ΠΑΝΕΠΙΣΤΗΜΙΟ ΔΥΤΙΚΗΣ ΜΑΚΕΔΟΝΙΑΣ
ΤΜΗΜΑ ΜΗΧΑΝΟΛΟΓΩΝ ΜΗΧΑΝΙΚΩΝ
ΤΟΜΕΑΣ ΠΑΡΑΓΩΓΗΣ ΚΑΙ ΜΕΤΑΦΟΡΑΣ ΕΝΕΡΓΕΙΑΣ

ΑΝΑΛΥΣΗ ΠΡΟΓΡΑΜΜΑΤΟΣ ΣΥΝΤΗΡΗΣΗΣ ΣΤΟΛΟΥ ΑΕΡΟΣΚΑΦΩΝ
AIRFLEET MAINTENANCE CASE STUDY

ΔΙΠΛΩΜΑΤΙΚΗ ΕΡΓΑΣΙΑ

ΝΙΚΗΤΟΠΟΥΛΟΣ ΠΑΝΑΓΙΩΤΗΣ 1238

ΕΠΙΒΛΕΠΩΝ ΚΑΘΗΓΗΤΗΣ : **ΑΝΤΩΝΙΟΣ ΤΟΥΡΛΙΔΑΚΗΣ**

Κοζάνη, Νοέμβριος 2015

ΠΑΝΕΠΙΣΤΗΜΙΟ ΔΥΤΙΚΗΣ ΜΑΚΕΔΟΝΙΑΣ
ΤΜΗΜΑ ΜΗΧΑΝΟΛΟΓΩΝ ΜΗΧΑΝΙΚΩΝ
ΤΟΜΕΑΣ ΠΑΡΑΓΩΓΗΣ ΚΑΙ ΜΕΤΑΦΟΡΑΣ ΕΝΕΡΓΕΙΑΣ

ΑΝΑΛΥΣΗ ΠΡΟΓΡΑΜΜΑΤΟΣ ΣΥΝΤΗΡΗΣΗΣ ΣΤΟΛΟΥ ΑΕΡΟΣΚΑΦΩΝ
AIRFLEET MAINTENANCE CASE STUDY

ΔΙΠΛΩΜΑΤΙΚΗ ΕΡΓΑΣΙΑ

ΝΙΚΗΤΟΠΟΥΛΟΣ ΠΑΝΑΓΙΩΤΗΣ 1238

Τριμελής Εξεταστική Επιτροπή :

Α. Τουρλιδάκης **Ι. Μπακούρος** **Δ. Γιαγκόπουλος**

Κοζάνη, Νοέμβριος 2015

ABSTRACT

Nowadays, aircraft operators are trying to minimise their expenses. Most of the cost for an aircraft operator is allocated to the engine maintenance overhaul. Therefore, each shop visit should be as efficient as possible taking into account both life and non-life limited parts.

This thesis attempts to analyse the influence of a typical maintenance program to the lifing of non-life limited parts. A Boeing 777-200ER equipped with a General Electric GE90-94B engine was selected for this project. Turbomatch and Hermes models were used to simulate the operation of both engine and aircraft over a variety of operating conditions. In addition, a reference flight for this type of long haul aircraft was simulated. Next step was the creation of the maintenance program for such an engine. In order to predict the interval and the cost for each engine shop visit, cost estimate relationships had to be created. A regression process enabled the author to create five cost estimate relationships, which can be used to predict a basic maintenance program for the GE90-94B.

The thesis progresses with the non-life limited parts lifing study and more specifically it focuses on the high pressure compressor blades. A preliminary compressor design as well as, a detailed analysis of the first stage rotor blades were conducted, revealing the stresses imposed on the blade surface. The next step involved a fracture mechanics analysis for the blades. By using an Advisory Circular issued by the Federal Aviation Administration and a fracture mechanics model the author was able to estimate the probability for a blade to develop a 1mm length crack over a specific amount of flight cycles. Finally, a Double Goodman Diagram analysis was performed to evaluate the effect of the combine low and high fatigue on the blades.

Keywords:

General Electric GE90, Cost Estimate Relationship, Regression, Preliminary Compressor Design, Fracture Mechanics, Low and High Cycle Fatigue

ΠΕΡΙΛΗΨΗ

Στην σημερινή εποχή οι αεροπορικές εταιρείες προσπαθούν να περιορίσουν με κάθε δυνατό τρόπο τα έξοδα τους. Μια από τις μεγαλύτερες δαπάνες των αεροπορικών εταιρειών αποτελεί η συντήρηση των κινητήρων του αεροσκάφους. Κατά συνέπεια, κάθε κύκλος συντήρησης του κινητήρα θα πρέπει να είναι όσο το δυνατόν πιο αποδοτικός, λαμβάνοντας υπόψιν τόσο τα εξαρτήματα περιορισμένης διαρκείς ζωής όσο και αυτά που δεν έχουν κάποιο περιορισμό (life limited parts / non-life limited parts).

Η διπλωματική αυτή αποτελεί μια προσπάθεια να αναλυθεί ένα τυπικό πρόγραμμα συντήρησης αεροστροβίλου αεροπορικής χρήσης και να μελετηθεί η επίδραση των εξαρτημάτων που δεν έχουν περιορισμό στο προσδόκιμο ζωής τους. Για την επίτευξη αυτού ένα αεροσκάφος τύπου Boeing 777-200ER εξοπλισμένο με έναν κινητήρα General Electric GE90-94B επιλέχθηκε. Εν συνεχεία χρησιμοποιήθηκαν μοντέλα Turbomatch και Hermes για να προσομοιωθούν τόσο το αεροσκάφος όσο και ο αεριοστρόβιλος. Το επόμενο βήμα περιλάμβανε την εκτίμηση του προγράμματος συντήρησης. Χρησιμοποιήθηκε η διαδικασία παλινδρόμησης προκειμένου να σχηματίσουν συνολικά πέντε μαθηματικές σχέσεις, ικανές να προβλέψουν την συχνότητα και το κόστος κάθε κύκλου συντήρησης για τον κινητήρα GE90-94B.

Στην συνέχεια η προσοχή στράφηκε στα εξαρτήματα χωρίς περιορισμό στην διάρκεια ζωής (non-life limited parts) και πιο συγκεκριμένα στην πρώτη σειρά πτερυγίων του συμπιεστή υψηλής πίεσης. Αρχικά πραγματοποιήθηκε ένας προκαταρκτικός σχεδιασμός του συμπιεστή υψηλής πίεσης, καθώς και μια αναλυτική μελέτη του πρώτου σταδίου, που απέδωσε τις ασκούμενες στα πτερύγια τάσεις. Εν συνεχεία ακολούθησε μια ανάλυση θραυστομηχανικής στα πτερύγια του συμπιεστή. Χρησιμοποιώντας αναλυτικές οδηγίες του Federal Aviation Administration καθώς και ένα μοντέλο θραυστομηχανικής, εκτιμήθηκε η πιθανότητα δημιουργίας ρωγμής ενός χιλιοστού σε ένα προκαθορισμένο χρονικό διάστημα. Τέλος, εφαρμόστηκε η τεχνική Double Goodman Diagram για να εκτιμηθεί η επίδραση του συνδυασμένου κύκλου κόπωσης (low and high cycle fatigue) στη πρώτη σειρά πτερυγίων του συμπιεστή.

ΕΥΧΑΡΙΣΤΙΕΣ

Στο σημείο αυτό θα ήθελα να εκφράσω τις ευχαριστίες μου στον επιβλέπων καθηγητή από το Πανεπιστήμιο του Cranfield κ. **Anthony Haslam**. Η συμβολή του ήταν καθοριστικής σημασίας τόσο για την κατανόηση όσο και για την ολοκλήρωση της διπλωματικής. Επιπλέον, ο κ. Haslam μου επέτρεψε να έχω την απαραίτητη ευελιξία σε αυτή την διπλωματική ώστε να παραμείνω αφοσιωμένος καθ' όλη την διάρκεια του εγχειρήματος.

Επίσης θα ήθελα να ευχαριστήσω τον κ**, Θεοκλή Νικολαΐδη** για την βοήθεια του. Η τεχνική συμβολή του στο κώδικα του Turbomatch ήταν σημαντικότατη.

Επιπλέον οφείλω να αναγνωρίσω την πολύτιμη βοήθεια των κ. **Παναγιώτη Λασκαρίδη**, κ. **Davaiah Nalianda** και του υποψήφιου διδάκτορα κ. **Alex Nind**. Η τεχνική τους υποστήριξη ήταν καθοριστική στην επιτυχία στην προσομοίωσης του αεροσκάφους, μέσω του κώδικα Hermes.

Οφείλω ακόμα να ευχαριστήσω όλους τους παράγοντες τόσο στο Πανεπιστήμιο Δυτικής Μακεδονίας όσο και στο Πανεπιστήμιο του Cranfield. Πιο συγκεκριμένα θα ήθελα να εκφράσω την εκτίμηση μου στις επιτροπές Erasmus των δύο Πανεπιστήμιων και ειδικά στην κ. **Χριστίνα Πεταλωτή**, καθώς χωρίς την δικά τους σκληρή δουλεία δεν θα είχα στην ευκαιρία να ολοκληρώσω τις μεταπτυχιακές μου σπουδές στα πλαίσια του προγράμματος Erasmus

Επιπλέον θα ήθελα να ευχαριστήσω τον κ. **Αντώνη Τουρλιδάκη**. Ο κ. Τουρλιδάκης έθεσε τις βάσεις για την συνεργασία του Πανεπιστημίου Δυτικής Μακεδονίας και του Πανεπιστημίου του Cranfield.

Θέλω να ευχαριστήσω όλους τους αξιότιμους καθηγητές μου τόσο στο Πανεπιστήμιο Δυτικής Μακεδονίας όσο και στο Πανεπιστήμιο του Cranfield που μου μεταλαμπάδευαν τις πολύτιμες γνώσεις και την επιστημονική κατάκτηση παράλληλα με την ηθική τελείωση του χαρακτήρα μου. Θα ήθελα να εκφράσω την ευγνωμοσύνη και την αγάπη μου στην οικογένεια μου και ειδικά σε αυτούς που δεν βρίσκονται μαζί μας σήμερα. Τέλος, η στήριξη όλων των φίλων μου κατά την διάρκεια των σπουδών μου την καθοριστική.

TABLE OF CONTENTS

LIST OF FIGURES

LIST OF TABLES

LIST OF EQUATIONS

LIST OF ABBREVIATIONS

AC	Advisory Circular
ALC	Airfoil Lift Coefficient
BM	Bending Moment
CER	Cost Estimate Relationship
DDF	Denominator Degree of Freedom
DOF	Degree of Freedom
EASA	European Aviation Safety Agency
ECI	Employment Cost Index
ECM	Engine Condition Monitoring
EFC	Engine Flight Cycle
EFH	Engine Flight Hour
EGT	Exhaust Gas Temperature
EGTM	Exhaust Gas Temperature Margin
ET	Engine Thrust
FAA	Federal Aviation Administration
HPC	High Pressure Compressor
HPT	High Pressure Turbine
IGV	Inlet Guide Vane
ISA	International Standard Atmosphere
LE	Leading Edge
LLP	Life Limited Part
LLPC	Life Limited Parts Cost
LPC	Low Pressure Compressor
LPT	Low Pressure Turbine
MRO	Maintenance Repair and Overhaul
NDF	Numerator Degree of Freedom
OAT	Outside Air Temperature
PPI	Producer Price Index
PR	Pressure Ratio
TE	Trailing Edge
TET	Turbine Entry Temperature
TWR	Thrust to Weight Ratio

NOMENCLATURE

α_1	Blade Inlet Angle
α_2	Blade Outlet Angle
β	Compliance Factor
δ	Deviation Angle
ζ	Stagger Angle
θ	Blade Camber Angle
Θ	Compressor Shape Factor
μ	Hub / Tip diameter
ρ	Density
σ	Stress
σ_e	Endurance Limit
σ_{ult}	Ultimate Tensile Stress
Φ	Stage Flow Coefficient
Ψ	Stage Loading
a	Half Flaw Length
C	Absolute Velocity
C_a	Axial Velocity
C_D	Drag Coefficient
C_L	Lift Coefficient
D_h	Hub Diameter
D_t	Tip Diameter
E	Young's Modulus of Elasticity
I	Second Moment of Area
i	Incidence Angle
K_B	Blockage Factor
M	Bending Moment
$\dot{m}$	Mass Flow
P	Total Pressure
p	Static Pressure
Q	Flow Function
R	Coefficient of Determination
T	Total Temperature
t	Static Temperature
U	Blade Rotational Speed
V	Relative Velocity
Vol	Volume
W	Weight

1 Introduction

For a modern gas turbine, maintenance cost constitutes a significant portion of the total operating cost. Therefore it is no surprise that aircraft operators attempt to minimise engine maintenance cost. Typical maintenance program nowadays, are based on strict rules governing the life limited parts such as the heavy metal rotating parts of the engine. Engine manufacturers issue guidelines suggesting the life expectancy for the life limited parts. Consequently, the rest of the gas turbine components follow the same scheduling.

The management of the maintenance schedule can became inefficient and costly, because many components are removed from the gas turbine before they have reached their life expectancy limit. Specially the high pressure compressor blades.

1.1 Main Objectives

The main objectives of this project are as follows:

- Simulate the engine and aircraft operation using the Cranfield Turbomatch and Hermes Codes for a reference flight.
- Create cost estimate relationships to predict the cost and interval of the engine shop visits.
- Perform a preliminary compressor design. Define the blade shape and calculate the stresses on the blades.
- Calculate the probability of a blade failing inspection in a specified number of flight cycles and study the effect of the combined high and low cycle fatigue on the blades.

1.2 Thesis Structure

This thesis comprises the following chapters.

Chapter 2 Gas Turbine Maintenance. The basics for the aircraft engine maintenance are described. The strategies which the airlines follow and their implications are also included. The main causes of engine removal, as well as the non-life limited parts are also discussed.

Chapter 3 Methodology. This chapter explains the methodology the author followed in this project.

Chapter 4 Engine Simulation. The simulation of the engine was conducted in this chapter. A brief discussion of the way that Turbomatch works is included. The results of the simulation and the points where the model was validated are also presented.

Chapter 5 Aircraft Simulation. The simulation of the Boeing 777-200ER was the subject of this chapter. First an example of the calculations that Hermes computes is presented. The description of the model used and the verification process follow. The simulation of a reference flight for London Heathrow to New York JFK airport concludes this chapter.

Chapter 6 Cost Estimate Relationships. The processes of creating and normalizing an engine database are described. In addition, the basic theory of cost estimate relationships is included. The final cost estimate relationships which can predict the cost and interval for the engine overhaul are also presented.

Chapter 7 High Pressure Compressor Design. A preliminary compressor design is conducted. The annulus geometry is extracted and compered with the actual geometry. The velocity triangles for the first stage of the compressor are also defined and by using them the basic shape of the blades is created. The blade stresses imposed by the centrifugal load as well as the changes in pressure and velocity over the blade are derived for the leading and trailing edge.

Chapter 8 Fracture Mechanics. This chapter include a fracture mechanics analysis for the first blade row of the HPC. The probability for a detectable crack appearing under a specific number of flight cycles is calculated. In addition, a Double Goodman Diagram technique was used to evaluate the effect of the combine high and low cycle fatigue on the blades.

Chapter 9 Conclusion and Recommendations. The final chapter contains the author's conclusions relating with the influence of the maintenance program to the lifing of the non-life limited parts. In addition, the author made several recommendations concerning some future work on the same subject.

2 Gas Turbine Maintenance

2.1 Airlines Cost Structure

The air transportation market has seen an excessive growth over the past years. In addition to that the market itself has become very aggressive and competitive. Most of the airlines today are seeking new ways to reduce their expenses in order to stay profitable in a market where low fare carriers are thriving. This is the reason why we observe a change in the airline cost structure nowadays. Airlines are implementing new technologies that can potentially contribute to the reduction of the operation cost for an aircraft throughout its life. Maintenance, repair and overhaul (MRO) costs for an airline gas turbine constitutes a major component of that total operating cost [1].

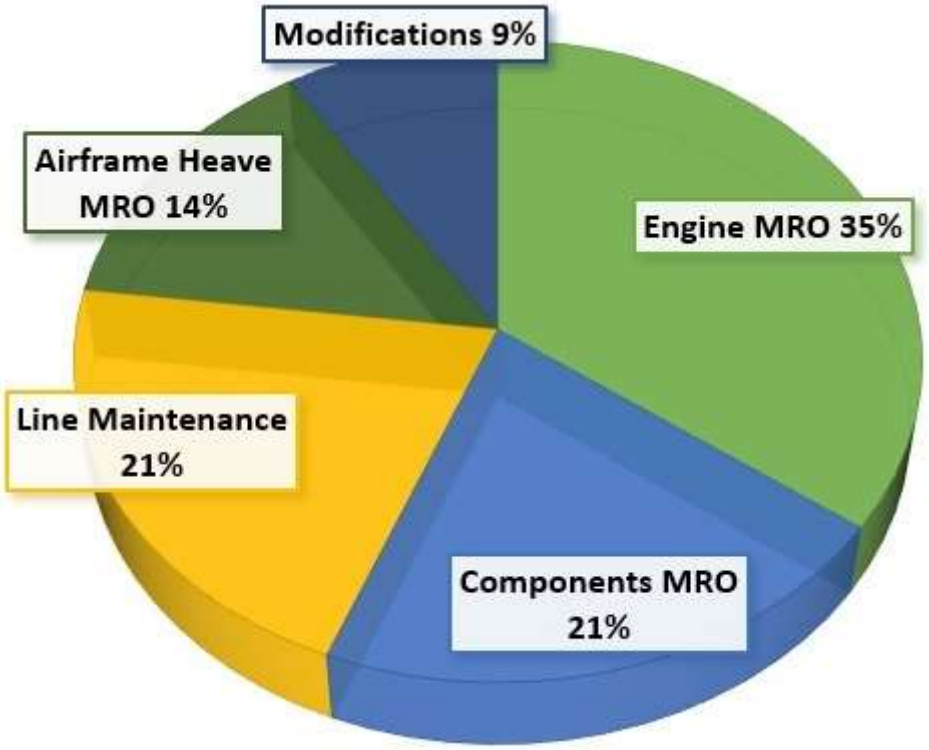

Figure 2-1 Aircraft Maintenance Cost [2]

The cost of maintaining an aircraft engine is such a large proportion of the total MRO costs due to the complexity of those machines. Inspection, disassembly, reassembly and testing of a modern gas turbine requires many man hours that result in a high labour cost.

Moreover the high temperatures and stresses exerted on the components of the engine require expensive materials that can withstand those severe conditions. This is why an engine overhaul can cost many times more that the initial purchase cost and also is the reason why the MRO is purely a cost driven process. Therefore many aircraft operators develop complex monitoring and cost estimating tools that can help them predict the costs associated with the operation of a gas turbine over its life cycle.

2.2 Maintenance Strategies

It is obvious that maintenance is a significant part of any airline organization. It involves a lot of planning and management in order to minimize the costs. There are several strategies which can be applied but not all of them are suitable for an aircraft engine. The simplest maintenance strategy is called run-to-failure. This technique allows the equipment to operate until failure occurs. For obvious reasons related to the safety of the aircraft that type of maintenance program is not applicable for an airline engine. In the earlier age of aviation a technique called time-based maintenance was used. Aircraft engines were removed for an overhaul on a fixed interval rate. This time based schedule attempts to prevent failures by replacing the components before a critical situation occurs. The disadvantage of this method is the assumption that all the components age at the same rate regardless of the operating conditions. In recent years the most frequently used maintenance strategy is called condition – based maintenance. This method prevents failures by monitoring the deterioration level of the gas turbine components. The repair or the replacement of a component can take place when the monitored value exceeds a predetermined limit. Further techniques like opportunity maintenance and design out method, are also not suitable for a gas turbine since the risk of failure is not tolerable [2] [3].

2.3 Engine Condition Monitoring

Engine Condition Monitoring (ECM) is necessary when a condition-based maintenance strategy is applied.

Before the evolution of this technique the maintenance crew used to rely on the pilot to retrieve the various parameters, using the instrumentation inside the aircraft cockpit. Data was manually recorded once during take-off and once in cruise conditions. Therefore the reliability and the efficiency of the whole maintenance program suffered. Modern aircraft engines are equipped with electronic engine control systems. Those devices apart from controlling the safe operating of the gas turbine, also monitor the engine using a separate maintenance software. They can collect data at a much faster pace that a manual system and with higher accuracy. Those systems also have the option to transmit information directly to a ground station [4]. The collected data can be classified into two categories. The first category includes data which is not directly related to the engine trust level and the operating conditions, like the oil temperature and the vibration level of the engine. While the second category consists of measurements like the gas path temperature, fuel consumption and rotational speed for the high and low pressure shafts of the engine. In addition to those a set of characteristics flight parameters like the altitude and flight speed are also collected. All the gathered information is being used to produce trend lines. By comparing the produced trend lines with base lines provided by the engines manufacturer the faulty component can be found and replaced. Apart from data collection, engine condition monitoring also includes the physical monitoring of an engine such as borescope inspections [2].

2.4 Engine Shop Visit

Even though in recent years engine original equipment manufacturers (OEMs) have tried to improve the on-wing maintenance by making the internal components more accessible, the engine deterioration will eventually make the operation of the engine unsafe and perhaps non profitable. At that point the engine is removed from the wing for an overhaul. Also worth mentioning is that the engine is replaced so that the aircraft can continue to operate while the engine is refurbished. The whole process of removing and replacing an engine can be completed by a group of 3-4 mechanics in under 8 hours [2].

2.4.1 Primary causes of engine removal

A shop visit can be either a scheduled or unexpected event. An unexpected shop visit could be the result of foreign object damage.

Debris can enter the engine while the aircraft is taxing, taking off or landing, as well as when the aircraft flies. In a case of a scheduled shop visit there are three usual causes:

- Hardware Deterioration
- Exhaust Gas Temperature (EGT) Margin Deterioration
- Expiry of Life Limited Parts (LLPs)

The type of the engine influences the cases of an engine removal. As the following diagram suggests short haul engines are more likely to be removed due to the depletion of the EGT margin and the expiry of their life limited parts. On the other hand medium to long haul engines suffer more from hardware and EGT deterioration [5]. The reasons of this difference are going to be explained in the next chapter. This thesis project is focused more on the medium to long haul aircraft engines.

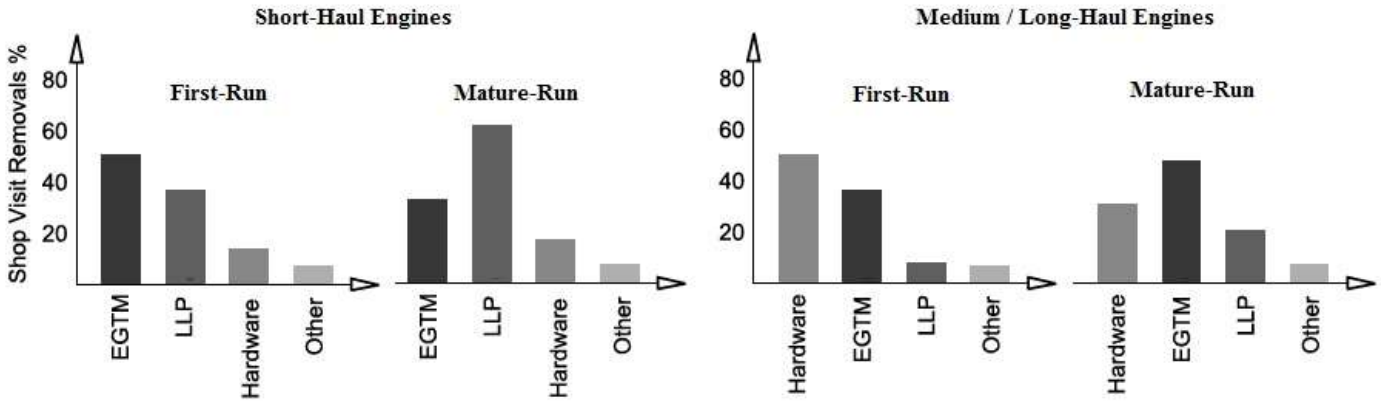

Figure 2-2 Primary Causes for Engine Removal [5]

EGT Margin Deterioration

The exhaust gas temperature is one of the most important measurements for a gas turbine, because it can be easily related to the efficiency of the machine at a specific thrust level. The increase in the EGT depends on the component deterioration that the engine experiences.

A possible cause for the degradation of the EGT can be the wear of the turbomachinery in the engine's compressor and turbine. That wear increases the components losses, through mechanisms like the over tip leakage, making the whole engine less efficient.

In order for the engine to provide the same amount of thrust more fuel is introduced into the combustor resulting in a higher exhaust gas temperature. If the EGT exceeds a predetermined limit and the engine continues to operate, the safety of the components can be compromised. This is why every engine is certified with a maximum value of EGT called red line EGT. The difference between the monitored EGT and the red line EGT is the EGT margin. Also worth mentioning is that the Outside Air Temperature (OAT) influences the EGT and the relationship between the two is almost linear.

Life Limited Parts Expiry

Another possible cause for the removal of the engine is the expiry of LLPs. The parts on an aircraft engine are called limited parts if their failure results in an uncontrolled situation. As the name suggests those components are certify for a specific number of engine flight cycles (EFC). The LLPs on a gas turbine comprise of rotating parts such as shaft and disks, and stationary parts such as casings and engine mounts. For example the booster shaft on a General Electric 90-94B engine is certified for 20,000 EFC [6]. After the utilization of those flight cycles the engine has to visit the workshop for an overhaul. Usually short haul engines experience LLPs expiry as the cause of engine removal. Those engines operate with a low ration of flight cycles to flight hours resulting in a higher rate of LLPs life consumption.

Hardware Deterioration

The last reason for an engine overhaul is the degradation of the engine's hardware. The components inside an engine are exposed to high temperatures and stresses, particularly the high pressure compressor and turbine. The non-life limited parts like blades that operate under those conditions, suffer from low and high cycle fatigue, thermo-mechanical fatigue and corrosion.

This results in a reduction in the life of the components or ever failure. To prevent failure each component is closely examined as part of the engine condition monitoring procedure and necessary the defective part is replaced.

2.4.2 Typical Shop Visit Planning

Engine Module Construction

Modern aircraft engine like the GE 90-94B are built using separate assemblies called modules. This is an attempt by the OEMs to reduce the time required to replace a component of the engine. A twin spool engine usually consists of 6 modules [7]. The fan, the low pressure compressor (LPC), the high pressure compressor (HPC), the combustion chamber, the high pressure turbine (HPT) and the low pressure turbine (LPT).

In many cases the high pressure compressor, turbine and the combustor are referred to as the core of the engine. A typical modular construction for a twin shaft gas turbine can be seen in the following figure.

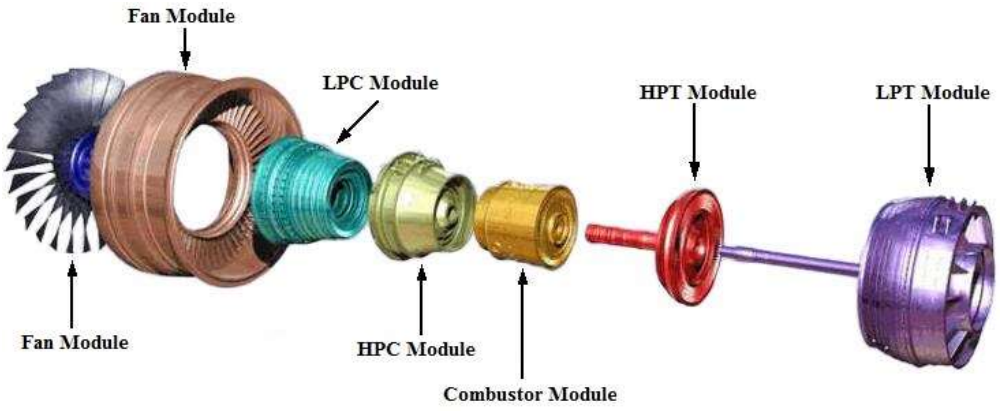

Figure 2-3 Twin Spool Module Architecture [8]

Shop Visit Planning

The overhaul of an engine comprises two major activities. The first is the restoration of the EGT, while the second is the replacement of the life limited parts.

More specifically when an engine visits the workshop the first step is the disassembly of the engine and the inspection of each module individually. The following procedure is the removal of parts, such as blades, and the inspection for their serviceability. If those part are considered serviceable a restoration can take place. The last steps are the reassembly and testing of the restored engine.

At this point it is noteworthy that from the total cost the material cost constitutes approximately 60% - 70%, labor cost is equal to 20% - 30% and remaining 10% - 20% accounts for the repair cost.

Different modules on the engine do not experience the same level of stress and temperature, so they do not require the same level of attention at each workshop visit. For this reason there are three level of work scope that can be applied to each module separately. A typical example of the different level of work scopes for each module is illustrated in the table below.

Modules	1st Shop Visit	2nd Shop Visit	3rd Shop Visit
Fan & LPC	Minimum Level	Performance Level	Minimum Level
Core	Performance Level	Full Overhaul	Performance Level
LPT	Minimum Level	Performance Level	Minimum Level

Table 2:1 Typical Engine Work Scope

The Minimum work scope includes only the exterior inspection of the module and some negligible repairs. The Performance level requires the disassembly of the module and the inspection of parts like blades, seals and shrouds. Lastly the Full Overhaul level calls of a full teardown of the module and the individual inspection and replacement of each of the parts. The manufacturer of the engine usually issues guidelines of the level of work scope for every module of an aircraft engine [5].

2.5 Shop Visit Cost and Interval

As it is already mentioned the shop visit intervals are caused due to EGT margin depletion, hardware deterioration, LLP expiry or unexpected events like foreign object damage.

All the causes apart for the debris damage depend on the operation conditions of the gas turbine. Therefore there is a relationship between the shop visit cost and interval with the thrust rating of the engine, the operational severity and the utilization of the engine.

2.5.1 Engine Utilization

A useful way to describe the usage of an aero engine is the ratio between engine flight hours per engine flight cycles (EFH / EFC). A typical flight for a commercial aircraft consists of a high thrust level at take-off, a steady thrust level at cruise and a decrease in the thrust level at the descent and landing phases. Those changes in the thrust level correspond to one full engine cycle. In addition to that many aircraft use reverse thrust to decelerate after touching down. This also correspond to an engine cycle, but since this phase is only few seconds long it usually tends to be ignored. Using the EFH / EFC ratio the distinction between short and long haul aircraft is simpler. Usually short haul aircraft have a ration equal to 1-2 while long haul can reach values of 7-10.

2.5.2 Thrust Rating

As the thrust level increases for a gas turbine so does to the temperatures inside the engine. Consequently, the core components experience greater thermal stresses. That has an effect on the depletion of the EGM margin of the gas turbine.

2.5.3 Operational Severity

The operational severity include all the conditions that create more challenging operating conditions for the gas turbine.

The first one is the flight length. For a long flight the engine spends more of the time at cruise conditions which are not demanding. Therefore a longer flight is less severe to an aircraft engine than a short one.

The second conditions is the take-off derate and it relates with the trust rating mentioned above. When an aircraft do not require all the available thrust from the engine the take-off thrust can be reduce, that results in a reduction of the rate of EGT margin depletion.

The next operating conditions that affects the severity is the ambient temperatures. The Outside Air Temperature (OAT) is linked with the EGT margin and the trust level of the engine. For the same thrust level as the OAT increases the EGM margin decreases, making the operating of the engine more demanding. Lastly the environment in which a gas turbine operates is crucial to the severity. An environment containing dust and sand particles than enter the engine will results in higher deterioration especially in the compressor and turbine blades.

2.6 Non-Life Limited Parts

The objective of this thesis project is to study the influence of the maintenance schedule to the non-life limited parts of an airline engine. More specifically, it is focused on the high pressure compressor blades of a General Electric 90-94B. The airfoils on a high pressure compressor are not life limited parts but they are critical parts. This means that if they fail, the safe operation of the gas turbine can be compromised. Blades are also a part that requires the manufacturer's approval. This concept was introduced by the Federal Aviation Administration and it ensures that the replacement blade will be designed and manufactured under certain regulations [5]. The first step in analyzing the influence of the compressor blade to the maintenance program is to understand the mechanisms that make the blades fail.

2.6.1 Compressor Blade Failure Modes

There are two major categories of failure modes which apply to compressor blades. First are the mechanical failure modes that include High Cycle Fatigue (HCF), Low Cycle Fatigue (LCF) and Thermo-Mechanical fatigue. The second category of failure modes include corrosion which is an environmental driven process. In this project the blade life analysis will be based on high and low cycle fatigue.

Compressor blades experience a variety of different loads. The most severe of them is the centrifugal load caused by the rotation of the shaft. The resulting tensile stress is a maximum at the root of the blade. Apart from this loading, gas bending moments due to change in the pressure and the velocity in both tangential and axial direction are also imposed on the blade. Those gas bending moments are fluctuating because of the interaction between stationary and rotational components on the compressor.

At the inlet of the high pressure compressor of the GE 90-94B inlet guide vanes (IGVs) are installed to turn the flow in the desirable direction. IGVs are stationary blades that create at region of low flow velocity behind them, called a wake. As the rotor blades cross the IGVs the gas bending moments acting on them change and a cyclic loading is created. The frequency of that loading depends on the number of IGVs installed on the engine, the rotational speed and the time that the gas turbine is in operation. This situation produces what is known as high cycle fatigue. On the other hand, low cycle fatigue is caused by starting and stopping operation of the machine. HCF is usually associated with low stresses and high frequency while LCF is the exact opposite condition.

Fatigue Mechanism

Fatigue is a phenomenon where a material can fail at a much lower stress level than the material static strength, if the loading is fluctuating. The cyclic loading combined with the crystalline nature of the materials used on compressor blades are what drives the fatigue mechanism. The process of fatigue can be divided into three phases: Crack Initiation, Crack Propagation and Failure by Fracture [9].

Crack Initiation

It is typical for cracks to initiate from the surface of the material. The bonds that hold the outside layer of grains are weak making the distortion more likely at the surface. In addition to that the stress concentration and the corrosive conditions at the surface of the blade enhance the creation of initial cracks.

The slippage between crystals which are aligned with the cyclic loading is responsible for the formation initial micro-cracks. The defects in the material increase the local stress concentration and quickly can be developed into macro-cracks.

Propagation of Crack

The next phase is more important for identifying the fatigue resistance of a material. Since every sample of a material will include impurities it is safe to assume that the material will have initial micro-cracks. The propagation of cracks can be spilt in two segments. At the first, the slippage between crystals in the direction of maximum shear stress takes place.

While in the second one the propagation of the crack changes direction to avoid planes that slippage cannot occur. At low stress conditions the propagation of a crack can account for up to 90% of the material life [9].

Failure by Fracture

The propagation of a crack continues until the size of the crack reaches a critical value. At that point the structural integrity of the material is compromised, since the loading is applied at a small cross sectional area and the stress concentration is very high. The failure can then occur by a gross yielding, ductile shear or a fast running brittle fracture [9]. The mechanism of crack propagation and fracture will be discussed in greater detail in the chapter 8.

2.7 Non-Life Limited Parts Inspection

The non-life limited parts and more specifically the blades of the high pressure compressor are located deep in the core of the engine. It is not practical to disassemble the gas turbine each time an inspection has to take place. In order to simplify the process manufacturers have installed inspection ports in several key locations. The maintenance crew can use them to insert a borescope and monitor the condition of the interior of the engine without removing the casing. Borescope inspection follows a schedule determined by the OEMs buy unscheduled inspections can occur in the case of a malfunction.

A borescope is comprised of an eyepiece where a magnification lens is located, a flexible or rigid tube that includes the optical relay and optical fiber systems and at the end an objective lens [10]. Light for the light source travels to the object through the optical fibre system and returns back to the eyepiece through the relay system.

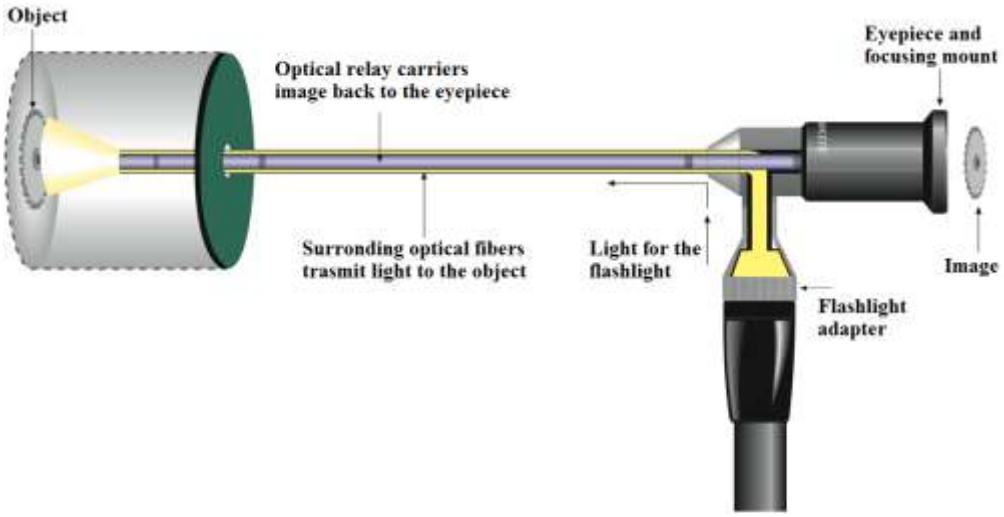

Figure 2-4 Borescope [11]

Another feature of flexible borescope is the ability to control the movement of the objective lens. Articulated borescopes can either move into two or four directions and are much easier to navigate inside the small cavities of the engine. Lastly borescope inspections are an effective means of detecting degradation because the smallest detectable crack size is slightly less than 1mm [12].

2.8 Chapter Conclusion

This chapter was dedicated to the maintenance schedule of an airline gas turbine. The importance of the maintenance was discussed and the different types of maintenance programs were explained. In addition to that, the procedures involved in engine overhaul and the causes of an engine shop visit were described. This thesis project focuses more on the influence of a typical engine maintenance program to the life of a non-life limited part such as a compressor blade. Therefore a quick description of the mechanisms responsible for the failure of the blades and the inspection techniques used for them was included in this chapter.

3 Methodology

This chapter provides an overview of the methodology used by the author in his research. The main objective is to identify the influence of a normal maintenance schedule on the high pressure compressor of a General Electric 90-94B engine. The first step is the creation of the maintenance program. In order to achieve this the author used the Cranfield Turbomatch and Hermes codes to simulate the performance of the engine and the aircraft. Next step involved the formation and usage of cost estimate relationships to predict the maintenance program. After calculating the total amount of Engine Fight Cycles (EFC) a blade lifing model, based on fracture mechanics, is used to determine the probability of a blade failure.

3.1 Turbomatch Simulation

Turbomatch is a gas turbine simulation code developed at Cranfield. It is used to simulate the performance of the GE90-94B engine at both design point and off design conditions. Initial the process starts by matching the results of the simulation with the available data in the literature. When satisfied that the model represents as closely as possible the actual engine, the Turbomatch code is used as an input to the Hermes program to simulate the performance of the aircraft.

3.2 Hermes Simulation

Hermes is an integrated engine-aircraft simulation code. It combines some geometrical characteristics of the airframe with the results from the Turbomatch code to simulate the operation of the aircraft over a mission. The model used in this thesis represents the Boeing 777-200 ER aircraft and the first step was the formation of a payload /range curve that matched the actual one provided by Boeing. When an acceptable simulation was achieved the model was used to represent a specific flight from London, Heathrow to New York JFK.

3.3 Maintenance Schedule

With the results available for the reference flight, the cost estimate relationships can be used to predict the maintenance program for the specific aircraft.

The creation of the cost estimate relationships is a procedure that involves the collection of data for a large engine database and a back step regression process. This process will be fully explained in chapter six.

3.4 Blade Sizing

This step includes the necessary procedures to retrieve a basic shape for the compressor blades. In a high pressure compressor the first stage will experience the higher stresses. The first row blades are longer and therefore the centrifugal stresses will be higher. The basic shape for the first stage blades will arise from a preliminary compressor design study.

3.5 Blade Lifing

The last step consists of the lifing analysis of the compressor blade. Having calculated the basic dimensions of the blade, the stresses imposed on it can be derived. For the lifing of the blade two methods will be used. The first is a fracture mechanics model that predicts the crack propagation. The second is a basic high cycle fatigue lifing study using a Goodman diagram approach.

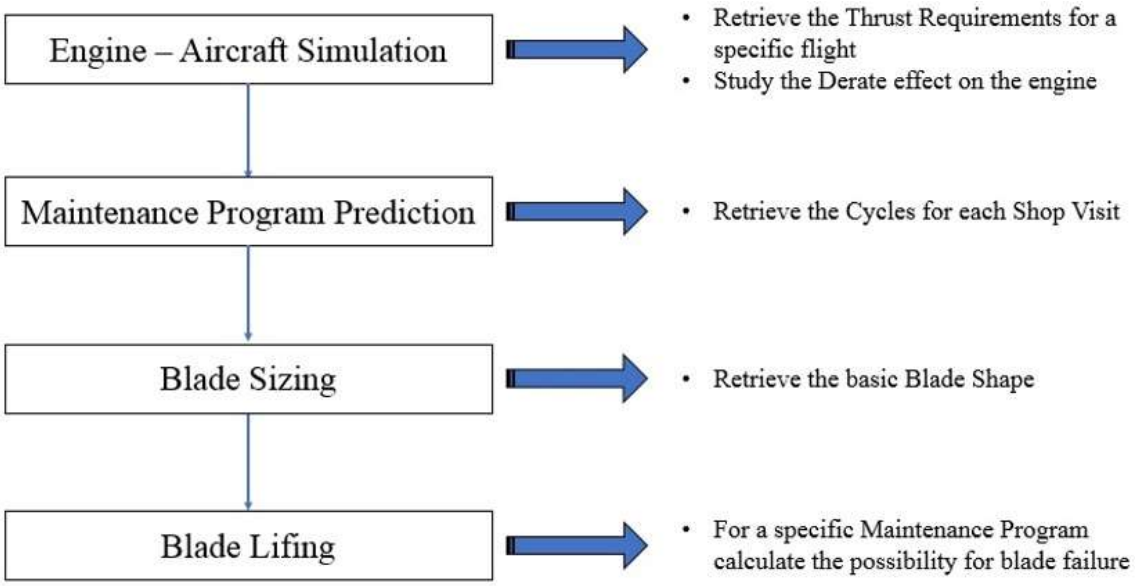

Figure 3-1 Methodology

4 Engine Simulation

This chapter includes the specifications for the selected engine, the basic function of the Turbomatch code, the model the author used to simulate the performance of the engine and the results from the matching process.

4.1 General Electric 90-94B

Initially the study was conducted using a larger more powerful and newer gas turbine the GE 90-115B1. However the lack of data available for that specific engine made the matching process difficult. To avoid this problem the author decided to change his selection and work with a slightly older engine the GE 90-94B. The General Electric GE 90 was developed from the Nasa Energy Efficient Engine. It is a twin spool large turbofan engine. The fan has a diameter of 3.4 meters and includes 22 blades constructed from carbon composite material with a titanium leading edge. After the fan, the flow splits and follows either the path through the core of the gas turbine or the bypass duct. Inside the core of the engine, a low pressure compressor or booster is located to increase the core mass flow. The high pressure compressor, which follows, initially had 10 stages but it was decided that the final stage was not necessary. The HPC in the GE 90-94B is a 9 stage compressor with a pressure ratio of 23:1 at take-off conditions. In order to ensure stall free operation of the front stages at part speed, 5 rows of variable stator vanes were also included in the design. The combustion chamber is constructed using two concentric chambers, a design that GE calls Dual-Annular Combustor. There are two rings of 30 fuel nozzles each, with only one of the rings spraying fuel during starting and low power setting. The high pressure turbine of the engine consists of two air-cooled stages and an active clearance system is also present in the HPT casing. The following component is the low pressure turbine, which has 6 stages for improved efficiency and work extraction. An active clearance control system is also present in the LPT [13]. The figure below depicts the airflow and major components for a General Electric GE 90.

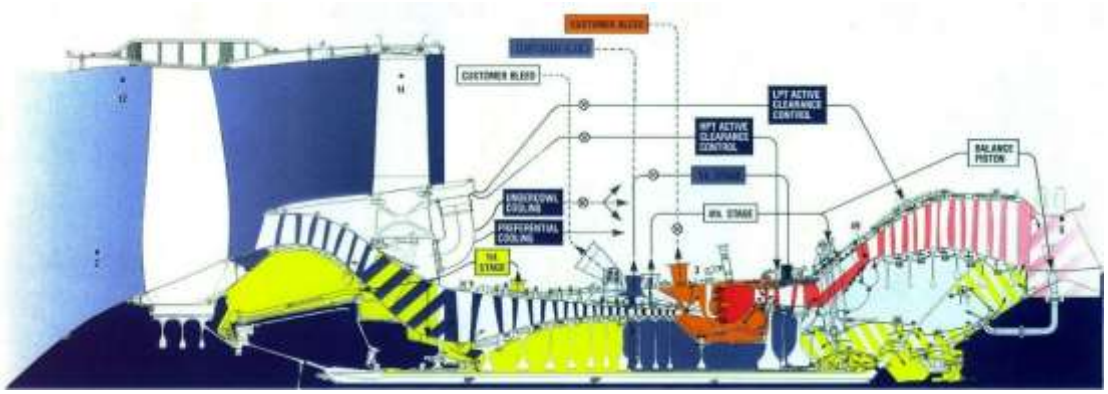

Figure 4-1 GE90 Airflow [14]

4.2 Turbomatch

Turbomatch is a gas turbine performance simulation code. It has been developed by the School of Mechanical Engineering in Cranfield. The latest version, Turbomatch 2.0 can perform design-point, off-design and transient performance calculations. Is uses a brick design construction that enables it to simulate a wide range of industrial and aero engines. These bricks represent the major components of the gas turbine such as the compressor, turbine and combustion chamber. The method that Turbomatch uses to simulate the operation of the engine is based on mass flow and energy equilibrium between the bricks. The interface between bricks is known as a station and the gas properties in this position are called station vectors [15].

Initially Turbomatch calculates the design point for the gas turbine. It uses inputs such as the ambient conditions and the values selected for the handle and calculates the gas properties at each station. Using these it can derive outputs like the trust and fuel consumption for the gas turbine. In addition Turbomatch also selects scaling factor for the design point calculations. It uses those to adjust the generic component maps to fit the particular simulation.

For the off – design calculations Turbomatch applies a technique where it guesses values like the pressure ratio, the rotational speed and the components efficiencies. It then checks if the guesses are correct using mass flow, energy and rotational speed equilibriums.

At this stage, it is worth mentioning that the biggest uncertainty introduced to the simulation arises from the use of generic component maps. Turbomatch includes 5 compressor and 6 turbine maps that it scales to match the design point. Since the component maps are generic they cannot fully simulate the operation of the components. However the scaling process has been optimized to such an extent that the error from the use of the generic maps is almost unnoticeable.

4.3 General Electric 90-94B Model

To simulate the GE90-94B a typical brick construction was used. A simplification was made to the design of the model, regarding the bleed extraction from the HPC. The air used for cooling the HPT was taken only at the outlet of the high pressure compressor, while the actual engine incorporates 3 bleed ports at the fourth, seventh and ninth stage. The model used in this simulation is described by the figure 4-3.

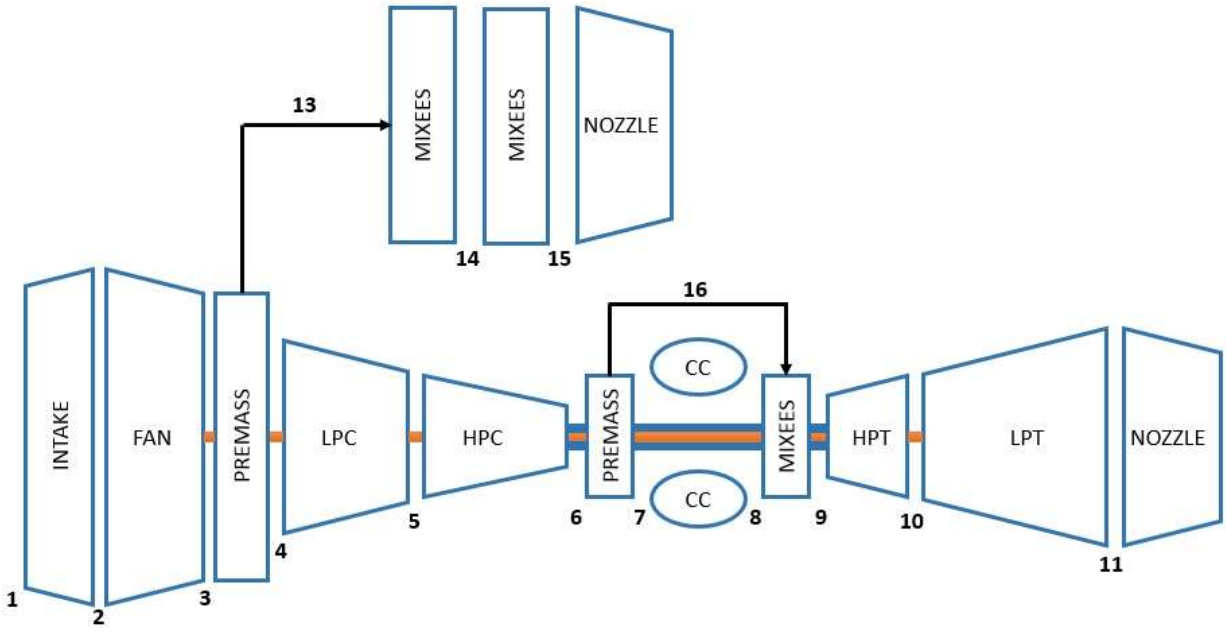

Figure 4-2 GE90-94B Turbomatch Model

The simulation process for any gas turbine starts by collecting all the available specifications for the design point. In the case of the GE90-94B most of the data were available at take-off conditions, hence that point was chosen as the design point of the engine. The available data for the take-off condition can be seen in the table 4-1 below.

Engine Specifications at Take-Off	
Item	**Value**
Inlet Mass Flow [Kg/s]	1467
By-Pass Ratio	8:4
Fan Pressure Ratio	1.58:1
HPC Pressure Ratio	23:1
HPT Auxiliary Work [kW]	288.1

Table 4:1 Engine Specifications [13]

Another parameter that affects the operation of the gas turbine is the amount of air extracted from the compressor, which is used to cool the high pressure turbine.

The total amount allowed for extraction depends on the power setting of the engine. The following table contains the maximum permitted air extraction in relation to the non-dimensional rotational speed of the low pressure spool (N1).

Allowable Bleed Limits (Percent)				
	Stage 4	Stage 7	Stage 9	Total
Below 23% N1	7.8	1.8	13.6	15.4
23% to 31% N1	7.6	1.6	12.8	14.4
31% to 57.4% N1	7.4	1.3	12.6	13.9
57.4% to 80% N1	7.2	1.3	12.6	13.9
80% to 96.8% N1	7.0	1.3	6.5	8.3
Above 96.8% N1	6.5	1.3	6.5	7.8

Table 4:2 Maximum Bleed Extraction [16]

For the take-off condition the maximum air bleed allowed is equal to 7.8 percent of the total mass flow through the core of the engine. Finally the last variables that need to be specified were the component efficiencies. This is another possible cause of inconsistencies, since the actual values for the efficiencies are not available in the public domain. These values are assumed and they were kept within reasonable limits. The individual component isentropic efficiency selected for the final model are illustrated in the table below.

Component	Isentropic Efficiency
Fan	0.915
Low Pressure Compressor	0.89
High Pressure Compressor	0.88
Combustion Efficiency	0.99
High Pressure Turbine	0.92
Low Pressure Turbine	0.93

Table 4:3 Component Isentropic Efficiency

4.4 Turbomatch Model Validation

The model of the GE0-94B engine was verified using three different operating conditions. Three points were selected in order to ensure a proper working model. The difficulty at this stage originates from the available data in the literature. In two of the cases the author was forced to compere the model of the GE90-94B with data available for the GE90-85B.

4.4.1 Take-off

This is the design point of the model. Apart from the specifications of the engine presented in the table 4-1, the only other available data was the thrust level produced at take-off. The actual engine produces 416671.3 N of thrust and the result from the simulation was 416735.35 N. The resulting error is equal to -0.01537%. Also noteworthy is the Turbine Entry Temperature (TET) used in the design point simulation.

The only data that was available, came from a less powerful engine the GE90-85B. These two models share the same basic construction and most of the components, the difference between them is the level of thrust they produce. For the GE90-85B at take-off conditions the TET was 1592K, while in his model the author used a TET of 1659K. The 67K difference is reasonable given the higher thrust level of the 90-94B.

Design Point			
	Literature	**Turbomatch**	**Error %**
Thrust Level [N]	416671.3	416735.35	-0.01537

Table 4:4 Design Point Simulation Results

4.4.2 Cruise Conditions

For the simulation of the cruise conditions the author could not find any reliable data for the specific model of the GE90. Therefore again a comparison between the GE90-94B and the GE90-85B was chosen. In order to simulate cruise, the ambient conditions were changed to an altitude of 30000 ft (10668 meter) and a cruise speed of 0.85 Mach.

The TET was used as a handle and the engine was spooled down until the required thrust level was achieved. The results are shown in the table 4-5 below.

Cruise Condition			
	Literature / GE90-85B	**Turbomatch**	**Error %**
Thrust Level [N]	69100	69117.18	-0.0249
SFC [kg/N]	15.6	15.4	1.28

Table 4:5 Cruise Conditions Simulation Results

4.4.3 European Aviation Safety Agency (EASA) Certification

The last point chosen for validation of the model was the certification test from the EASA. The engine in this test is allowed to operate without any bleed extraction from the compressor and without any auxiliary work produced by the high pressure turbine. The air required for blade cooling is provided by an external

source. In addition to this, the test takes place under static sea level conditions with an International Standard Atmosphere (I.S.A.) temperature deviation of 15 °C. The comparison between the actual test results and the simulation can be seen in the table 4-5 below.

EASA Certification Condition			
	EASA Certification	**Turbomatch**	**Error %**
Thrust Level [N]	432811	432936.36	-0.0289
EGT [°C]	1030	932.34	9.482

Table 4:6 EASA Certification Simulation Results

The error that occurs in the measurement of the exhaust gas temperature seems significant. Indeed an error of 9.482% in a simulation is considered to be high. However there are three possible causes for such a large error. Firstly Turbomatch is a thermodynamic tool that works adiabatically, so it does not take into account the heat fluxes through the casing of the gas turbine. Heat could be transferred for a hotter combustion case to the measurement equipment, something that Turbomatch does not account for.

Secondly an error can arise from the measurement itself. During the EASA certification the EGT is measured between the HPT and LPT. At this location a measurement of homogenous temperature is difficult. Thirdly the EASA does not specify the temperature of cooling air provided to the HPT. The temperature of this cooling mass flow affects the measured exhaust gas temperature.

The design point code as well as the results from each validation point are presented in the Appendix A.

4.5 Turbomatch Results

The creation of a reliable Turbomatch model was essential for this thesis project. Hermes uses as an input the design point created in Turbomatch, to simulate the performance of the engine during a whole flight. Therefore the model was validated using three different operation conditions. However the results contain error due to three major assumptions:

1. The way Turbomatch code works introduces an error. The actual component maps are not available and generic maps are used after they have been scaled. Consequently this is a reason for generating errors, especially in off-design simulation.

2. The assumption of the component efficiencies. Full specification for the components of a gas turbine are not published in the literature. Subsequently some assumptions have to be made. In many cases the chosen efficiencies do not agree with the actual data.

3. The comparison with the GE90-85B. The author was forced to validate the operation of the engine in cruise conditions using data from a different engine. Even though both engines are quite similar, this probably has introduced some error to the simulation.

4.6 Chapter Conclusion

This chapter included a brief summary of the specifications of the General Electric 90-94B and a description of the Turbomatch model used to simulate it. The validation process that followed tests the accuracy of the model using three different operating points and the resulting errors were within acceptable limits. Lastly an explanation for the causes of those errors was given.

5 Aircraft Simulation

This chapter focuses on the analysis of the flight path using an aircraft performance model called Hermes. The basic way that Hermes works, the inputs it needs and the results it produces are also explained. The chapter is continuous with a description of the model used in this project, and concludes with the validation of the results.

5.1 Hermes

Hermes constitutes an aircraft performance model develop in Cranfield. It uses the appropriate input data to calculate mainly the thrust required from the engines, the maximum range of the aircraft for a specific amount of fuel or alternatively the fuel needed for a predetermined mission. It is constructed in such a way, that a wide variety of aircraft can be simulated using the code. The user also has the capability to interfere with variables such as the rate of climb and the configuration of the aircraft during take-off and landing. The tool has been validated using as a baseline many aircraft with errors that do not exceed 1% [17] [18].

5.2 Hermes Modules

Hermes is built with a modular construction following the logic behind Turbomatch. This gives the code the necessary flexibility to adapt to many different simulation scenarios. The different modules of Hermes are:

1. The Input data
2. The Mission Profile
3. The Atmospheric
4. The Engine Input data
5. The Aerodynamic
6. The Aircraft Performance Module

The modules are independent of each other, but data from all of them are combined to calculate the aircraft characteristics and produce the desired results such as the range, the fuel consumption and the time spent at every phase of the flight [17].

5.2.1 Input Data Module

The module contains all the necessary aircraft data. The geometrical characteristics of the airframe are defined in this module. More specifically data such as the area, the aspect ratio, the sweep angle, the taper ratio etc. for the plane's wings, fins and tailplane are required as an input. In addition to, the basic configuration of the aircraft such as the landing gear characteristics and high lift systems are also included in this module. All the information in this module is used by the aerodynamics or the performance modules to produce the aircraft variables such as the lift and drag coefficient [17].

5.2.2 Mission Profile Module

All the data describing the mission that the aircraft is flies are included in this module. The profile of the flight is defined by the inputs in order for the performance module to calculate the range, duration and fuel required for the mission. There are two option that the user can choose in this module either for a fixed amount of fuel to calculate the maximum range of the airplane, or to calculate the necessary fuel for a specific flight.

5.2.3 Atmospheric Module

The function of this module is to provide the others modules with the correct atmospheric operating conditions. The module calculates the ISA temperature and pressure at the exact flight level the plane flies and these are used as input to the performance and aerodynamic modules. The user can choose a typical ISA temperature or input a different temperature to study the influence on the flight characteristics [17].

5.2.4 Engine Data Module

In this module the operating condition for the engine is defined. The user inputs the maximum TET at take-off, climb, cruise, approach and idle, as well as a range which Hermes will uses in order to converge to a solution for the required thrust.

The data for the engine data module with some additional information from the atmospheric module are used to describe the operating condition of the engine in the Turbomatch code [17].

5.2.5 Aerodynamic Module

The aerodynamic profile of the airframe is calculated in this module, in particular the drag coefficient for each surface of the airplane [17].

5.2.6 Aircraft Performance Module

The final module that uses as inputs the results from all the other modules is the performance module. The outputs are presented in the aircraft flight path performance file that Hermes produces and include among others the distance, the duration and the fuel consumption for each segment of the flight. An example of how the aerodynamic and performance modules calculate the required thrust at cruise conditions follows.

The Aerodynamic module is responsible for computing the drag coefficient for the whole airplane. The drag coefficient can be divided into a constant part and a part that depends on the lift coefficient.

$$C_D = C_{D0} + C_{DI} \qquad \textbf{(5-1) Drag Coefficient}$$

Where*:*

C_D = Drag coefficient

C_{D0} = Zero lift drag coefficient

C_{DI} = Lift influenced term

The zero lift drag coefficient is calculated using profile drag of each surface of the aircraft. The expression for the C_{D0} is:

$$\boldsymbol{C_{D0}} = \frac{\sum(\boldsymbol{Cf_c} \times \boldsymbol{\varphi_c} \times \boldsymbol{Q_c} \times \boldsymbol{Swet_C})}{\boldsymbol{S_{Ref}}} \qquad \textbf{(5-2) Zero Lift Coefficient}$$

Where:

Cf_c = Skin friction coefficient

φ_c = Form factor

Q_c = Interference factor

$Swet_c$ = Wetted area

The term that depends on the lift coefficient is calculated using the equation below.

$$C_{DI} = \left[\left(\frac{C_1}{C_2 \times \pi \times A \times R}\right) + C_3 + C_4 + C_{D0}\right] \times C_L^2$$ **(5-3) Lift Influenced Term**

In equation 5-3 the terms C_1 and C_2 relate to the geometrical characteristics of the plane's wings. The term C_3 adjusts the result of any non-optimum wing twist, while the term C_4 accounts for the viscous effects [17].

Having established the method for deriving drag coefficient the lift coefficient calculation follows. The aircraft performance module determines the lift coefficient using the equation 5-4.

$$C_L = \frac{W}{1/2 \times \rho \times v^2 \times S_{Ref}}$$ **(5-4) Lift Coefficient**

In the above equation W stands for the total weight of the aircraft, ρ for the density of the outside air, v for the aircraft velocity and S_{Ref} for the reference area of the airframe. This relationship explains the reason why in cruise as the aircraft consumes fuel and looses weight it requires less thrust for the engines.

The final equation for calculating the thrust in level flight conditions is based on a simple force equilibrium on the aircraft.

Assuming that the airplane flies at a constant speed the thrust is equal to the drag force and the lift produced by the wings is equal to the weight of the aircraft. Hence:

$$\text{Thrust} = \frac{W}{E} \qquad \textbf{(5-5) Thrust Equation}$$

Where:

W = Aircraft weight

E = Aerodynamic efficiency C_L / C_D

Hermes uses similar equations to compute the range and fuel consumption of the airplane not only at cruise conditions but also at take-off, climb and descent.

5.3 Payload Curve

The payload curve includes all the performance information for the aircraft in one diagram. The payload curve is unique for each aircraft and it describes the range for a given payload. It is defined using three separate lines. The first is called maximum payload (A-B), the second maximum take-off weight (B-C) and the third maximum fuel capacity (C-D). The three lines indicate the three different operating conditions for the airplane. In addition, there are also three noteworthy points on the figure below.

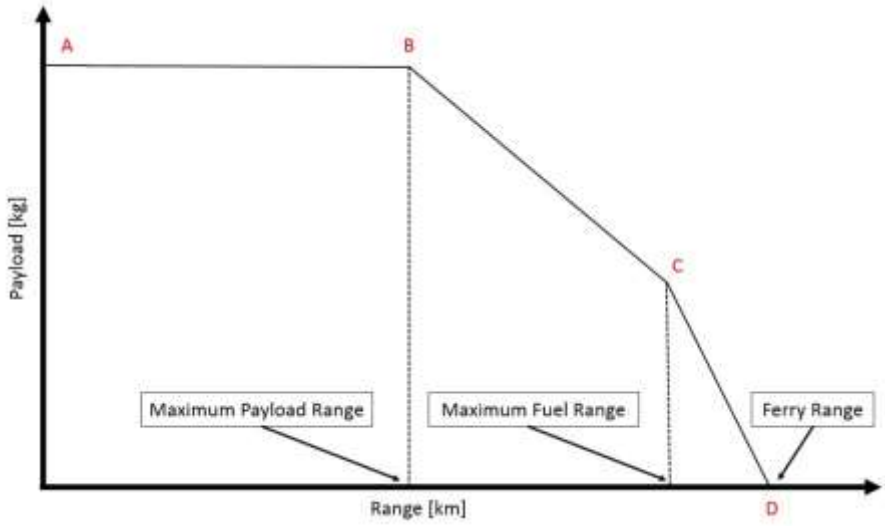

Figure 5-1 Typical Payload Curve [19]

5.3.1 Maximum Payload Range

This point indicates the maximum range that the aircraft can fly, carrying the maximum payload. The maximum payload capacity for an airplane can be defined either by using the maximum volumetric payload, or the maximum zero fuel mass limitation [19].

- Maximum Volumetric Payload

The payload of the aircraft using this method is calculated by adding the mass of the passengers, baggage and cargo using standard densities for all of them.

- Maximum Zero Fuel Mass Limited Payload

The payload in this case is determined by subtracting the maximum zero fuel mass from the aircraft empty operating mass.

5.3.2 Maximum Fuel Range

In this situation all of the airplane's fuel tanks are completely full with fuel. The payload in this case is the remaining weight up to the maximum take-off weight is reached [19].

5.3.3 Ferry Range

The last significant point on the payload curve is the ferry range of the aircraft. This represent the maximum range the aircraft can be flown if only the maximum fuel was carried. This point does not correspond to the maximum take-off weight and therefore the lift to drag coefficient will be different [19].

Beside these points the manufactures also defines the design point of the plane. For civil aircraft the design point usually exists between the maximum payload range and maximum fuel range [19].

5.4 Boeing 777-200ER Model

The aircraft which the author chose to simulate in this thesis project is a Boeing 777-200ER. It is a medium to large range aircraft first flown in 1994. The ER version stands for extended range. In order to simulate the aircraft in Hermes the geometrical characteristics have to be obtained. The author used the drawings provided in the Boeing website [20] to derive variables such as the wings taper ration, aspect ratio and sweep angle.

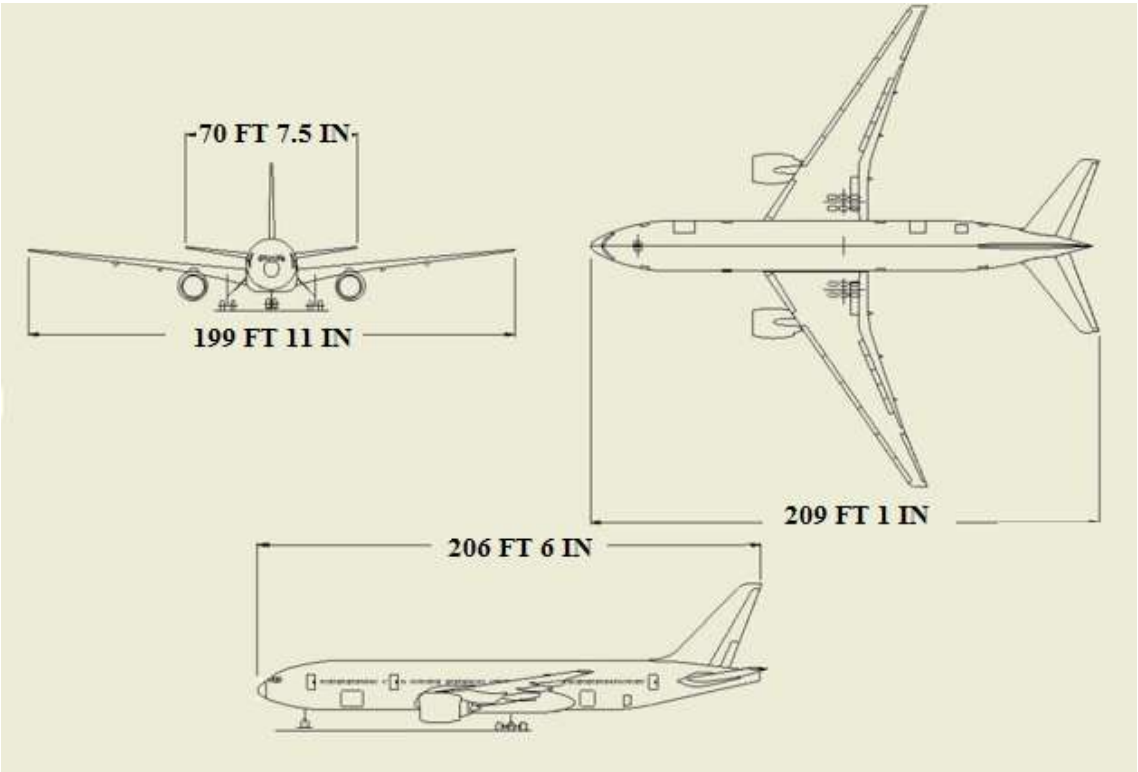

Figure 5-2 Boeing 777-200ER Drawing [20]

In addition to these geometrical specifications, Hermes requires some weight specifications for the aircraft. These are also found through the Boeing website. The table below lists all the weight specifications used in the model.

Boeing 777-200ER with GE90-94B	
Maximum Take-off Weight [Kg]	297550
Maximum Landing Weight [Kg]	213180
Maximum Payload [Kg]	54635
Engine Weight [Kg]	7550
Fuel Capacity [Litres]	171170

Table 5:1 Boeing 777-200ER Weight Specifications [21]

To complete the basic model the author input additional information for the configuration of the aircraft, such as the landing gear characteristics and the number and angle of the flap surfaces. The full model used to simulate the Boeing 777-200ER can be seen in Appendix B.

5.5 Hermes Model Validation

After constructing the Hermes model the validation process began. The payload / range curve created by Hermes was compared with the actual curve from Boeing [22]. In order to produce the payload / range curve for the model in the Hermes the program was used three times with a different set of inputs each time. Hermes was used with a fixed payload and fuel weight and the result of each simulation was the range of the aircraft.

The first simulation targets the ferry range of the aircraft. Therefore the maximum fuel weight of the aircraft was used. It is noteworthy that the maximum tank capacity is given by the manufacturer in terms of volumetric capacity. Using an aviation fuel density of 0.813 kg/L [23] the author convert this volumetric capacity to weight capacity. This is an approximation because density depends on the temperature and the weight of the fuel that the tanks of the aircraft can store depends on the ambient conditions.

The second range simulated with Hermes was the maximum fuel range. In this case the fuel tanks were again completely full and the payload was increased until the maximum take-off weight was achieved.

The last point in the validation process was the maximum payload range. Following the logic of the previous cases the maximum payload weight was inserted in Hermes and the rest of the available weight was used as the fuel weight for the mission.

The results of the simulation compared with the payload / range curve from Boeing are illustrated in the figure 5-3 below.

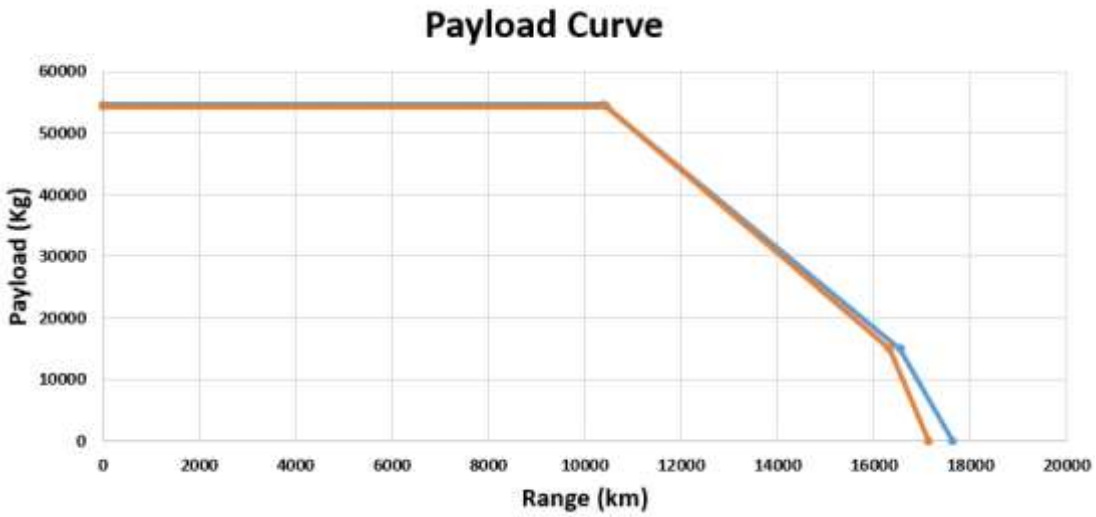

Figure 5-3 Payload/Range Curve

The maximum error occurs in the ferry range calculation and it is 2.8379%. This error is considered to be substantially small, thus making the simulation successful. The trend that arises for the results is noteworthy. The error increases as the range of the aircraft increases. The reason why this occurs could be some discrepancies in the simulation of the engine in the cruise conditions. As the aircraft flies farther the engines operate for a greater amount of time in cruise conditions and therefore the error increases. However, since the maximum error is under 3% no change in the Turbomatch module of the Hermes codes is required.

5.6 Reference Flight

After the successful matching of the payload curve, a reference flight was also simulated using the created code. The flight selected initiate from London Heathrow to New York JFK airport. The flight has a length of 5545.8 Km and accordingly with the British Airways website [24] the flight takes 7.5 hours. The Boeing 777-200ER is capable of much longer flights than that, but since this is a popular route the author decided to use it as the reference flight.

All the necessary values were inputted in the Hermes model and a fixed range for a given payload scenario was chosen. The selected payload for this simulation was equivalent of 368 passengers fling under the medium / long range rules configuration as the [22] suggested. Those passengers and luggage translate to 35000 Kg of payload. The last variable changed was the derate level at take-off. A 15% derate at take-off was selected to study the influence of derating the engine.

After the simulation the important results from Hermes was the thrust level of the engines at take-off conditions as well as the total time for completing the flight. The engines with a 15% derate level were producing a maximum thrust at take-off equal to 357.71 KN per engine. In addition to that the whole flight time was equal to 7.05 hours. A difference between the 7.5 hours for the British Airways website was no observed. There are two main reasons for this difference.

1. The true airspeed that British Airways uses to fly that mission is not known. For the simulation the author selected a typical Mach Number equal to 0.80 for the cruise segment of the flight, but a different value will affect the total time of the mission

2. The time spent for taxing. Both Heathrow and JFK are two of the busiest airports in the world. Usually taxi in and out of those airports takes a lot of time. Hermes has a fixed for taxi in and out. Specifically for international flight start and taxi-out is set to 12 minute, while taxi-in is only 5 minute [17]. The actual time required for those segments of the flight could be longer, resulting in the difference of 25 minutes in the simulation.

The results for the simulation of the reference flight are consider to be acceptable from the author and are going to be used in order to calculate a reference maintenance program for a Boeing 777-200ER using the Cost Estimate

Relationships. In addition to that, results for this simulation are going to be used to perform a stress analysis in the first stage of the high pressure compressor blades in the Chapter 7 of this thesis.

5.7 Chapter Conclusion

This chapter provides an overview of the Hermes program and the simulation of a Boeing 777-200ER. The structure and the operation of the code were explained. In addition, an example of how Hermes calculates the required thrust was presented. Lastly the model used to simulate the aircraft was described and a detailed analysis of the results of the validation process was given.

6 Cost Estimate Relationships

The process of creating a reliable and cost effective maintenance program for an airline engine is a very complicated task. A simplified method that can give an estimation of the engine shop visit intervals and cost associated with maintenance is the usage of cost estimate relationships (CERs) developed for an aircraft engine. The process involves the creation of an engine database and the collection of the specifications related to the maintenance schedule. After normalizing the data, a back step regression process results in the desire CERs. This chapter describes the steps required to calculate those CERs.

6.1 Data Collection

The collection of data and the creation of the engine database is probably the most crucial aspect of this study. Initially the engines which are going to be included in the database must be selected. Since the thesis project focuses on medium to large haul aircraft, the engine chosen are equivalent to the GE90-94B used in the Turbomatch – Hermes models. After establishing the selection of the engine the specifications of each have to be collected. The specifications can be divided into two categories. The first includes all the cost drives. Those are non-cost variables that affect the maintenance schedule of an engine. The second category contains all the information for the shop visit intervals and the cost related to them [25].

6.1.1 Non-Cost Specifications

The maintenance schedule and the money required for each shop visit usually depend on some key engine performance characteristics. More specifically the thrust of an engine, the weight or the ratio between the engine flight hours per engine flight cycles (EFH / EFC) influence the maintenance program. Therefore for the formation of CERs the rated thrust, the engine weight, the EFH / EFC and EGT margin were collected.

6.1.2 Cost Specifications

In addition to the information above, in order to complete the regression process, cost specifications are also essential. For this data the author relied on the literature available on the aircraft-commerce website [26]. The data gathered included information for the non-mature and mature shop visit intervals, the shop visit costs as well as the reserves for the life limited parts.

A full description of the reference for each engine is given in Appendix C.

The Table below lists all the data collected for the engine database. It is also worth mentioning that for the General Electric 90-90B engine, data were available for different EFH / EFC ratios hence this engine appears twice in the table 6-1 below.

					Removal Intervals				SV Cost				LLP Cost
					1st Removal		Mature Removal		1st Removal		Mature Removal		
Engine Name	Thrust (kN)	Weight (kg)	EFH/EFC	EGTM	EFH	EFC	EFH	EFC	Cost ($ mi)	$/EFH	Cost ($ mi)	$/EFH	LLP Reserve $/EFC
RB211-535 E4	178.37	3449	3	30	18000	6000	18000	6000	3	166.67	3.5	194.44	185
Trent 553	235.756	4990	10.75	40	28000	2600	24725	2300	5.7	203.57	6.4	258.85	710
Trent 556	249.1	4990	8.5	40	22100	2600	19550	2300	5.4	244.34	6	306.91	710
Trent 768	298.03	6160	6	45	26400	4400	21000	3500	4.65	176.14	5.5	261.90	374
Trent 772	316.284	6160	7	45	30100	4300	23100	3300	4.75	157.81	5.6	242.42	374
Trent 877	342.519	6078	3.5	50	18550	5300	16450	4700	5.5	296.50	6.5	395.14	524
Trent 892	407.457	6078	7	50	24500	3500	17500	2500	5.1	208.16	6.75	385.71	596
Trent 895	413.684	6078	9	50	22500	2500	20700	2300	5.6	248.89	7	338.16	844
Trent 970	311.375	6246	8.5	50	23000	2700	19000	2200	5	217.39	6.3	331.58	618
Trent 977	338.065	6246	10.75	50	28000	2600	15000	2300	5.25	187.50	6.5	433.33	618
CF6 - 80E1	320.27	5092	5.75	33	18000	3300	16000	2500	2.25	125.00	3.25	203.13	305
GE 90-90B	400.34	7550	3.65	45	13125	3500	19000	5000	5	380.95	6	315.79	445
GE 90-90B	400.34	7550	6	45	17000	2850	14500	2450	6.25	367.65	7	482.76	445
GE 90-94B	416.798	7550	8	45	20450	2550	17500	2150	6.25	305.62	7	400.00	445
GE 90-110B	489.304	8283	10	45	29000	2900	20000	2000	6.75	232.76	7.75	387.50	432
GE 90-115B	511.546	8283	8.5	45	25000	3000	19000	2200	6.25	250.00	7.25	381.58	432
PW 2040 RTC	182.38	3221	3	47.5	14000	4700	14000	4700	2.2	157.14	2.8	200.00	189
PW 4077	351.409	6847	1.5	40	15000	10000	12000	8000	4	266.67	5	416.67	514
PW 4090	404.788	6847	7	50	18500	2800	15550	2350	4.5	243.24	5.75	369.77	661

Table 6:1 Engine Database

6.2 Database Normalization

The reports containing the cost data for the engine database were not published for the same year. The problem when working with historic cost data is that they do not compare with each other. This is because cost data are influenced by inflation. As mentioned in the second chapter, a shop visit cost can be divided into labour cost and cost for replacement parts with each one influencing to a different extent the total cost. Inflation occurs differently for the two categories of costs. To account for this the total inflation has been calculated using the following equation [5].

$$\text{Inflation Factor} = 0.3 \times \frac{ECI}{ECI_{base}} + 0.7 \times \frac{PPI}{PPI_{base}} \qquad \textbf{(6-1) Inflation Factor}$$

Where:

ECI = Employment Cost Index

PPI = Producer Price Index

The baseline for the calculations was chosen as the year 2015. In addition to this, the factors 0.3 for the employment cost index and the 0.7 for the producer price index indicate that the labour cost constitutes 30% of the total cost, while the remaining 70% is the cost for the replacement parts. The data for the PPI and ECI were found in the bureau of labor statistics website [27], and are presented alongside with all the normalized data and the inflation factors used in the Appendix C.

6.3 Regression Process

Regression is the process in which mathematical expressions are developed, reflecting how one or several independent variables influence a dependent one. All the independent variables are not significant. The process of regression involves finding the variables which are significant in determine the results and forming a mathematical expression.

The simplest way of creating cost estimate relationships is by using a linear multiple stepwise backwards regression. In this case the produced expression would have a form such as:

$$\mathrm{Y} = \mathrm{a} + \mathrm{b} \times X_1 + c \times X_2 + d \times X_3 \ldots \qquad \textbf{(6-2) Typical Linear CER}$$

Where Y is the dependent variable and the X_1, X_2, X_3 are the independent variables. However in most cases the cost estimate relationships are not linear. To resolve this, a variation of different functions must be used in order to produce the best combination that creates the smallest error. In this situation a general CER has the following form:

$$\mathrm{Y} = \mathrm{a} + \mathrm{b} \times \ln X_1 + c \times {}^{1}/_{X_2} + d \times X_3^2 \ldots \qquad \textbf{(6-3) Typical Non-Linear CER}$$

The software of choice to perform the regression process was Excel. Excel does not have an automatic tool to perform a stepwise backwards regression process, so it has to be performed manually. Initially, all the non-cost variables are collected and functions of them are created. Unfortunately Excel does not support regression processes for more than 16 independent variables. Using the data analysis tool in Excel a regression step is performed. After the first iteration, the least significant variable is recognized and removed from the database before the whole procedure is repeated.

The criterion in order to remove the independent variables is based on a statistical test that involves the usage of the t-value. The user can calculate the minimum t-value using the degree of freedom and the appropriate t-value charts. The degree of freedom (DOF) can be calculated using the equation below:

$$\mathrm{DOF} = \mathrm{N} - \mathrm{k} - 1 \qquad \textbf{(6-4) Degree of Freedom}$$

With N stands for the number of observations (essentially the number of engines used in the engine database) and k the explanatory variables. The user also has to describe the level of confidence required. For this study the level of confidence is 90%. The t-value chart used for the regression can be seen in the Appendix C.

The critical value is then compared with the actual value for each independent variable. If the expression below is not satisfied the variable is removed from the process. The iterations continue until all the actual t-values are greater than the critical.

$$|\text{Actual t} - \text{value}| \geq |\text{Critical t} - \text{value}| \qquad \textbf{(6-5) T-stat Check}$$

6.3.1 Mature Shop Visit Interval Removal Example

This paragraph explains in more detail the regression process for the formation of the mature shop visit interval removal CER. In order to form the cost estimate relationship, five independent variables and their functions were used. More specifically the thrust, the weight of the engine, the EFH / EFC, the Thrust to Weight ratio (TWR) and the EGT Margin (EGTM) were used. The results for the first step of the regression are illustrated in the table below.

ANOVA

	df	*SS*	*MS*	*F*
Regression	13	47884654.47	3683434.96	26.9764151
Residual	5	682713.9463	136542.7893	
Total	18	48567368.42		

	Coefficients	*Standard Error*	*t Stat*	*P-value*
Intercept	3029550.253	2157793.035	1.404004093	22%
Thrust	56.66079524	1429.088638	0.039648202	97%
Thrust^2	0.110283343	2.101002887	0.05249081	96%
Thrust^3	-0.00013676	0.001317171	-0.10382804	92%
ln(Thrust)	-25885.7838	172275.8414	-0.15025777	89%
Weight	238.3459276	189.2340855	1.259529577	26%
Weight^2	-0.02066571	0.016787057	-1.23105	27%
Weight^3	7.55295E-07	6.43102E-07	1.174454954	29%
ln(Weigth)	-429626.485	357366.3808	-1.20220174	28%
EFH/EFC	-1441.28238	1312.886472	-1.09779665	32%
(EFH/EFC)^2	79.07276644	58.65437722	1.348113648	24%
ln(EFH/EFC)	-404.271359	3136.167583	-0.12890617	90%
EGTM	-80.6117756	66.35082133	-1.2149326	28%
TWR	-63858.2434	546374.0177	-0.11687643	91%

Table 6:2 First Step Regression Results for Mature Shop Visit Interval

For the first iteration the degree of freedom can be calculated, using the equation 6-3.

$$DOF = N - k - 1 \Rightarrow DOF = 19 - 13 - 1 \Rightarrow DOF = 5$$

By referring to a t-value chart for a confidence level of 90% and a DOF = 5 the critical t-value is equal to 2.015. All the resulting t-values for the first iteration are lower than 2.015, therefore the variable with the lowest t-value has to be removed. Subsequently, the thrust^2 was removed and the whole procedure was repeated until the equation 6-4 was satisfied for all the independent variables. The results for the final iteration can be seen in the table below.

ANOVA

	df	*SS*	*MS*	*F*
Regression	6	47182208.09	7863701.348	68.125266
Residual	12	1385160.333	115430.0277	
Total	18	48567368.42		

	Coefficients	*Standard Error*	*t Stat*	*P-value*
Intercept	79453.11442	26076.25064	3.046953165	1%
Thrust	46.00247056	18.47528576	2.489946362	3%
ln(Thrust)	-17208.7998	6368.43781	-2.70220112	2%
(EFH/EFC)^2	15.90910013	5.448771635	2.919759021	1%
ln(EFH/EFC)	-4061.64105	360.4800424	-11.2673118	0%
Weight	4.493623046	1.560095277	2.880351677	1%
Weight^2	-0.0003353	0.000121613	-2.75708414	2%

Table 6:3 Seventh Step Regression Results for Mature Shop Visit Interval

After removing 6 variables, the degree of freedom in this case is equal to 12 and the critical t-value is 1.782, making the condition imposed from equation 6-4 true for all the variables. Therefore the iteration process stops and the final mathematical expression for the cost estimate relationship can be derived.

The method explained in this paragraph was used to create all of the CERs. It is noteworthy at this point that the user should be careful when conducting a regression process in Excel. Apart for the t-value check the user should also use logical thinking when choosing which variable should be removed.

For instance, it is not logical to remove all the thrust related variables from a CER, since the thrust level of an engine influences the maintenance schedule. Even though it would satisfy the t-value check, a CER without any thrust related variable would not perform correctly.

6.4 Final Cost Estimate Relationships

In total five cost estimate relationships were developed, in order to predict the maintenance schedule for an airline engine. These mathematical formulas can predict the shop visit intervals, the shop visit cost and the reserve cost for the LLPs.

Non - Mature Removal Interval CER

$$NMRI = 5901.894 - 63.679 \cdot ET + 0.08587 \cdot ET^2 + 5.3701 \cdot W - 0.00041 \cdot W^2 + 475.0095 \cdot {EFH}/{EFC} - 6091.27 \cdot \ln\left({EFH}/{EFC}\right)$$

Where:

NMRI = Non – Mature Removal Interval [EFC]

ET = Engine Thrust [KN]

W = Engine Weight [Kg]

Mature Removal Interval CER

$$MRI = 79453.114 + 46.002 \cdot ET - 17208.8 \cdot \ln(ET) + 15.909 \cdot \left({EFH}/{EFC}\right) - 4061.64 \cdot \ln\left({EFH}/{EFC}\right) + 4.4936 \cdot W - 0.0003353 \cdot W^2$$

Where:

MRI = Mature Removal Interval [EFC]

ET = Engine Thrust [KN]

W = Engine Weight [Kg]

Non – Mature Shop Visit Cost CER

$$NMSV = -11191.37 - 17.46 \cdot TR + 0.04366 \cdot ET^2 - 3.57 \times 10^{-3} \cdot ET^3 - 0.2335 \cdot W + 1862.97 \cdot \ln(W) + 59.5 \cdot \left(EFH/EFC\right) - 1140.734 \cdot \frac{1}{\left(EFH/EFC\right)} - 569.1316 \cdot \ln\left(EFH/EFC\right) - 0.01108 \cdot NMR$$

Where:

NMSV = Non – Mature Shop Visit Cost [$ / EFH]

ET = Engine Thrust [KN]

W = Engine Weight [Kg]

NMR = Non – Mature Removal [EFH]

Mature Shop Visit Cost CER

$$MSV = 11289.91 + 21.84982 \cdot ET - 0.01264 \cdot ET^2 - 10237 \cdot \log(ET) - 1.5 \times 10^{-5} \cdot W^2 + 3443.99 \cdot \log(W) + 0.6830 \cdot \left(EFH/EFC\right) - 822.039 \cdot \log(MR)$$

Where:

MSV = Mature Shop Visit Cost [$ / EFH]

ET = Engine Thrust [KN]

MR = Mature Removal [EFH]

Life Limited Parts Reserves Cost CER

$$LLPR = 27930.779 + 17.5747 \cdot ET - 13238.889 \cdot \log(ET) + 1.8065 \cdot W - 0.000186 \cdot W^2 + 62.4223 \cdot \left(EFH/EFC\right) - 1324.406 \cdot \log(NMR)$$

Where:

LLPR= Life Limited Parts Reserves Cost [$ / EFC]

ET = Engine Thrust [KN]

NMR = Non – Mature Removal [EFH]

It is obvious that all the CERs are influenced by the trust level and the weight of the engine as well as the ratio between flight hours and flight cycles. This result is reasonable since the thrust level of an engine reflects the operating conditions and therefore has an effect on the maintenance schedule. Moreover the weight of the engine is an indication of its size and lastly the EFH / EFC accounts for how severe the operation of the engine is. Consequently, all the existing terms in the CERs constitute cost-drive variables.

After the formation of all the necessary cost estimate relationships the following step is the evaluation of them. The next chapter describes the validation process for the CERs.

6.5 Cost Estimate Relationship Validation

The validation of the cost estimate relationships was conducted using two statistical tests. The first on involves the adjusted R^2 and the second the F-stat value.

6.5.1 Adjusted R^2

The adjusted coefficient of determination known and as R^2, is a modified version of the coefficient of determination. The adjustment accounts the usage of multiple observations in the regression model. The regular R^2 is a measurement of the errors for each observation compared with the mean value. The mathematical expression of R^2 can be seen in the equation below [28]:

$$R^2 = \frac{\sum(\acute{y} - \bar{y})^2}{\sum(y_i - \bar{y})^2}$$ **(6-6) Coefficient of Determination**

Where:

y_i = Observed value

$\bar{y}_i$ = Mean value

$\hat{y}_i$ = Fitted value

Using the value of R^2 the adjusted R^2 can be also defined using the equation 6-6 below:

$$R^2_{adj} = 1 - (1 - R^2) \times \frac{n-1}{n-p-1}$$ **(6-7) Adjusted Coefficient of Determination**

Where:

n = Number of observations (essentially number of engines used in the engine database)

p = Number of independent variables

6.5.2 F-value Test

In order to check that the data used in the regression process were correctly fitted to the final mathematical expression, a statistical test called F-value test was conducted for each of the cost estimate relationships. This test, actually checks the hypothesis that the independent variables coefficient are equal to zero. This is kwon as the nun hypothesis. The F-value test can be easily conducted since the value of F is given in the results spreadsheet of the regression.

The F-value test is similar to the t-value test mentioned above, with the difference that it applies to all the variables simultaneously.

To perform the test the user has to compare the F-value in the results with a critical value derived from the F distribution chart presented in the Appendix C. In order for the test to be successful the actual value of F should be greater than the critical. It is noteworthy that to retrieve the critical value for the F distribution chart two more values are required. These numerator degree of freedom and the denominator degree of freedom [29].

$$Numerator\ degree\ of\ freedom = P - 1$$ **(6-8) NDF**

$$Denominator\ degree\ of\ freedom = odservations - P$$ **(6-9) DDF**

Where:

P = Independent variable + 1

The table below illustrates the results of the aforementioned tests to the five cost estimate relationships develop for this project.

Cost Estimation Relationships Validation Results				
CER	**Adjusted R^2**	**DOF**	**F-value**	**Critical F-value**
NMRI	0.9344	11	41.354	3.09
MRI	0.9573	12	68.125	3
NMSV	0.7940	9	8.71	3.02
MSV	0.8384	11	14.349	3.09
LLPR	0.8144	12	14.166	3

Table 6:4 CER Validation Results

The F-value test for all the created cost estimate relationships was successful, indicating that all the independent variables used to describe the CERs are significant. Moreover the adjusted R^2 values for the Non – Mature Removal Interval and the Mature Removal Interval CERs are above 0.9 which makes the error in those relationship significantly small. The remaining values of the adjusted R^2 vary from 0.7940 to 0.8384. The results are acceptable according to the author, because for this thesis project the prediction of the engine shop visits are considered to be more important than the shop visit cost prediction. The number of cycles the engine experiences until an overhaul are going to be used in the fracture mechanics analysis in the chapter 8.

6.6 Reference Flight

In the Chapter 5.6 a reference flight was simulated. A flight for London Heathrow to New York JFK was used as a reference Boeing 777-200ER flight. The results from that simulation are going to be used to create a reference maintenance program for the GE90-94B that the Boeing 777-200ER uses.

The aforementioned Cost Estimate Relationships require the maximum thrust level of the engine, the weight of each engine and the ratio of flight hour per flight cycles can the aircraft experiences. The weight of the GE90-94B is 7550 Kg [16].

For the engine thrust level and the EFH / EFC the results for the Hermes simulation are going to be used. More specifically, with a take-off derate level of 15% the maximum thrust was 357.71 KN per engine and the flight had a duration of 7.05 hours. Taking into account the assumption that each flight represents one full engine cycle, the resulting EFH / EFC is equal to 7.05. By using those results in the developed CERs an estimation of the basic maintenance program can be derived. In addition to that, a comparison between the reference maintenance program for the GE90-94B and the literature data is presented in the table below.

Reference Maintenance against Literature Maintenance		
Variable	**Literature**	**Reference**
EFH / EFC	8	7.05
Thrust Level [kN]	416.798	357.71
NMRI [EFH]	20450	19499.72
MRI [EFH]	17500	16905.68
NMSV [$ / EFH]	325.45	315.72
MSV [$ / EFH]	400	396.64
LLPR [$ / EFC]	445	336.32

Table 6:5 Reference Flight against Literature

In order to understand the results two things must be taken into consideration. First the engine thrust level is reduced, making the operation of the engine less severe. This has an impact in the cost of each shop visit. The deterioration occurring in the core components of the engine is less severe due to the lower temperature which exist inside the engine. Fewer parts may require replacement at each shop visit lowering the total shop visit cost. In addition to that the engine's EFH / EFC ratio is lower. This influences the interval for the shop visits. With a lower EFH / EFC ratio the engine experiences a greater amount of cycles per day and therefore the hours required pes shop visit interval are fewer.

To conclude the reference maintenance program suggests that the engine will be removed for an overhaul more often that the literature data, but less money will be needed to replace all the worn parts, reducing the total cost per shop visit.

6.7 Chapter Conclusion

This chapter give an overview in the development of the cost estimate relationships. The steps required in order to perform a successful regression process were fully explained. Moreover, an example of the procedure followed to create the CERs was described. This chapter also included a description of the five cost estimate relationships developed as part of this thesis project. Finally, the evaluation method and the results from the validation process were presented.

7 High Pressure Compressor Blade Design

One of the objective of this project is to identify the influence of a typical maintenance program on the non – life limited parts and more specifically the blades of the high pressure compressor. In order to perform an analysis of the lifing of these components, their basic design characteristics have first to be determined. Therefore a preliminary compressor design is necessary to estimate the basic shape of the compressor blades.

7.1 Preliminary Compressor Design

A preliminary compressor design enables the designer to initiate the design process for an actual compressor. The annulus area in the inlet and the outlet is determined. In addition, the main task is to calculate the fluid properties at various meridional planes. The properties which are most critical, are the fluid relative and absolute speed magnitudes and angles. The following diagram illustrates the velocity triangles in a typical compressor stage.

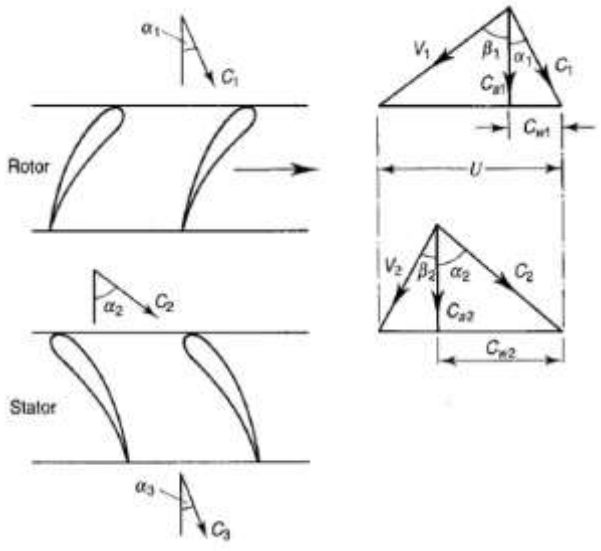

Figure 7-1 Typical Velocity Triangles [30]

In the illustration above the absolute velocities use the symbolisms C, while the relative velocities are denoted V.

In that respect the absolute velocity at the stage inlet is the C_1 and the angle at which the fluid enters the stage is α_1. The rotational speed of the blades is symbolized with U. If the rotational speed and the inlet speed are combined the result is the relative inlet velocity V_1 and the relative inlet angle β_1. At the outlet of the blade row the flow has an absolute velocity equal to C_2 at an angle α_2 while the relative outlet velocity is equal to V_2 with an angle equal to β_2. Lastly this stage is designed by a repeating stage concept were the outlet velocity from the stator matches the next stage inlet velocity. This concept is really helpful when designing a multi – stage compressor [30].

7.1.1 Preliminary Design Assumptions

In order to perform the preliminary design of the high pressure compressor for the General Electric 90-94B engine, some major assumptions were made. Since data related to the construction of the compressor were not available, the author had to assume a number of the inputs to the design process.

Axial Velocity

The first assumption involves the inlet axial velocity to the HPC. A high axial velocity is required in order to sustain a high mass flow rate thought the compressor. At the same time the axial Mach number in the inlet of the HPC must be restricted under the subsonic. Typical values for axial velocities at the inlet of the HPC for modern aircraft engines are between 130 m/s and 250 m/s. The chosen value for the preliminary design was 205 m/s which results in a Mach number equal to 0.612015 in the inlet of the compressor. In addition, the axial velocity is consider to be the same at the inlet to each stage.

Design Point

The second assumption made by the author concerned the design point for the compressor. The compressor of a large turbofan engine like the GE90-94B will work most of the time at cruise conditions. Consequently, for the design point the cruise point was selected. In addition, for the input gas properties to the HPC, the results for the cruise simulation of Turbomatch were used.

IGVs Angle

Since the compressor was design at cruise conditions, the rotational speed of the spool was lower than the take-off rotational speed. In order to avoid surge in the front stages for the compressor, the GE90 incorporates variable inlet guide valves (IGVs), as well as variable stator vanes in the first four stages. The angle of the IGVs was unknown to the author. Therefore a typical value of 16^{o} degrees was selected for the IGV angle in the cruise conditions.

Blade Shape

A typical assumption for a preliminary compressor design is to use the free vortex theory in order to obtain the velocity triangles at the tip and the hub of the blade. Unfortunately, this theory does not satisfy radial equilibrium for the specific compressor design. In addition the objective of the thesis is to study the influence of the maintenance program to the blades of the HPC. Therefore a detailed design for the compressor is not necessary considering that the author decided to calculate the blade shape only in the mean meridional plane and extent the blade from the hub to the tip of the annulus. This will result in the introduction of some error to the calculation of the blade stresses. More specifically the stresses resulting from the bending moments in the axial and tangential directions will be affected, but since the biggest stress is the centrifugal stress the error is consider acceptable by the author.

Annulus Shape

Another assumption concerned the annulus shape of the high pressure compressor of the GE90-94B. Typical compressor have a rising, constant or falling mean line. The compressor of the General Electric GE90-94B can be represented by a rising mean line for the first four stages and a constant mean line for the remaining stages. This unique construction of the compressor forced the author to use a ‘Θ’ parameter to describe the mean line rising angle. The values of the ‘Θ’ parameter used in the design can be seen in the table below.

'Θ' Parameter									
Stage	1	2	3	4	5	6	7	8	9
Θ	5	3.3	2	1.5	1	0	0	0	0

Table 7:1 'Θ' Parameter

Blockage Factor

In the above it is stated that the axial velocity is consider to be constant between the stages of the compressor. In reality as the air progresses into the compressor it is subjected to an adverse pressure gradient. This results in the growth of the boundary layers. To account for this phenomenon, a blocking factor was introduced into the design. The factor is applied to the annulus area calculations increasing the required area to account for the reduced work that each stage can achieve [31].

$$K_B = \frac{A_{ANN}(Uniform\ C_a)}{A_{ANN}(Non-Uniform\ C_a)}$$ **(7-1) Blockage Factor**

The values used in the design of the HPC for each stage are illustrated in the table below.

Blockage Factor									
Stage	1	2	3	4	5	6	7	8	9
K_B	0.99	0.95	0.92	0.9	0.88	0.88	0.88	0.88	0.88

Table 7:2 Blocking Factor [31]

Hub / Tip Diameter

Another assumption the author had to make was the ratio of the hub to tip diameter in the inlet of the compressor. The value selected for the ratio, known also as μ, was 0.508. In addition, hub / tip diameter ratios over 0.93 are not acceptable due to the increased tip leakage losses in comparison to the overall height of the blade [31].

Gas Properties

Lastly the gas constant (R) and the heat capacity ratio (γ), which is the ratio of the heat capacity at constant pressure to heat capacity at constant volume, are consider constant thoughtout the compressor design.

7.1.2 Annulus Design

First Stage Inlet Annulus Area

The table 7-1 below describes the inlet conditions to the HPC. The values of pressure, temperature and mass flow are the results from the Turbomatch simulation of the cruise conditions.

HPC Design Point Conditions		
Variable	**Inlet**	**Outlet**
Pressure [KPa]	67.5615	1511.83
Temperature [K]	300.97	772.63
Mass Flow [Kg/s]	64.595	
Axial Velocity [m/s]	205	
Rotational Speed [rpm]	9800	
Inlet Hub / Tip Ratio	0.508	

Table 7:3 HPC Design Point Conditions

In order to calculate the necessary annulus area at the inlet of the first stage, the flow function [Q] is used. Using the isentropic flow charts from [31] the ratio between the absolute velocity and the total temperature at the inlet, can be related to the flow function. For the following calculations the symbols defined in figure 7-1 are used.

$$\frac{C_1}{\sqrt{T_1}} = \frac{{Ca_1}/{\cos(\alpha_1)}}{\sqrt{T_1}}$$

(7-2) V_{axial} upon root T

Using the isentropic flow charts the value of the flow function Q can be derived. This function can be used to calculate the required inlet annulus area, using the equation below.

$$Q_1 = \frac{W_1 \times \sqrt{T_1}}{K_B \times A_1 \times P_1} \Rightarrow A_1 = \frac{W_1 \times \sqrt{T_1}}{Q_1 \times K_B \times P_1}$$ **(7-3) Q Function**

Since the ratio between the hub and tip diameters for the inlet is know the D_t and D_h can be calculated thus:

$$D_{t1} = \sqrt{\frac{4 \times A_1}{\pi \times (1 - \mu_1)^2}}$$ **(7-4) Tip Diameter**

$$D_{h1} = D_{t1} \times \mu_1$$ **(7-5) Hub Diameter**

Since the ratio of hub to tip diameter is unknown for the outlet of the compressor the outlet annulus area cannot be defined yet. A stage to stage design process on the other hand is feasible, since the assumption of the 'θ' parameter can link the diameters for the hub between each stage.

First Stage Outlet Annulus Area

The outlet total temperatures for the compressor are 772.63K and 300.97K respectively, resulting in a temperature rise of 471.66K. Usually this temperature rise is distributed equally between the stages of the compressor. This could affect the De Haller number of the first stages. To avoid this situation the author distributed the temperature rise unevenly between the compressor stages. The derivation of the De Haller number and its impact on the compressor design will be analyzed in the next paragraph of the thesis. The table below illustrates the temperature rise per stage used in the preliminary design.

Temperature Rise									
Stage	1	2	3	4	5	6	7	8	9
Label	49	52	52	53.11	53.11	53.11	53.11	53.11	53.11

Table 7:4 Temperature Rise per Stage

By consulting the table above the total temperature at the outlet of the first stage can be calculated.

$$T_2 = T_1 + \Delta T_1$$ **(7-6) 1st Stage Outlet Temperature**

In order to calculate the first stage outlet pressure a stage polytropic efficiency has to be assumed. After applying the polytropic efficiency at all of the compressor stages, the compressor outlet total pressure must agree with the result from Turbomatch. In order to achieve this an iterative process was followed in Excel. The final stage polytropic efficiency selected was given by: n_{pol} = 0.92741. At this point, the stage pressure ratio can be defined by equation 7-7.

$$PR_{stage} = \left[n_{pol} \times \frac{\Delta T_{stage}}{T_1} + 1\right]^{\left(\gamma/\gamma-1\right)}$$ **(7-7) Stage Pressure Ratio**

By following exactly the same process as before the first stage outlet annulus area can be derived. It is noteworthy that the repeating stage concept is used to define the outlet absolute velocity.

An Excel spreadsheet was created in order to perform the calculations described above for all of the nine compressor stages. Each time the absolute velocity and the total temperature of the stage were used to derive from the isentropic flow chart the flow function. Using the value of Q, the blockage factor and the pressure ratio for each stage, the annulus area can be estimated. The table below illustrates the dimensions of the tip and hub for each stage in addition to the resulting annulus area.

High Pressure Compressor Annulus Design										
Stage	1	2	3	4	5	6	7	8	9	10
Ann [m^2]	0.4759	0.3411	0.2508	0.1892	0.1528	0.1204	0.0971	0.0797	0.0665	0.0562
D_t [m]	0.9081	0.8615	0.8332	0.8123	0.8050	0.7942	0.7830	0.7688	0.7577	0.7491
D_h [m]	0.4676	0.5548	0.6124	0.6473	0.6734	0.6909	0.6996	0.6996	0.6996	0.6996

Table 7:5 HPC Annulus Design

The author consider it useful to have a visual comparison between the designed high pressure compressor with the actual compressor used in the GE90-94B. To achieve this comparison figure 4-1 was used to derive a sketch of the actual shape of the HPC. The figure depicts the actual compressor shape against the one that resulted from the preliminary compressor design process.

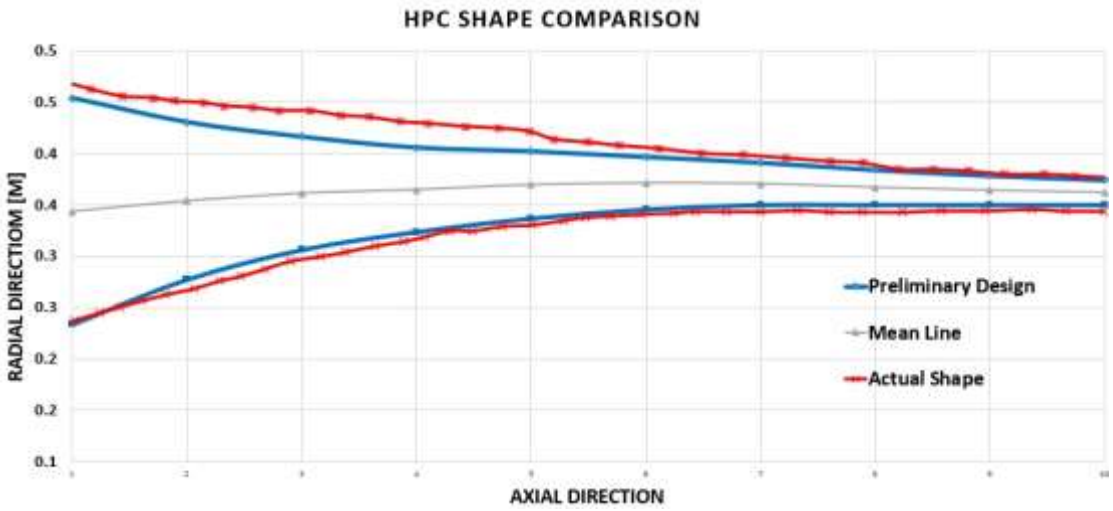

Figure 7-2 HPC Shape Comparison

7.1.3 Velocity Triangles

The aim of the preliminary first stage design is to estimate the shape of the compressor blades. In order to achieve this, the velocity triangles in the mean span have to be calculated. The following methodology will describe the calculations needed for the first stage velocity triangles. The study is focused on the first stage of the high pressure compressor. The main reason for this is that this stage experiences the higher stress level due to centrifugal forces.

The rotational speed of the compressor spool can be easily translated to a mean blade speed at the inlet of the stage using the following equation.

$$U_{1m} = \frac{2 \times \pi \times N}{60}$$ **(7-8) Stage Inlet Blade Speed**

Where:

N = rotational speed of the compressor [rpm]

The outlet angle for the IGVs and the axial flow velocity at the inlet of the stage are known. Therefore the velocity triangle in the inlet of the first stage can be derived.

To connect the triangle for the inlet to the outlet firstly a total energy estimate, per unit mass flow, at equilibrium has to be performed. In addition, the work produced per unit mass flow has to be linked with the swirl velocities in the inlet and outlet of the stage using the conservation of momentum thought the rotor. The resulting equation is known as the Euler's Turbine Equation [31] and it is one of the most useful relationships in turbomachinery. The following formula is the Euler's Turbine Equation:

$$\Delta H = U_2 \times C_{w2} - U_1 \times C_{w1} \qquad \textbf{(7-9) Euler's Equation}$$

The difference in enthalpy for the rotor inlet to the outlet can be expressed using the following equation.

$$\Delta H = C_p \times \Delta T_{stage} \qquad \textbf{(7-10) Enthalpy Difference}$$

Therefore using the temperature rise per stage as described in the table 7-4, the swirl velocity at the outlet of each stage can be calculated. According to the [31] the outlet absolute velocity must correspond both with the stage work (swirl velocity C_{w2}) and with the mass continuity within the stage. Since the swirl velocity at the outlet is predetermined by the Euler's equation, the outlet axial velocity is initial guess and by using the mass flow conservation the outlet absolute flow angle (α_2) is calculated. This is an iterative process and it was performed in Excel.

After the iterations the axial velocity at the outlet in addition to the absolute velocity and flow angle can be determine, completing the velocity triangle at the outlet of the blade row. The same methodology was used for all the stages of the compressor.

Feasibility of the Design

The author used the guideline presentment in [31] to check if the resulting velocity triangles are feasible. More specifically the compressor loading chart was used. To identify the position of each stage at the loading chart three values must we calculated first.

1. Degree of Reaction

   The last variable checked was the degree of reaction. This is a ratio between the increase in total pressure in the rotor and the increase in total pressure over the whole stage. A degree of reaction equal to 50% represents a symmetrical velocity triangle where the rotor and stator contributes the same to the total pressure increase in the stage. It is also noteworthy that lower degrees of reaction are related to higher swirl velocities in the rotor and therefore higher aerodynamic losses [30].

2. Stage Flow Coefficient

   The stage flow coefficient (Φ) is used to quantify the mass flow that passes though the stage [31]. It can be derived using the relationship 7-11

$$\Phi = \frac{Axial\ Velocity}{Rotor\ Speed} \Longrightarrow \Phi = \frac{C_a}{U} \qquad \textbf{(7-11) Flow Coefficient}$$

3. Stage Loading Coefficient

   The stage loading (Ψ) is an indication of the work required to achieve the desired stage pressure ratio [31]. The following equation represents Ψ.

$$\Psi = \frac{Stage\ Work}{Rotor\ Speed^2} \Longrightarrow \Psi = \frac{C_p \times \Delta T_{stage}}{U^2} \qquad \textbf{(7-12) Stage Loading}$$

4. De Haller Number

A measure of the diffusion that takes place in the stage is the De Haller Number. It can be derived using the static pressure rise coefficient presented in the equation below.

$$\frac{\Delta p}{D} = \frac{\Delta p}{{}^{1}/_{2} \times \rho \times V^{2}} \Longrightarrow$$

(7-13) Pressure Rise Coefficient

$$\frac{\Delta p}{{}^{1}/_{2} \times \rho \times V^{2}} = 1 - \left(\frac{V_2}{V_1}\right)^{2}$$

Since the pressure gradient though the compressor stage is positive, a high diffusion could easily lead to excessive losses. To avoid this, a limit of 0.69 was selected by the author.

The De Haller number was calculated using the expression below.

$$\mathrm{dH} = \frac{V_2}{V_1}$$

(7-14) De Haller Number

The diagram illustrated in the figure 7-3 below, represents typical values of the aforementioned parameters for a core compressor. In addition, the design point for the first stage of the compressor is also visible in the diagram.

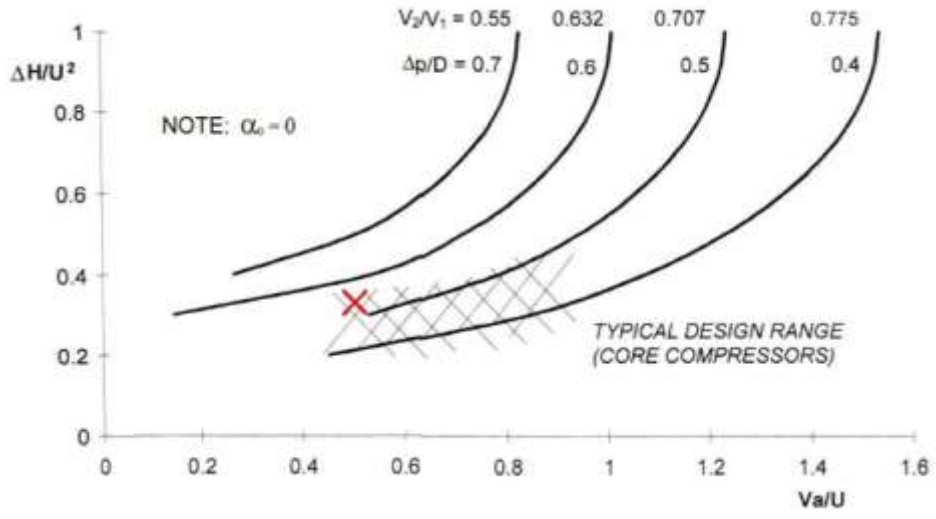

Figure 7-3 Compressor Loading Chart

The final design satisfies the limitations on the De Haller number, Stage Loading and Stage Flow Coefficient. Consequently, the final design parameters for the first stage of the compressor are presented in the table below.

Parameter	Value	Parameter	Value
Inlet absolute angle	16°	Inlet absolute velocity	213.26 m/s
Inlet relative angle	55.13°	Inlet relative velocity	358.58 m/s
Outlet absolute angle	45.82°	Outlet absolute velocity	275.26 m/s
Outlet relative angle	39.96°	Outlet relative velocity	250.25 m/s

Table 7:6 Final First Stage Flow Angles and Velocities

The velocity triangle at the mean meridional plane can be seen in the figure 7-4 below.

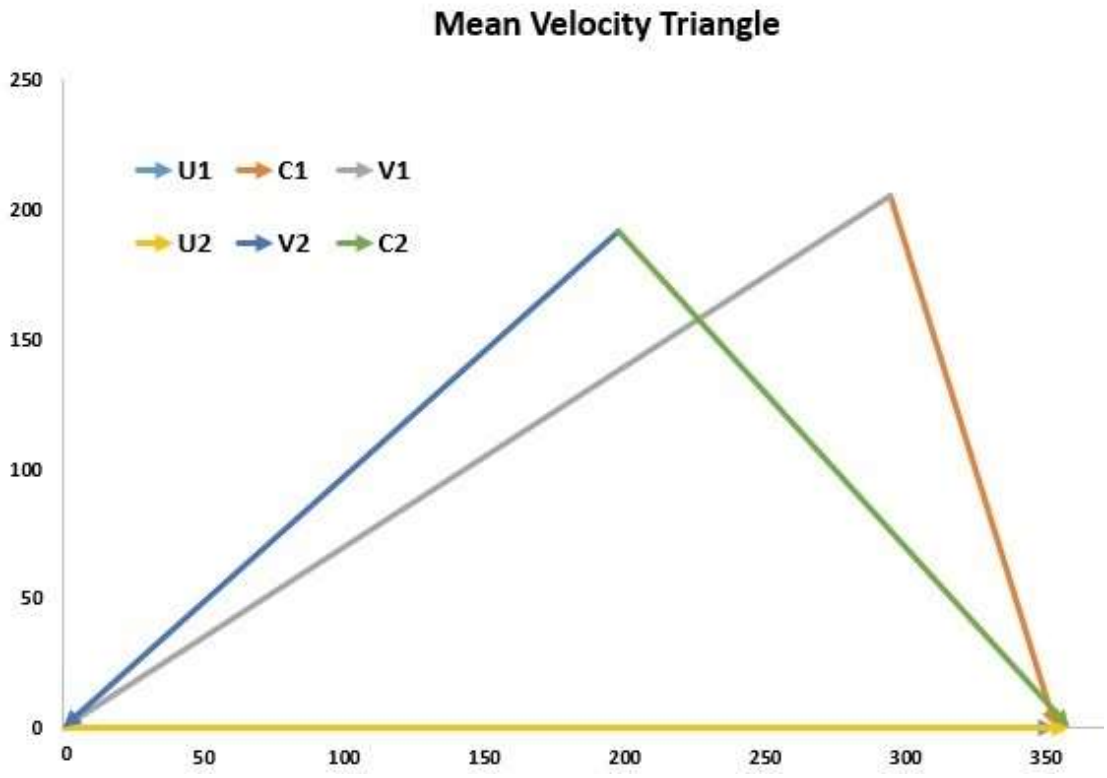

Figure 7-4 Mean Velocity Triangle

The velocities and angles calculated above represent the movement of the flow that will result in the desired pressure rise per stage for the compressor.

The next step is to translate these flow angles into blade angles from which the actual shape of the blade can be estimated. The compressor blades have to turn the flow and perform a diffusion at the same time. Due to the losses taking place over the surfaces of the blade, air does not enters and exit the compressor blades at the blade metal angles. This phenomenon has to be taken into account when choosing the blade metal angles. In addition, the blade angles have to be selected in such a way that will allow the operation of the compressor over a wide range of operating conditions. With those considerations in mind the next paragraph includes the calculation of the blade metal angles.

7.2 Blading Design

The following diagram for Saravanamutto's Gas Turbine Theory [30] will be used to define the necessary angles.

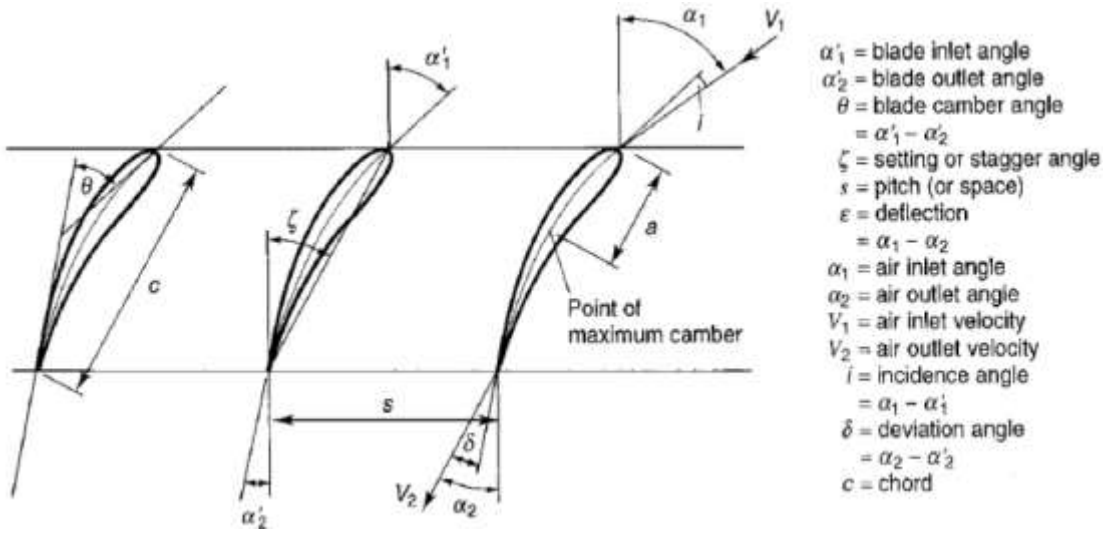

Figure 7-5 Angles Notation [30]

The desired angles for the following analysis are the incidence angle (i) and the deviation angle (δ). Both angles quantify the difference between the relative angle and the blade angle at the inlet and outlet of the rotor blade. The selection of incidence angle is crucial since the value of this angle is related to the losses over the blade. Incidence angle with a value higher than $\pm 10^o$ must be avoided [30].

In order to calculate these angles an iterative process has to be performed. The process begins by defining blade pitch to chord ratio using the airfoil lift coefficient. The airfoil lift coefficient is expressed by equation 7-15.

$$Cl_{v2} = \frac{Lift}{0.5 \times \rho \times C \times (V_2)^2}$$ **(7-15) Airfoil Lift Coefficient**

Experiments have shown that the value of the airfoil lift coefficient should not exceed 1. Using the maximum allowed value for the airfoil lift coefficient and by expressing it with another mathematical formula, the desired pitch to chord ratio can be derived.

$$Cl_{v2} = 2 \times \left(\frac{S}{C}\right) \times (\tan(\alpha_1) - \tan(\alpha_2)) \times \frac{(\cos(\alpha_2))^2}{\cos(\alpha_m)}$$ **(7-16) Zweiffel ALC**

Where:

$$a_m = \frac{\tan(\alpha_1) - \tan(\alpha_2)}{2}$$ **(7-17) Zweiffel mean Angle**

This method is called Zweiffel's method. An additional method to determine the pitch to chord ratio is known as Howell's method and it was used to verify the results.

Having calculate the S /C ratio, two initial guesses have to be made. The first is for the blade camber angle and the second for the difference between the blade angles at the inlet and outlet known as stagger angle (ξ). For the initial guesses the following expressions can be used.

$$\theta = 1.2 \times (\alpha_1 - \alpha_2)$$ **(7-18) Blade Camber Angle Initial**

$$\xi = 0.5 \times (\alpha_1 + \alpha_2)$$ **(7-19) Blade Stagger Angle Initial**

The incidence and deviation angles can be calculated using the formulae below.

$$i = K - 0.19 \times \theta \times {}^{S}/_{C}$$ **(7-20) Blade Incidence Angle**

With:

K = 6.5 for rotors and 3.5 for stators [32]

$$\delta = m \times \theta \times \sqrt{s/c}$$ **(7-21) Blade Deviation Angle**

The value of factor m depends on the stagger angle ξ and experiments have shown that the relationship between them can be expressed with equation 7-22.

$$m = 0.20996 - 0.00108 \times \xi + 0.0003 \times \xi^2$$ **(7-22) m Factor**

After the initial iteration the equations used to describe the chamber and the stagger angle are presented below.

$$\theta = a_1' - a_2'$$ **(7-23) Blade Camber Angle Final**

$$\xi = a_1' - \theta/2$$ **(7-24) Blade Stagger Angle Final**

Four iterations were needed to achieve constant value for the incidence and deviation angle. In addition, the number of blades was also calculated. Using the pitch to chord ratio and an assumed height to chord ratio. Typical values for the height to chord ratio for compressor blades are in the range between 3 and 3.5 [30]. Moreover the blade height can be easily derived by the annulus design process. Finally, by combining all the aforementioned equations the number of blades as well as the metal blade angles for the first row of blades and IGVs are presented in the table 7-7.

Final Blading Design		
Variable	**Rotor Blade**	**IGV Blade**
Blade Inlet angle	52.06	0
Blade Outlet angle	34.01	13.11
Blade Stagger angle	-43.03	6.562
Incidence angle	3.07	0
Deviation angle	5.94	2.894
Number of Blade	37	43

Table 7:7 Final Blading Design

7.3 Blade Geometry

Having calculated the metal angles for the blade, the geometry had to be imported into a drawing program. The software used was the BladeGen, which is a program developed by ANSYS to easily extract blade geometry. The shape of the first stage of rotor blades was imported and a 3D IGES file was created. This file was then used in AutoCAD Invertor to create a 3D basic model of the blade. The geometry of this blade was simplified as mentioned above. The airfoil in the mean span extended for tip to hub was used to create the final blade geometry. This approach will result in a small error, but this thesis is not focused on a detailed design of the high pressure compressor. The objective is to obtain the stresses imposed on the blades in order to predict the life of the blade and a geometry such as that used by the author is sufficient. The resulting blade geometry in Inventor can be seen in the figure 7-6.

Figure 7-6 Blade Geometry

Apart from a visualization of the final blade geometry, Inventor can provide additional information. Specifically the mass of the blade and the cross sectional area can be calculated using Inventor. Both these measurements are essential to the process of deriving the blade stresses.

Moreover due to the simplification in the shape of the blade, there is no need to divide the blade into sections to perform the blade stresses calculations. Therefore in the next paragraph the blade stresses will be calculated using the blade as one element.

7.4 Blade Stresses Calculation

7.4.1 Sources of Blade Load

There are five main causes of blade loading. The most obvious and significant load results from the rotational speed of the shaft. As the blades rotate a force is exerted upon them called centrifugal force. Apart from that, there are two types of bending moments. The first one is caused by changes in the momentum and pressure, while the second is an indirect result of the centrifugal force. More specifically the first type of bending moment is the result of the forces produced by the fluid as the momentum and pressure change across the blade. Lastly there are shear loads created by the untwisting of the blade due to the pressure change across the blade span and complex loads due to the temperature gradients in the blade. The stress analysis in this chapter will concentrate in the centrifugal loads and the bending moments due to the momentum and pressure changes [33].

7.4.2 Centrifugal Stress

In order to calculate the stress resulting from the centrifugal loads the following expression was used.

$$CF = W \times r_{cg} \times \omega^2 \qquad \textbf{(7-25) Centrifugal Load}$$

Where:

W = The mass of the blade [Kg]

r_{cg} = The distance for the center of gravity of the blade to the center of the rotating shaft

ω = Rotation speed [rad / s]

7.4.3 Gas Bending Moment

The gas bending moment consists of two components. The bending moment due to the pressure change, acting in the axial direction and the bending moment due to momentum change acting in both axial and tangential diractions. The expression used to derive the first component can be seen below.

$$B.M.(pressure) = Ann \times {}^{\Delta p}/_{N} \times r_{mom} \qquad \textbf{(7-26) Pressure BM}$$

Where:

Ann = Annulus inlet area [m^2]

Δp = Change in static pressure across the blade [Pa]

N = Number of blades

r_{mom} = The radius from the center of gravity to the base of the blade [m]

The second component of the gas bending moments can be quantified using the expression below.

$$B.M.(momentum) = \frac{\dot{m}}{N} \times \Delta V \times r_{mom} \qquad \textbf{(7-27) Velocity BM}$$

Where:

$\dot{m}$ = Mass Flow [kg / s]

ΔV = Change in velocity [m / s]

The equation above is used to calculate both the bending moment in the axial and tangential direction. The difference is the appropriate ΔV used in the calculations.

The calculated bending moments can then be converted into stress on the blade using engineers bending theory [33].

$$\frac{M}{I} = \frac{\sigma}{y}$$ **(7-28) Engineer Bending Theory**

Where:

M = Bending Moment

I = Second moment of area

σ = Direct stress

y = Distance from neutral axis

7.4.4 Operating Conditions

For the calculations above the operating conditions of the HPC are essential. In order to calculate the stresses and predict the life expectancy of the blade the reference flight was used. The simulated flight in the chapter five was from London Heathrow to New York JFK airport. The results from the Hermes simulation were used to determine the operating conditions for the high pressure compressor of the GE90-94B. More specifically the total pressure and temperature at the inlet and outlet of the HPC, as well as the mass flow though the core of the engine are easily derivable from the Hermes results.

The author had to select the operating conditions at which the calculation will be performed. The worst case scenario for the blade stresses was selected, which was the take-off operating condition. At this point the rotational speed of the high pressure spool is at a maximum value. In addition the bending moments are maximum at take-off due to the high value of mass flow though the compressor. The following table 7-8 contains all the operating conditions for the HPC.

High Pressure Compressor Operating Conditions	
P_{in} [KPa]	164.14
P_{out} [KPa]	3465.49
T_{in} [K]	337.69
T_{out} [K]	842.93
$\dot{m}$ [Kg/s]	142.71

Table 7:8 High Pressure Compressor Operating Conditions

In addition to the operating conditions of the HPC, the velocity changes in the first stage is required to calculate the blade stresses. These were derived using the same process described in the chapter 7.2.3. It is worth mentioning that at take-off conditions the IGVs angle used in the velocity triangle calculation was zero so the flow was consider to enter the compressor axially. The following table presents the changes in the axial and tangential velocity across the rotor blade.

HPC First Stage Velocity Changes	
Inlet Axial [m/s]	217.15
Outlet Axial [m/s]	174.78
Inlet Tangential [m/s]	363.942
Outlet Tangential [m/s]	234.517

Table 7:9 HPC First Stage Velocity Changes

The resulting bending moments are:

$$M_{Axial} = 68.476\ Nm$$

$$M_{Tangential} = 44.686\ Nm$$

By using the AutoCAD Inventor the center of gravity was determine for the blade and the required distances were derived.

The following sketch illustrates the final bending moments in the axial and tangential direction and the distances from the center of gravity to the leading edge (LE) and the trailing edge (TE).

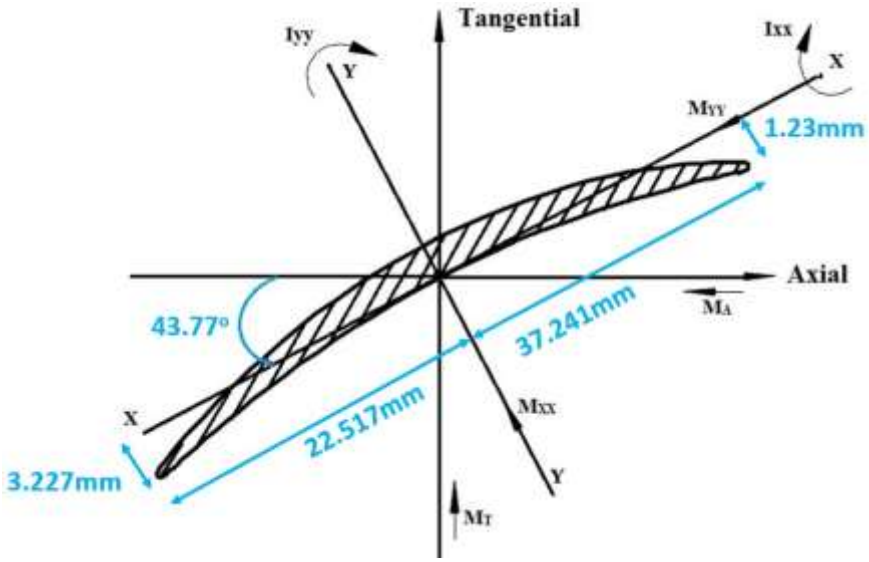

Figure 7-7 Blade Profile

The reference axis for the bending moments changes from the axial and tangential to X-X and Y-Y, therefore the bending moments have to be converted.

$$M_{yy} = M_{axial} \times \cos(\xi) - M_{tangential} \times \sin(\xi) \Longrightarrow M_{yy} = 18.536\ Nm$$

$$M_{xx} = M_{axial} \times \sin(\xi) + M_{tangential} \times \cos(\xi) \Longrightarrow M_{xx} = 79.638\ Nm$$

In addition to the bending moments, in order to use engineer's bending theory the second moment of area in both X-X and Y-Y axis is essential. To simplify the calculations the blade is consider to be shaped as a rectangular, with a length equal to 60mm and a width equal to 3.5mm.

$$I = \frac{b \times d^3}{12}$$ **(7-29) Second Moment of Area**

By applying the equation 7-28 to the two axis the I_{xx} and I_{yy} can be estimateded. The final stresses for the LE and TE of the blade can be derived using the expression below.

$$\sigma_{LE} = \frac{M_{xx} \times U_{LE}}{I_{xx}} - \frac{M_{yy} \times V_{LE}}{I_{yy}} \Longrightarrow \sigma_{LE} = 41.024\ MPa$$

$$\sigma_{TE} = \frac{M_{xx} \times U_{TE}}{I_{xx}} + \frac{M_{yy} \times V_{TE}}{I_{yy}} \Longrightarrow \sigma_{TE} = 16.61\ MPa$$

The resulting centrifugal stress in the blade is equal to 358.149 MPa. In total all the aforementioned stresses are tensile and if combined together the results for the leading and trailing edges are as follows:

$$\sigma_{LE} = 399.174\ MPa \qquad \sigma_{TE} = 374.759\ MPa$$

The most severe stress occurs at the leading edge of the blade. The centrifugal load accounts for most of the created stress and the remaining is generated from the gas bending moments. In order to perform the fracture mechanics analysis and the high cycle fatigue analysis in the next chapter a simplification has to be made. The gas bending moments are acting on the blade when the flow across the blade is not block by the IGVs located in front for it. There is a region of low velocity behind the IGVs known as the wake. The author assumed that the gas bending moments behind the IGVs are equal to zero. It is an approximation because even behind the IGVs the blade will experience a bending moment due to velocity and pressure changes but in order to calculate the magnitude of those a CFD simulation is required. The final tensile stress on the leading edge of the blade can be seen in the figure 7-8 below.

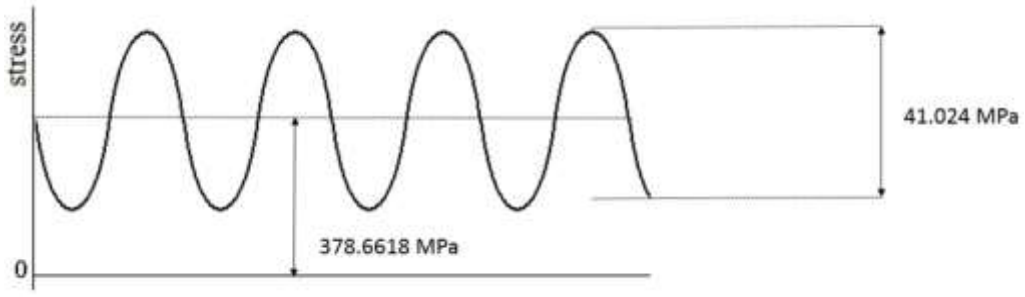

Figure 7-8 Leading Edge Stress

8 Fracture Mechanics

Fracture mechanics is the field of engineering that determines when a crack within a material becomes critical. More specifically it investigates when the crack propagation changes from stable to unstable. The strength of a material and the size of the crack are closely linked. As a crack size increases the strength of the material decreases. This is caused because the stress concentration in the region of the crack increases. This phenomenon can lead to a component failure during normal operation. By analyzing the crack and the stresses experienced by the component, fracture mechanics can provide expressions that relate the crack propagation rate with the stresses imposed on the component.

The following figure depicts the three typical modes of cracks propagation. This projects focuses on the rotating blades of the high pressure compressor and therefore the first of the crack modes is applicable in this situation.

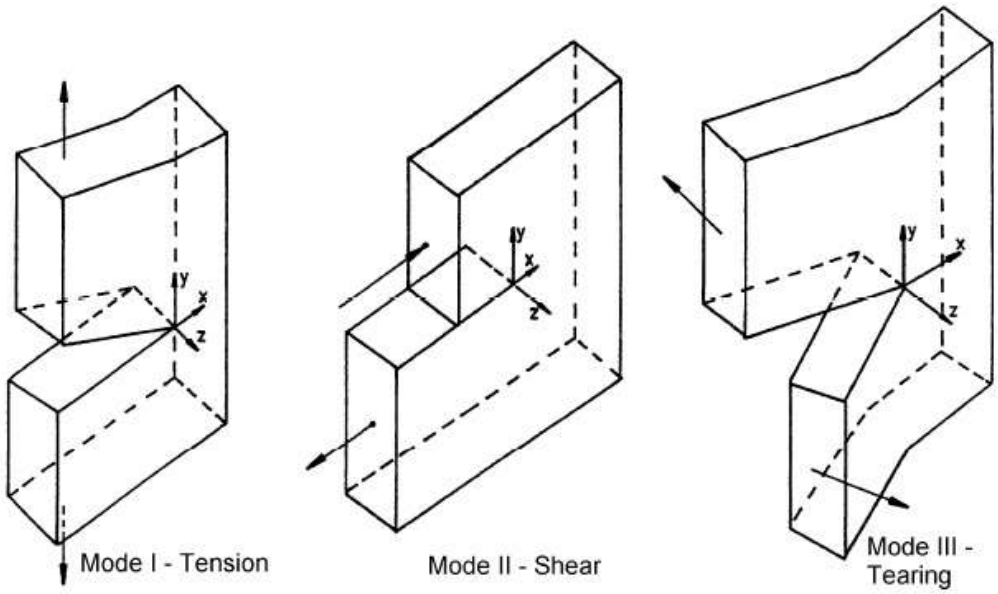

Figure 8-1: Typical Crack Modes [9]

In order to explain brittle fracture of glass, AA Griffith developed a radical idea. His approach involved the use of an energy equilibrium. He suggested that in order for a crack to propagate, it will have to overcome the cohesive energy between the atoms of the material.

A different way to express this is to calculate the increase in surface energy for a material. Using this approach, Griffith was able to calculate the stress required for a crack to propagate though a brittle material.

$$\sigma = \sqrt{\frac{2 \times E \times u_s}{\pi \times a}}$$

(8-1) Griffith Equation

Where:

σ = Stress required for crack propagation [Pa]

u_s = Surface energy

E = Young's Modulus of Elasticity

a = Half flaw length

8.1 Stress Intensity Factor

The next milestone in the fracture mechanics theory came in late 1940's when the stress intensity factor (K) was introduced by Irwin. This factor provides a method of measuring the stresses surrounding a crack tip. This factor is useful because it can be derived using the theory of elasticity, by using finite element analysis modeling or by testing the actual component. Subsequently, equation 8-2 below can be used to relate the stress intensity factor with the crack size.

$$K = \sigma\sqrt{(\pi \times a)}$$

(8-2) Stress Intensity Factor

Where:

σ = Nominal stress

Moreover, by using the equation 8-2 the critical stress intensity (K_{IC}) can be found. This corresponds to the stress intensity at which the crack becomes unstable [9]. In addition, the stain energy release rate (G) and critical strain energy release (G_{IC}) are also significant variables, quantifying the energy required for a crack to become critical [9].

8.2 Fatigue Crack

There are three stages defining crack growth. The first one is the creation of the crack. Cracks are formed usually between the grains of the material. In the next phase the crack has grown and becomes a macro-crack. At this phase the crack size increases and the crack propagates in a plane normal to the maximum principal stress. Finally, the crack length has become critical and the stress intensity factor has reached its critical value. When this occurs the component fails. The three stages of the crack propagation are illustrated in figure 8-2 below.

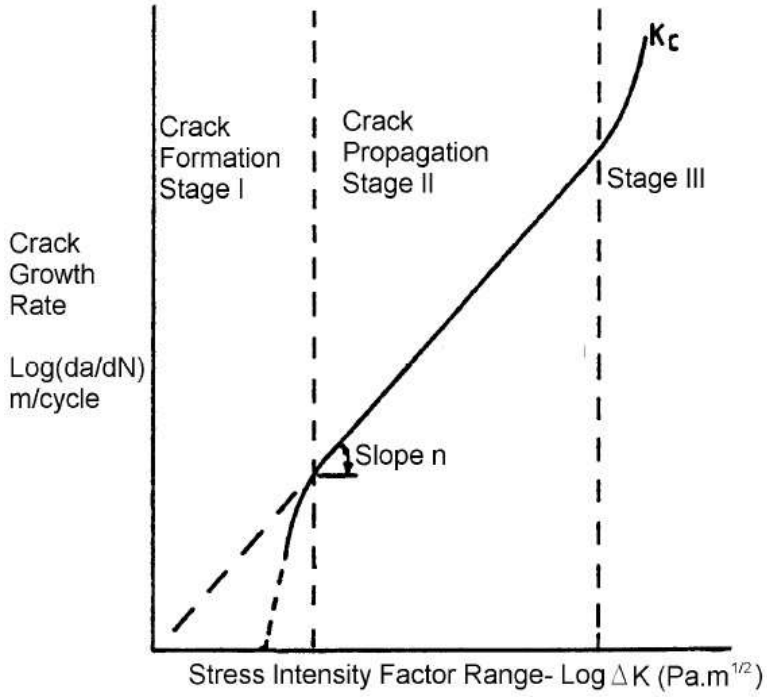

Figure 8-1 Crack Propagation Stages [9]

The time spent in the second stage of the fatigue crack growth is much greater that the time spend in the rest of the phases. Therefore relating the crack size with the cycles spent in this stage was essential. The first equation relating the rate of crack growth with the stress intensity factor was the Paris equation.

$$da/dN = C \times (\Delta K)^n \qquad \textbf{(8-3) Paris Equation}$$

And

$$\Delta K = \beta \times (\sigma_{max} - \sigma_{min}) \times \sqrt{\pi \times a} \qquad \textbf{(8-4) Stress Intensity Range}$$

Where:

da/dN = Crack growth rate

C = Experimentally determined constant

n = Experimentally determined constant

β = Crack shape factor (compliance factor)

If the relationship 8-3 is integrated and applied to a range of crack sizes from initial crack size (a_i) to critical crack size (a_c) the life of the material can be derived. The following expression illustrates the relationship between the a_i, a_c and the cycles to failure (N_f).

$$N_f = \frac{2}{(n-2) \times C \times \left(\beta \times \Delta\sigma \times \sqrt{\pi}\right)^n} \left[a_c^{\frac{2-n}{2}} - a_i^{\frac{2-n}{2}} \right] \qquad \textbf{(8-5) Life Cycles}$$

8.3 Walker's Law

An addition to the Paris law described above is the Walker's law which takes into account stress fluctuations where the mean stress is non equal to zero. It uses a stress ratio (R) which is defined as the ratio of the maximum to minimum stress imposed to the material. The crack propagation using Walker's law is expressed as follows [9].

$$da/_{dN} = C \times [\Delta K \times (1-R)^{m-1}]^n \qquad \textbf{(8-6) Walker's Equation}$$

Where:

m = Walker exponent

In order to use the above equation the ratio between the maximum and minimum stress must be greater than zero, otherwise the Paris equation is sufficient to determine the cycles to failure.

8.4 Advisory Circular 33.14-1

Advisory Circulars (AC) are published by the Federal Aviation Administration (FAA) of the USA and include guidelines in relation to the airworthiness regulations. The AC 33.14-1 [34] was published in 2001 and describes a lifing analysis for titanium alloy parts and more specifically for the compressor disk assembly. The AC is very useful to the author because apart from the material properties such as density, ultimate stress and fracture toughness, it also provides a distribution of Hard – Alpha Inclusions in titanium alloys.

The AC 33.14-1 includes a logarithmic diagram describing the range of material fault sizes and the probability of their occurrence in a tonne of material. This distribution is only applicable to titanium components manufactured after 1995. It is also worth mentioning that some assumptions were made in order to obtain that distribution.

1. The faults are distributed evenly throughout the material
2. The shape of the faults is spherical

The following figure depicts the distribution of hard – alpha faults in titanium alloys manufactured after 1995.

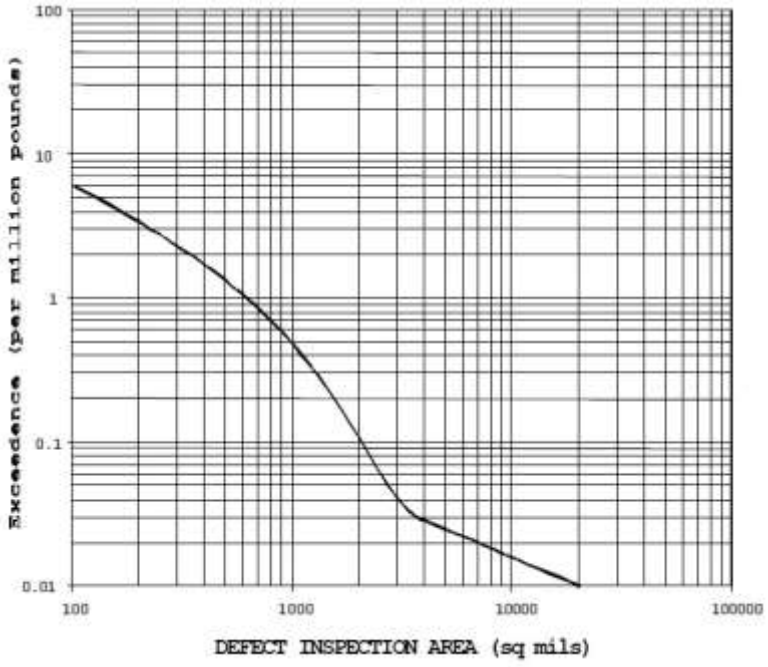

Figure 8-2 Fault Distribution [34]

8.5 Reference Flight

For the reference flight mentioned in chapters 5, 6 and 7 a basic maintenance program has been predicted and the blade stresses at take-off have been calculated. In this chapter a fracture analysis will be conducted. The AC 33.14-1 from the Federal Aviation Administration (FAA) will be used to calculate the probability of a HPC blade failing the inspection under a specified number of cycles. More specifically, in this chapter the probability of an initial crack big enough to cause a detectable crack in a specific number of flight hours will be derived. This probability will affect only the first stage compressor blades of the high pressure compressor for the reference engine which is the GE90-94B.The probability will arise from the usage of figure 8-2 that quantifies the number of exceedances per defect area.

Usually airlines change the compressor blades and the compressor shaft at the same time. The rotating shaft of a high pressure compressor is a life limited part and its life is limited by strict rules. In order to maximize the time that the engine is in operation, the shaft and blades are replaced at the same shop visit. This reduces the time that the engine spends in the workshop because a second shop visit is avoided, but the blades usually have not reached their life expectancy when removed. For a long haul engine like the GE90-94B a full overhaul of the HPC is expected at the second shop visit. Therefore, the author decided to investigate a blade replacement at the third shop visit. The number of cycles that correspond to the third shop visit according to the created CERs are 7562 EFC.

In addition, the fracture mechanics analysis focuses more on the low cycle fatigue, because a separate analysis for the high cycle fatigue is performed in the next chapter. This means that for the stresses used in the fracture mechanics analysis the maximum stress used is equal to the leading edge maximum stress calculated in the chapter 7, while for the minimum stress a value equal to zero was selected.

There are three additional significant factors for the fracture analysis, namely the compliance factor (β) and the two experimentally derived constants (C and n).

The experimental constants can be found on the AC 33.14-1 [34] for the specific titanium alloy and their values are:

$C = 9.25^{-11}$ [m/cycle]

n = 3.87

On the other hand there is no detail in the AC regarding the compliance factor. The Paris equation is very sensitive to the value of the compliance factor. The figure below illustrates the effect of the compliance factor on the number of cycles calculated with Paris equation 8-5.

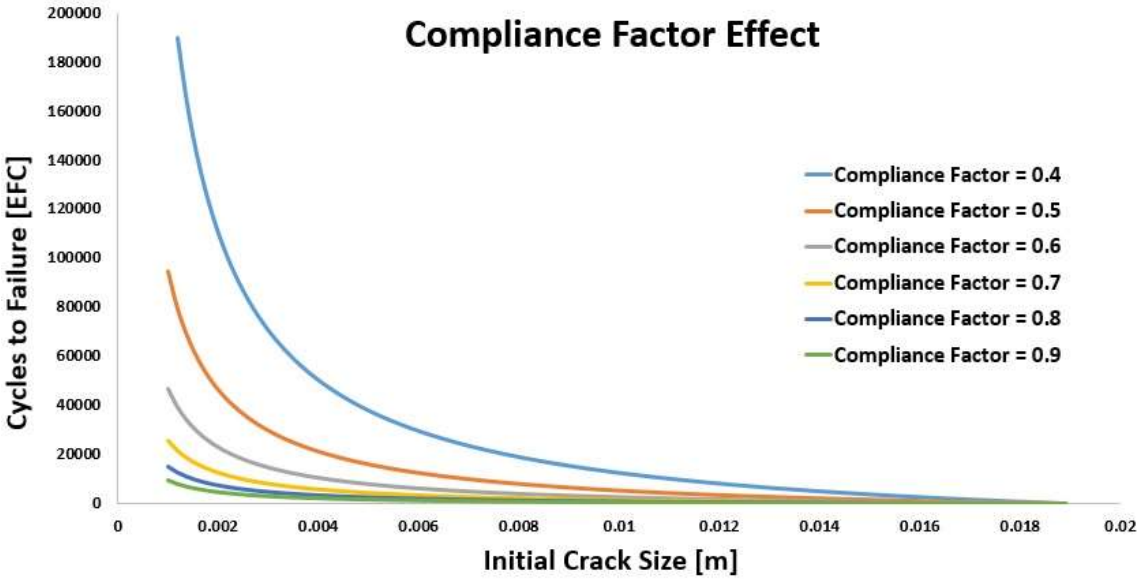

Figure 8-3 Compliance Factor Effect

The effect is more noticeable between the values 0.4 and 0.7. In addition, the difference between a compliance factor equal to 0.4 and 0.9 can exceed an order of magnitude in number of cycles to failure. Therefore the selection of the compliance factor is considered crucial for the fracture mechanics analysis.

The author therefore based his analysis on the work of Leigh Holland. As part of her thesis 'Probabilistic Prediction of Failure Events in Gas Turbine Due to Material Anomalies' [35] Holland calculated the compliance factor using a software called AFGROW. The selected value for surface cracks was 0.663.

The Paris equation also requires the critical crack size (a_c). The critical crack size represents the length of the crack at which the blade of the HPC will be replaced. As it is mentioned in the first chapter the non-life limited parts such as compressor blades are frequently monitor. The technique used is called borescope inspection. The borescope is inserted in the annulus of the HPC thought an observation port and the conditions of each blade is monitored. Borescope inspections are frequent because they do not require disassembly of the engine. The capability of detecting a crack depends not only on the borescope used but also on the skill of the technician working on the engine. Modern equipment and technician training have result in detectable crack sizes in the order of 1mm. Therefore for the fracture mechanics analysis the author selected a critical defect size as follows:

$$a_{IC} = 8 \times 10^{-4}\, m$$

Using the life cycles equation 8-5 a relationship between the initial crack size and the cycles to failure can be made. The following figure describes that relationship.

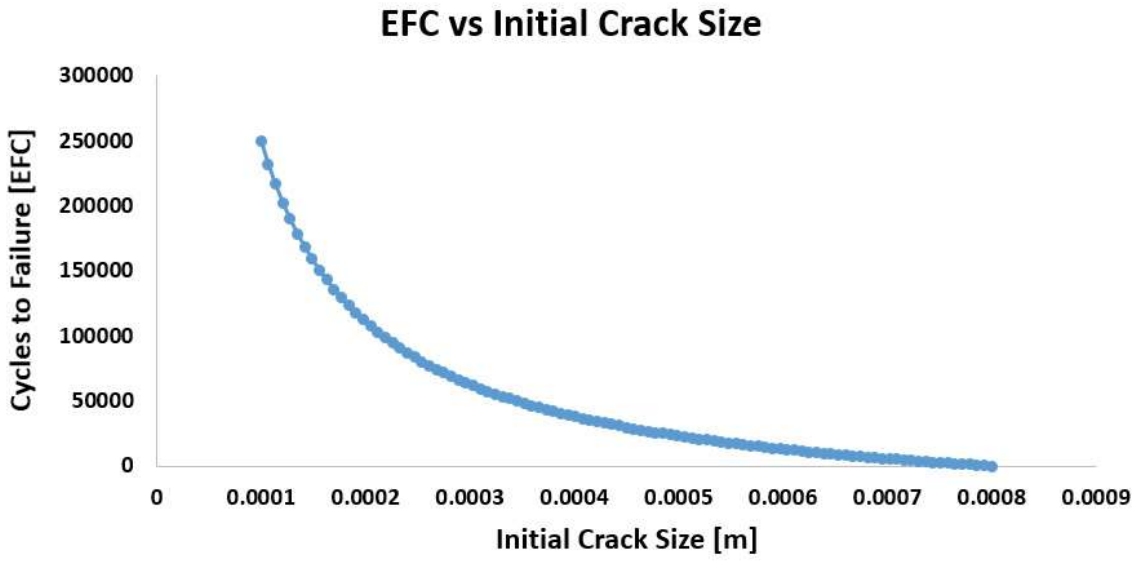

Figure 8-4 EFC vs Initial Crack Size

From the diagram above for a specified number of cycles equal to 7562 EFC the initial crack size can be derived.

$$a_i = 6.604 \times 10^{-4}\, m$$

Using the assumption that the flaws are spherical the area created by an initial crack with that size can be calculated.

$$A_i = 1.137014 \times 10^{-6}\, m^2$$

The resulting area can then be converted to square millionths of an inch (sq mils) knowing that 100 sq mils equal to $6.4516 \times 10^{-8}\, m^2$.

$$A_i = 1.137014 \times 10^{-6}\, m^2 \Longrightarrow A_i = 2123.72\, sq\ mils$$

Finally using the figure 8-2 the exceedances per million of titanium can be derived.

Exceedances / 1 million Kg of titanium = 0.0693

This anomaly occurrence has to be adapt to the mass of the blade on the first row of the HPC. In order to achieve that following equation is used.

$$P(\lambda_{zone}) = \frac{Vol_{zone}}{Vol} \times \lambda$$ **(8-7) Anomaly Probability**

Where:

λ_{zone} = anomaly occurrence rate for a specific volume Vol_{zone}

λ = anomaly occurrence rate for a volume Vol

The volume of all the blades in the first stage of the HPC is easily derivable using the density for titanium alloy found on the AC 33.14-1 [34]. The 37 blades have a volume equal to $Vol_{zone} = 1.405667 \times 10^{-3}\, m^3$. If the same density value is applied to the 1 million Kg of titanium a volume equal to $Vol = 101.9308\, m^3$ is the result.

Consequently, the probability of an initial crack big enough to cause failure in the first row of the HPC in 7562 EFC can be calculated.

$$P(\lambda_{zone}) = \frac{1.4055677 \times 10^{-3}}{101.9308} \times 0.0693 \Longrightarrow P(\lambda_{zone}) = 9.557 \times 10^{-7}$$

This probability is significantly low suggesting that the blades of the HPC could last 7562 EFC without a replacement required. It has to be emphasized, that this analysis only took into consideration the effects of low cycle fatigue. Moreover, the stresses used were derived using the assumption of an untwisted blade and only one operating condition (take-off).

In addition, the calculated probability affects only one engine of one aircraft. This probabilistic method can be extended into a fleet of aircraft. In order to do that the number of aircraft used by the operator and the operating conditions of each aircraft have to be defined.

8.6 High Cycle Fatigue

In order to analyze the effects of high cycle fatigue to the HPC blades the Double Goodman technique was selected. The life target for the blades is assumed equal to the third shop visit interval (7562 EFC). Moreover the stresses on the blade will change for this analysis. The cruise conditions are consider more important for the Double Goodman diagram analysis. Therefore by using the created Excel spreadsheet the author was able to estimate the stresses imposed on the blades. Most severe was the stress on the leading edge of the blade and the loading condition which is going to be used for this analysis can be seen in figure 8-5 below.

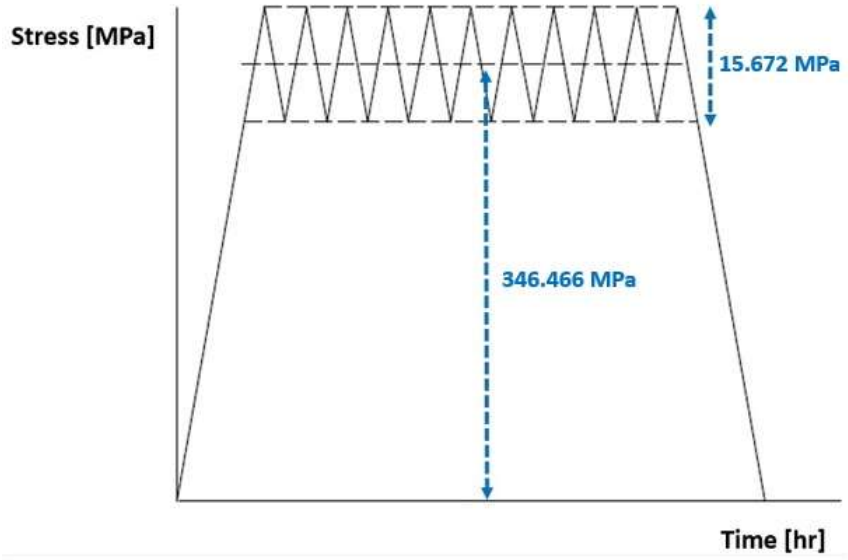

Figure 8-5 Combine Cycle

From the reference flight simulation the rotational speed of the shaft at take-off can be obtain, as well as the duration of the flight. In addition, the number of the IGVs have been defined in the chapter 7. Therefore the number of minor cycles experienced by the blades in 7562 engine flight cycles can be calculated as follows.

$$RPM \times Flight\ duration[min] \times Number\ of\ IGVs \times Target\ EFC \Rightarrow$$

$$9800 \times 7.05 \times 60 \times 43 \times 7562 = 1.348 \times 10^{12}$$

The first step in the Double Goodman diagram methodology is to define the cyclic strength of the material for the target life of 7562 cycles. In order to obtain that an S-N curve is required. To create the S-N curve for the material the ultimate strength and the endurance limit of the material are necessary. The ultimate strength of the material for the specific titanium alloy can be found on the AC 33.14-1 [34] σ_{ult} = 910 MPa.

The endurance limit of the material can be licked with the ultimate strength with the relationship below [36].

$$\sigma_e = 0.6 \times \sigma_{ult} \qquad \textbf{(8-8) Endurance Limit}$$

The resulting endurance limit for the material is σ_e = 546 MPa. Therefore the S-N diagram (on log-log axes) has the following shape.

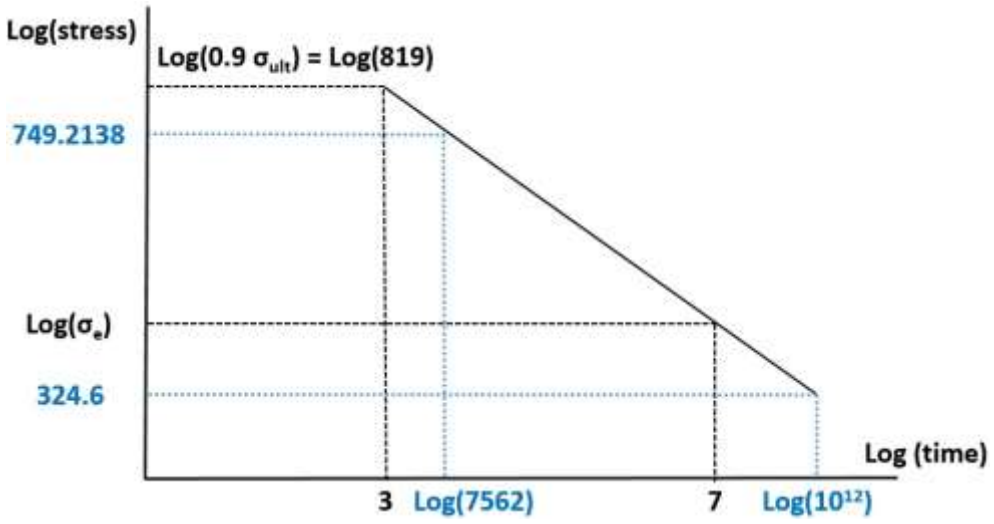

Figure 8-6 S-N Curve

Using similar triangles the cyclic strength is derived equal to 749.214 MPa. The Goodman diagram for the major cycle can therefore be drawn.

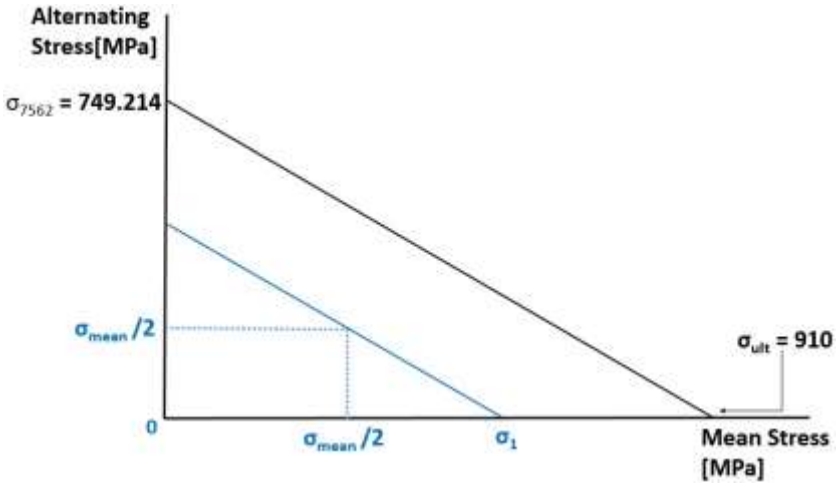

Figure 8-7 Major Cycle Goodman Diagram

The equivalent mean stress for the 7562 cycles can be calculated using again the similar triangles method. The result for σ_1 is 383.643 MPa. The second Goodman diagram for the combined cycle can be drawn and the calculated equivalent mean stress can be transferred to it. It is worth mentioning that from the S-N diagram in figure 8-6 the cyclic strength of the material for 1.348×10^{12} cycles is equal to 324.6 MPa. The mean stress of the minor cycle is equal to 15.672 / 2 = 7.836 MPa.

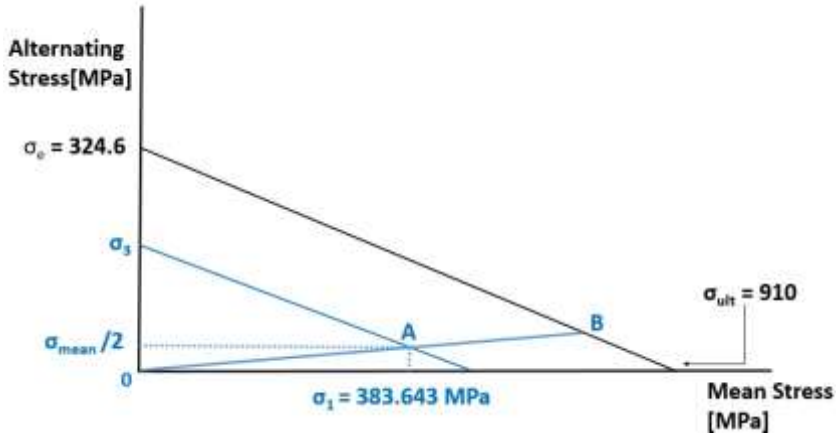

Figure 8-8 Combined Cycle Goodman Diagram

Finally the resulting safety factor is equal to 2.37 which is consider sufficient for the HPC blades.

8.6.1 Stress Concentration Factor

The Stress Concentration Factor (K_t) is the ratio of the actual stress to the nominal stress imposed on a component. The actual value of the stress can vary from the nominal due to variations in the geometry of the component. More specifically, between the airfoil and the base of the blade a shoulder fillet is created. This region is consider as an area of stress concentration.

The actual stresses created by the discontinuity in the shoulder fillet can be calculated using the theory of elasticity.

In the figure below the stress concentration factor is given for different geometrical variations according to the Peterson's Stress Concentration Factors [37].

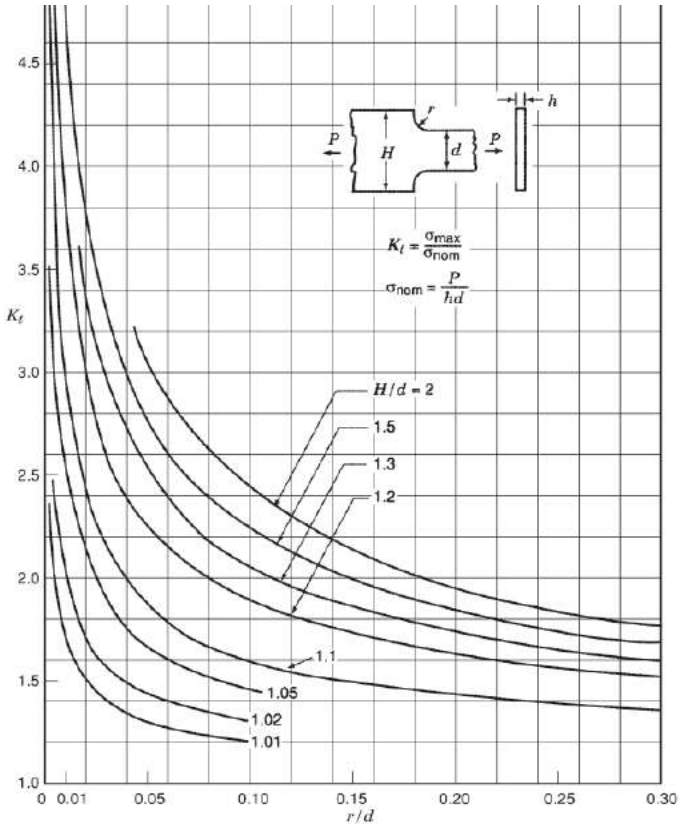

Figure 8-9 Stepped Flat Tension Bar K_t [37]

For the blade designed in chapter 7 the H/d = 1.2, but the shoulder fillet is not defined and can only be estimated. In order to evaluate the effect of the fillet

radius on the stress concentration factor a range of r/d between 0.05 and 0.25 is used. That range corresponds to shoulder fillet radius from 0.25 mm to 1.25mm.

Having calculated the stress concentration factor another Double Goodman Diagram analysis like the one described above is performed to derive the safety factor. The K_t is multiplied with the cyclic load of the major and minor cycle resulting in a greater alternating load for both cycles.

The figure 8-10 below depicts the effect of the stress concentration factor to the safety factor resulting from the Goodman Diagram analysis.

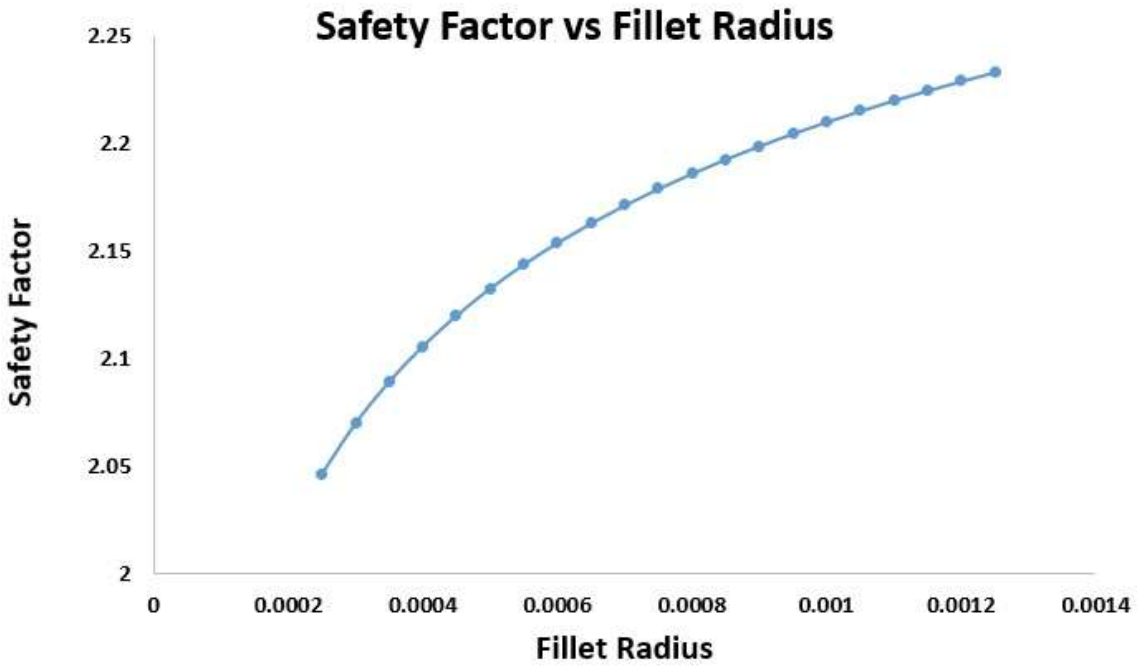

Figure 8-10 Safety Factor against K_t

It is obvious from the diagram that as the shoulder fillet radius increases the stress concentration in that region decreases. As a result, the stresses created are not so intense and the safety factor increases. This affect is reasonable since a larger radius of the fillet will result in a more graduate transition for the airfoil to the base of the blade, resulting in a lower stress concentration in that region.

Lastly, even a fillet radius equal to 0.25mm corresponds to a safety factor of 2.05, which the author considers to be acceptable for the blade design.

9 Conclusion and Recommendations

9.1 Conclusion

The objective of this project was to investigate the effect of the maintenance program on the lifing of the non – life limited parts. The project began with the simulation of the General Electric GE90-94B gas turbine and the Boeing 777-200ER aircraft. Both engine and aircraft simulations were verified using several operating conditions. The engine model was tested against the take – off, cruise and EASA certification condition and the maximum observed error was 9.482 % in the EGT, which can be explained by the way Turbomatch works. The Hermes model was validated using the payload / range curve with the maximum error reaching 2.8379 %. Apart from those simulations, a reference flight was also simulated. The flight was from London Heathrow to New York JFK airport.

The next step involved the creation of the cost estimate relationships. An engine data based was required in order to perform the regression process and it had to be normalized to account for inflation. Five CERs were created to estimate the interval and cost for the non-mature and mature shop visits.

The thesis was then focused on the high pressure compressor first row blades. A preliminary compressor design for the HPC was conducted and the annulus for each stage was calculated. The analysis continued with a more detailed design for the first row blades. The metal angles were defined and the blade shape was obtained. In addition, the stresses imposed on the blade were also calculated. The resulting stress on the leading edge was 378.66 ± 20.512 MPa. The analysis was conducted for the reference flight take-off condition.

Using the maximum calculated stress and the result for the flight cycles between shop visits a fracture mechanics analysis followed. The outcome of the analysis was a probability for a blade failing inspection under a specified number of engine cycles. More specifically the third interval (7562 EFC) was used and the resulting probability was of the appearance of a detectable crack was $P = 9.557 \times 10^{-7}$. This result suggests the blades of the HPC will not experience any significant cracking during 7562 engine flight cycles due to low cycle fatigue.

Accordingly to the fracture analysis the blades could be renewed at the fourth or fifth shop visit instead of the third. This would result in a great cost benefit for the operator. An unscheduled engine shop visit in order to replace the compressor blades can cost up to $ 150,000 [38]. The operator usually covers this cost with the revenue created for the operation of the aircraft. Therefore by allowing the aircraft to operate for a longer period of time before replacing the HPC blades will reduce the overall maintenance cost per engine flight cycle.

In an attempt to address the problem of the combined high and low cycle fatigue, a second analysis using a double Goodman diagram technique was performed. The outcome of this analysis was a safety factor equal to 2.37, which suggest that in the target life of 7562 EFC the combine cycle will not affect the first row blades. Also worth mentioning is that for the double Goodman technique the stresses on the blades during the cruise phases were used. Finally, a sensitivity analysis of the stress concentration factor was conducted.

9.2 Recommendation

The author has some recommendations regarding future work on the same subject. Due to time and technical limitations the compressor design was simplified significantly. A more detail analysis on the aerodynamic design of the blade has to be performed. In addition, a CFD analysis could be helpful to establish if the design blade can perform the desire pressure rise per stage.

Another aspect that can be improved is the calculation of the stresses imposed on the blades. The blade can be divided into multiple section and the stresses can be estimated for each section separately. Moreover a finite element analysis model could be used to establish in more detail the stress on the blades.

The fracture mechanics model can also be improved. A probabilistic fracture mechanics analysis could be performed, which would result in a Weibull distribution. This distribution would indicate the probability for a blade failing the inspection. Finally, the study could be applied to a fleet of aircraft instead of just only one aircraft, therefore increasing the probability for detectable cracks be present in the HPC blades.

REFERENCES

[1] Soares, Claire. (2008). *Gas Turbine A Handbook of Air, Land and Sea Applications*. Boston: Butterworht – Heinemann.

[2] Seemann R. (2010). *Modeling the Life Cycle Cost of Jet Engine Maintenance*. Hamburg: Technische Universitat Hamburg.

[3] Strarr, Al-Najjar, Holmberg, Jantunen, Bellew and Albarbar. (2010). *E – maintenance.* London: Springer.

[4] Linke – Diesinger. (2008). *Systems of Commercial Turbofan Engines.* Hamburg: Springer.

[5] Ackert. (2011). *Engine Maintenance Concepts for Financiers.* Aircraft Monitor

[6] GE90 family maintenance cost. Aircraft – Commerce. 84, s.l.: Aircraft Commerce, 2012

[7] Roux, E. (2007). *Turbofan and Turbojet Engines: Database Handbook*. Blagnac: Editions Elodie Roux.

[8] http://training.egyptair.com/Maintenance/EngineModuleChange (accessed August, 2015).

[9] Cookson R. A., Haslam A. S. (2015). *Fatigue and Fracture*. Course notes. Cranfield University.

[10] http://www.borescopes.info/how.asp (accessed August, 2015).

[11]https://upload.wikimedia.org/wikipedia/commons/3/37/BorescopeSchematic.png (accessed August, 2015).

[12] Schijve, J. (2009). *Fatigue of Structures and Material*. Dordrecht; London: Springer.

[13] Daly M., Gunston B. and FRAeS. (2012). *Jane's Aero Engines*. Jane's information group.

[14] http://cv01.twirpx.net/0355/0355593.jpg (accessed August, 2015).

[15] Pachidis V., Nikolaidis Th., (2015). *Gas Turbine Performance Simulation.* Course notes. Cranfield University.

[16] EASA. IM. E. 002 General Electric GE90 series engines. Available at: http://easa.europa.eu/system/files/dfu/EASA-TCDS-E.002_%28IM%29_General_Electric_GE90_series_engines-02-16032004.pdf (accessed August, 2015).

[17] Laskaridis P., Pilidis P. and Kotsiopoulos P. (2005). "An Integrated Engine – Aircraft Performance Platform for Assessing New Technologies in Aeronautics". Cranfield University.

[18] Whellens M. W., Singh R., (2002). Propulsion Systems Optimisation for Minimum Global Warming Potential. ICAS 2002, Congress, Toronto Canada.

[19] Jenkinson L. R., Lloyd R., Simpkin P., Rhodes D., (1999). Civil Jet Aircraft Design. London: Arnold.

[20] http://www.boeing.com/commercial/airports/3_view.page (accessed August, 2015).

[21] Boeing 777 Payload – Range Capability. Available at: http://www.boeing.com/assets/ (accessed March, 2015).

[22] Boeing 777-200ER Performance Summary. Available at: http://www.boeing.com/assets/ (accessed March, 2015).

[23] Goodger E., Ogaji S. (2011). *Fuels & Combustors in Heat Engines*. Bedfordshire: Cranfield Design and Print.

[24] http://www.britishairways.com/en-gb/destinations/new-york/flights-to-new-york (accessed August, 2015).

[25] International Society of Parametric Analysis. *Parametric Estimating Handbook*. Vienna: ISPA, 2008.

[26] http://www.aircraft-commerce.com/ (accessed August, 2015).

[27] http://www.bls.gov/ (accessed August, 2015).

[28] Draper, Norman R. (1998). *Applied Regression Analysis*. New York: Wiley

[29] Lindsey, James K. (2004). *Introduction to Applied Statistics: a modelling approach*. Oxford: Oxford University Press.

[30] Saravanamuttoo, H.I.H. (2008) *Gas Turbine Theory*, 6th Edition. Upper Saddle River, N.J.: Pearson Prentice Hall.

[31] Zachos P., Ramsden KW. (2015). *Turbomachinery Course Notes - Compressors.* Course notes. Cranfield University.

[32] Seyb N. (2015). *Turbomachinery Course Notes – Compressor Blade Design*. Course notes. Cranfield University.

[33] Cookson R. A., Haslam A. S. (2015). *Mechanical Design of Turbomachinery*. Course notes. Cranfield University.

[34] Federal Aviation Administration. Code of Federal Regulations, Advisory Circular 33.14-1, *Damage Tolerance for High Energy Turbine Engine Rotors*.

[35] Holland Leigh. (2007). *Probabilistic Prediction of Failure Events in Gas Turbine Discs to Material Anomalies.* MSc Thesis. Cranfield University

[36] http://www.roymech.co.uk/Useful_Tables/Fatigue/Fatigue.html (accessed August, 2015).

[37] Pilkey, Walter D. (2008). *Peterson's Stress Concentration Factors* 3rd Edition. Hoboken, N.J.: John Wiley

[38] General Electric Aviation. (2007). Service Solutions. Volume 7 (3). Available at: http://geaviationservicesolutions.com/lib/pdfs/v07i03.pdf

APPENDICES

Appendix A Turbomatch

A.1 Design Point Code

```
        TURBOMATCH SCHEME 2.0 - Windows 7 version
   ****************   VERSION 2.0   ***************
LIMITS:100 Codewords, 800 Brick Data Items, 50 Station Vector
15 BD Items printable by any call of:-
OUTPUT, OUTPBD, OUTPSV, PLOTIT, PLOTBD or PLOTSV
 Input "Program" follows
Engine: GE 90-948 (2-spool with booster)


Jane's Engines
_____________________________________________________________
Mid Cruise:
FPR: 1.65
BPR: 8.1
Mass Flow: 576 Kg/s
!#
Take-off:
Max Thrust (Take-off): 432811 N
Fuel Flow: 2.968 Kg/s
FPR: 1.58
BPR: 8.4
OPR: 39.6
Mass Flow: 1467 Kg/s
_____________________________________________________________
////
OD SI KE VA FP
 -1
 -1
INTAKE   S1,2          D1-6              R300
COMPRE   S2,3          D7-18             R305      V7    V8
PREMAS   S3,13,4       D19-22                      V19
DUCTER   S13,14        D23-27            R310
NOZCON   S14,15,1      D143,144          R351
COMPRE   S4,5          D33,8,35-44       R320      V33
COMPRE   S5,6          D53-64            R335      V53   V54
PREMAS   S6,16,7       D97-100
BURNER   S7,8          D105-112          R350
MIXEES   S8,16,9
TURBIN   S9,10         D113-127                    V114
TURBIN   S10,11        D128-142                    V129
NOZCON   S11,12,1      D145,146          R355
PERFOR   S1,0,0        D147-150,355,300,350,351,0,0,0,0,0
CODEND


BRICK DATA////
1 0.0                ! INTAKE: Altitude
2 15                 ! Deviation from ISA temperature
3 0.0                ! Mach number
4 -1.0               ! Pressure recovery, according to USAF
5 0.                 ! Deviation from ISA pressure [atm]
6 0.                 ! Relative humidity [%]

7 0.85             ! FAN - COMPRESSOR: Z = (R-R[choke])/(R[surge]-R[choke])
8 1.                 ! DP Relative rotational speed PCN
9 1.58               ! DP Pressure ratio
10 0.915             ! DP Isentropic efficiency
11 0.                ! Error selection
12 2.                ! Compressor Map Number
13 1.                ! Shaft number
14 1.                ! Scaling Factor of Pressure Ratio - Degradation factor
15 1.                ! Scaling Factor of Non-D Mass Flow - Degradation factor
16 1.                ! Scaling Factor of Isentropic Efficiency - Degradation fact
17 1.5               ! Effective component volume [m^3]
18 0.                ! Stator angle (VSV) relative to DP

19 0.893617      ! BYPASS - PREMAS: LAMDA W Cooling bypass (Wout/Win) BPR = 8.4
20 0.                ! DELTA W
21 1.                ! LAMBDA P
22 0.                ! DELTA P

23 0.              ! BYPASS DUCT - DUCTER: Air duct
24 0.01              ! Total pressure loss: DELTA(P)/Pin (Pressure loss = 1%)
25 0.                ! Combustion efficiency
26 0.                ! Limiting value of Fuel Flow (=100000 if not needed)
27 -1                ! Effective component volume [m^3]
```

```
33 0.85          ! COMPRESSOR-BOOSTER: Z = (R-R[choke])/(R[surge]-R[choke]) (if
!34 1.             ! DP Relative rotational speed PCN (The speed is taken from
35 1.0897          ! DP Pressure ratio
36 0.89            ! DP isentropic efficiency
37 1.              ! Error selection
38 2.              ! Compressor Map Number
39 1.              ! Shaft number
40 1.              ! Scaling Factor of Pressure Ratio - Degradation factor
41 1.              ! Scaling Factor of Non-D Mass Flow - Degradation factor
42 1.              ! Scaling Factor of Isentropic Efficiency - Degradation fact
43 0.1             ! Effective component volume [m^3]
44 0.              ! Stator angle (VSV) relative to DP

53 0.85          ! HP COMPRESSOR: Z = (R-R[choke])/(R[surge]-R[choke]) (if =-1.
54 1.              ! DP Relative rotational speed PCN
55 23              ! DP Pressure ratio
56 0.88            ! DP isentropic efficiency
57 1.              ! Error selection
58 5.              ! Compressor Map Number
59 2.              ! Shaft number
60 1.              ! Scaling Factor of Pressure Ratio - Degradation factor
61 1.              ! Scaling Factor of Non-D Mass Flow - Degradation factor
62 1.              ! Scaling Factor of Isentropic Efficiency - Degradation fact
63 -1              ! Effective component volume [m^3]
64 0.              ! Stator angle (VSV) relative to DP

97 0.078         ! HPT COOLING - PREMAS: LAMDA W
98 0.              ! DELTA W
99 1.              ! LAMBDA P
100 0.             ! DELTA P


105 0.04         ! COMBUSTOR: Pressure loss (=Total pressure loss/Inlet total p
106 0.99           ! Combustion efficiency
107 -1             ! Fuel flow (If -1. is given the TET must be determined in t
108 0.             ! (>0) Water flow [kg s-1 or lb s-1] or (<0) Water to air ra
109 288.           ! Temperature of water stream [K]
110 0.             ! Phase of water (0=liquid, 1=vapour)
111 1.             ! Scaling factor of ETAb (combustion efficiency) - Degradati
112 0.05           ! Effective component volume [m^3]

113 288100         ! HP TURBINE: Auxiliary or power output [288.1 KW]
114 -1             ! DP Relative non-dimensional massflow W/Wmax (if = -1, valu
115 -1             ! DP Relative non-rimensional speed CN (if = -1, value 0.6 i
116 0.92           ! DP isentropic efficiency
117 -1.            ! DP Relative non-dimensional speed PCN (= -1 for compressor
118 2.             ! Shaft Number (for power turbine, the value "0." is used)
119 5.             ! Turbine map number
120 -1.            ! Power law index "n" (POWER = PCN^n) If = -1, power is assu
121 1.             ! Scaling factor of TF (non-D inlet mass flow) - Degradation
122 1.             ! Scaling factor of DH (enthalpy change) - Degradation facto
123 1.             ! Scaling factor of ETAc is (Turbine isentropic efficiency)
124 181.9667       ! DP Rotor rotational speed [RPS]
125 30.            ! Rotor moment of inertia [kg.m^2]
126 -1             ! Effective component volume [m^3]
127 0.             ! NGV angle, relative to D.P.

128 0.           ! LP TURBINE: Auxiliary or power output [W]
129 -1             ! DP Relative non-dimensional massflow W/Wmax (If = -1, valu
130 -1             ! DP Relative non-rimensional speed CN (if = -1, value 0.6 i
131 0.93           ! DP isentropic efficiency
132 -1.            ! DP Relative non-dimensional speed PCN (= -1 for compressor
133 1.             ! Shaft Number (for power turbine, the value "0." is used)
134 5.             ! Turbine map number
135 -1.            ! Power law index "n" (POWER = PCN^n) If = -1, power is assu
136 1.             ! Scaling factor of TF (non-D inlet mass flow) - Degradation
137 1.             ! Scaling factor of DH (enthalpy change) - Degradation facto
138 1.             ! Scaling factor of ETAc is (Turbine isentropic efficiency)
139 241.0833       ! DP Rotor rotational speed [RPS]
140 150.           ! Rotor moment of inertia [kg.m^2]
141 0.15           ! Effective component volume [m^3]
142 0.             ! NGV angle, relative to D.P.

143 -1.          ! BYPASS NOZZLE: Swich set (= "1" if exit area "floats"
                   !                          = "-1" if exit area is fixed)
144 1.             ! Scaling factor


145 -1.          ! CONVERGENT NOZZLE: Swich set (= "1" if exit area "floats"
                   !                             = "-1" if exit area is fixed)
146 1.             ! Scaling factor


147 -1.          ! ENGINE RESULTS - PERFOR: Power output - Power or Power turbi
148 -1.            ! Propeller efficiency (= -1 for turbojet/turbofan)
149 0.             ! Scaling index ("1" = scalling needed, "0" = no scaling)
150 0.             ! Required DP net thrust(Turbojet,turbofan) or shaft power (
                   ! = 0 if Scaling index = 0

-1
1 2 1467.          ! Mass flow (kg/s)
8 6 1659           ! TET (K)
-1
```

Figure A-1 Design Point Code

A.2 Design Point Simulation Result

Station	F.A.R.	Mass Flow	Pstatic	Ptotal	Tstatic	Ttotal	Vel	Area
1	0.00000	1467.000	1.00000	0.99999	303.15	303.15	0.0	******
2	0.00000	1467.000	******	0.99999	******	303.15	******	******
3	0.00000	1467.000	******	1.57998	******	349.62	******	******
4	0.00000	156.064	******	1.57998	******	349.62	******	******
5	0.00000	156.064	******	1.72171	******	359.39	******	******
6	0.00000	156.064	******	39.59924	******	916.50	******	******
7	0.00000	143.891	******	39.59924	******	916.50	******	******
8	0.02239	147.113	******	38.01527	******	1659.00	******	******
9	0.02064	159.286	******	38.01527	******	1606.60	******	******
10	0.02064	159.286	******	7.25889	******	1132.91	******	******
11	0.02064	159.286	******	1.18772	******	750.86	******	******
12	0.02064	159.286	1.00061	1.18772	718.09	750.86	269.7	1.2037
13	0.00000	1310.936	******	1.57998	******	349.62	******	******
14	0.00000	1310.936	******	1.56418	******	349.62	******	******
15	0.00000	1310.936	1.00060	1.56418	307.50	349.62	292.0	3.9544
16	0.00000	12.173	******	39.59924	******	916.50	******	******

```
 Gross Thrust = 416735.35
Momentum Drag =      0.00
   Net Thrust = 416735.35
    Fuel Flow =    3.2217
       s.f.c. =   7.73072
   Sp. Thrust =   284.073
    Sim. time =   0.0000
          Time Now 16:14:00
```

Figure A-2 Design Point Results

A.3 Cruise Simulation Results

Station	F.A.R.	Mass Flow	Pstatic	Ptotal	Tstatic	Ttotal	Vel	Area
1	0.00000	629.201	0.23524	0.37501	218.81	250.26	251.8	******
2	0.00000	629.201	******	0.37501	******	250.26	******	******
3	0.00000	629.201	******	0.60333	******	290.92	******	******
4	0.00000	64.595	******	0.60333	******	290.92	******	******
5	0.00000	64.595	******	0.66678	******	300.97	******	******
6	0.00000	64.595	******	14.92062	******	772.63	******	******
7	0.00000	55.617	******	14.92062	******	772.63	******	******
8	0.01918	56.683	******	14.39117	******	1436.00	******	******
9	0.01651	65.662	******	14.39117	******	1351.70	******	******
10	0.01651	65.662	******	2.72961	******	940.61	******	******
11	0.01651	65.662	******	0.34085	******	577.05	******	******
12	0.01651	65.662	0.23524	0.34085	521.26	577.05	343.3	1.2037
13	0.00000	564.605	******	0.60333	******	290.92	******	******
14	0.00000	564.605	******	0.59729	******	290.92	******	******
15	0.00000	564.605	0.31522	0.59729	242.02	290.92	314.2	3.9544
16	0.00000	8.979	******	14.92062	******	772.63	******	******

```
 Gross Thrust = 227579.20
Momentum Drag = 158462.02
   Net Thrust =  69117.18
    Fuel Flow =    1.0666
       s.f.c. =  15.43159
   Sp. Thrust =   109.849
    Sim. time =   0.0000
          Time Now 16:16:51
```

Figure A-3 Cruise Point Results

A.4 EASA Certification Simulation Results

Station	F.A.R.	Mass Flow	Pstatic	Ptotal	Tstatic	Ttotal	Vel	Area
1	0.00000	1493.494	1.00000	0.99999	303.15	303.15	0.0	******
2	0.00000	1493.494	******	0.99999	******	303.15	******	******
3	0.00000	1493.494	******	1.59271	******	350.81	******	******
4	0.00000	160.474	******	1.59271	******	350.81	******	******
5	0.00000	160.474	******	2.82768	******	421.31	******	******
6	0.00000	160.474	******	41.79073	******	939.51	******	******
7	0.00000	160.474	******	41.79073	******	939.51	******	******
8	0.02125	163.884	******	39.85658	******	1645.00	******	******
9	0.02125	163.884	******	39.85658	******	1645.00	******	******
10	0.02125	163.884	******	9.06338	******	1205.49	******	******
11	0.02125	163.884	******	1.23074	******	769.58	******	******
12	0.02125	163.884	1.00000	1.23074	729.22	769.58	299.9	1.2037
13	0.00000	1333.019	******	1.59271	******	350.81	******	******
14	0.00000	1333.019	******	1.57678	******	350.81	******	******
15	0.00000	1333.019	1.00000	1.57678	307.80	350.81	295.1	3.9544
16	0.00000	0.000	******	0.00000	******	0.00	******	******

```
 Gross Thrust = 432936.36
Momentum Drag =      0.00
   Net Thrust = 432936.36
    Fuel Flow =    3.4099
       s.f.c. =   7.87620
   Sp. Thrust =   289.882
    Sim. time =   0.0000
          Time Now 10:28:11
```

Figure A-4 EASA Point Results

Appendix B Hermes

B.1 Geometrical Details

```
!GEOMETRIC DETAILS
! Wing Geometry
427.8          ! AcWingAInit - Wing area
8.67           ! AcWingAspr - Aspect ratio
0.10628        ! AcWingCThir - Thickness chord ratio
31.6           ! AcWingSwpa - Sweep angle (in degrees)
0.149          ! AcWingTpr - Taper ratio
0.16258        ! AcWingRtThir - Root thickness ratio
0.09318        ! AcWingOtThir - Outer thickness  ratio
! Tailplane Geometry
101.26         ! AcTailAInit - Tailplane area
4.5            ! AcTailAspr - Aspect ratio
0.09           ! AcTailCThir - Thickness chord ratio
35.0           ! AcTailSwpa - Sweep angle (in degrees)
0.30           ! AcTailTpr - Taper ratio
0.10           ! AcTailRtThir - Root thickness  ratio
0.07           ! AcTailOtThir - Outer thickness  ratio
! Fin Geometry
53.23          ! AcFinA - Fin area
9.24           ! AcFinSpan - Span
0.085          ! AcFinCThir - Thickness chord ratio
46.            ! AcFinSwpa - Sweep angle (in degrees)
0.29           ! AcFinTpr - Taper ratio
0.09           ! AcFinRtThir - Root thickness  ratio
0.08           ! AcFinOtThir - Outer thickness  ratio
! Fuselage Geometry
6.20           ! AcFusDia - Diameter
62.78          ! AcFusLen - Length
! Landing Gear Characteristics
2              ! AcLGTyp1 - Landing gear type ***0=default, 1=Bogie, 2=Small twin wheel***
2              ! AcLgTyp2= 0,1,2
1              ! AcLgTyp3= 0,1,2
-1             ! AcLgTyp4= 0,1,2,-1 *** -1=if the aircraft only has 3 LG -1 has to be declared
-1             ! AcLgTyp5= 0,1,2,-1 *** for the last 2 values
2              ! AcLGDepl - Number of segments with LG down for descent
! High lift systems
1              ! AcFlapSegTo -Number of Segments with flaps deployed during TO
3              ! AcFlapSegApp - Number of Segments with flaps deployed for approach
2              ! AcFlapSegLand - Number of Segments with flaps deployed during Landing
1.10           ! AcExtSrTo - Wing area extension ratio TO
1.15           ! AcExtSrApp - Wing area extension ratio approach
1.20           ! AcExtSrLand - Wing area extension ratio Landing
5.0            ! AcFlapAngleTo - Flap Angle TO IN DEGREES
20.0           ! AcFlapAngleApp - Flap Angle Approach
30.0           ! AcFlapAngleLand - Flap Angle Land
1              ! AcFlapSlots - Number of Flap Slots (1-3)
! Engine Geometry
3.40           ! EngNacDiaInit - Diameter
7.29           ! EngNacLenInit - Length
```

Figure B-1 Geometrical Data

B.2 Mission Weight Data

```
!MISSION/WEIGHT SPECIFICATION DATA
130410         ! AcAfrWtInit - Airframe weight
2              ! AcEngNb - Number of Engines
7550           ! EngWtInit - Engine weight,  (kg/engine)
13050          ! AcPldWt - Payload weight, (kg)
138990         ! AcFuelWtInit - Fuel weight,  (kg)
60000          ! AcPldWtmax  - Maximum payload weight, kg
200000         ! AcFuelWtmax - Maximum fuel weight,  kg   (greater than 138647.7 Kg)
213180         ! AcLandWtmax - Maximum landing weight, kg
297550         ! AcToWtmax - Maximum take-off weight, kg
0.01           ! DVFuelRatio - Diversion fuel weight to total fuel weight (%)
0.1            ! AcFuelContpc - Relative contingency fuel to remain after landing (%)
17634.7        ! AcRng - Range to be flown (km)       ! Mission (2)
340            ! AcRngdv - Diversion Range to be flown (km)
1              ! AcMisType - Mission to be flown
1              ! DvMission - specify if diversion mission is to be run
```

Figure B-2 Mission Weight Data

B.3 Cruise and Diversion Data

```
!CRUISE MAIN/DIVERSION AND HOLDING DATA
2              ! number of cruise altitudes and Mach numbers
1              ! number of cruise Temperature Deviations from ISA day
1              ! number of diversion cruise altitudes
5.             ! Cruise small segment time Interval in (min).
10688, 13106.4  ! Cruise altitudes in [m]
0.85, 0.85      ! Cruise Mach numbers, the same number with cruise altitudes
0.0            ! Cruise ambient temperature deviation from ISA, in [K]
6096.          ! Diversion cruise altitudes (m)
0.65           ! Diversion cruise Mach numbers,
0.             ! Diversion cruise ambient temperature deviation from ISA, in [K]
457.0          ! Holding altitude (m)
30.            ! Hold Time in (min)
```

Figure B-3 Cruise and Diversion Data

B.4 Climb and Descent Data

```
!CLIMB DATA
22                ! Climb segments Number
! Altitudes(m)   | DTisa(K) | EAS(knots) | Power(0.-1.)
557.20 0. 250. 1.
900.00 0. 250. 1.
1500.00 0. 250. 1.
1981.20 0. 250. 1.
2438.40 0. 250. 1.
2743.20 0. 250. 1.
3048.00 0. 250. 1.
3048.10 0. 320. 1.
3657.60 0. 320. 1.
4267.20 0. 320. 1.
4876.80 0. 320. 1.
5486.40 0. 320. 1.
6096.00 0. 320. 1.
7620.00 0. 320. 1.
8077.20 0. 320. 1.
9144.00 0. 320. 1.
10058.00 0. 320. 1.
10668.00 0. 320. 1.
11227.00 0. 320. 1.
11887.00 0. 320. 1.
12000.00 0. 320. 1.
12496.8 0. 320. 1.
!XXXXXXXXXXXXXXXXXXXXXXXXXXXXXXXXXXXXXXXXXXXXXXXXXXXXXXXXXXX
!DESCENT DATA
10                ! Descent segments Number
! The altitudes are dependant on the final cruise altitude.
! DTisa(K)       | TAS(knots) | Power(0.-1.)
3. 233.1 1.                                  ! Flight Idle Rating
3. 221.5 1.                                  ! Flight Idle Rating
3. 202.9 1.                                  ! Flight Idle Rating
3. 195.0 1.                                  ! Flight Idle Rating
3. 183.1 1.                                  ! Flight Idle Rating
3. 164.7 1.                                  ! Flight Idle Rating
3. 150.9 1.                                  ! Flight Idle Rating
3. 145.0 1.                                  ! Approach Rating
3. 140.0 1.                                  ! Approach Rating
3. 139.0 1.                                  ! Approach Rating
```

Figure B-4 Climb and Descent Data

Appendix C Cost Estimate Relationships

C.1 Engine References

Engine Name	Manufacturer	Puplication Title	Data of Publication
RB211-535 E4	Rolls - Royce	Big Engine in-service Performance & Maintenance	August 2008
Trent 553	Rolls - Royce	Rolls-Royce Trent Family Maintenance Cost	September 2012
Trent 556	Rolls - Royce	Rolls-Royce Trent Family Maintenance Cost	September 2012
Trent 768	Rolls - Royce	Rolls-Royce Trent Family Maintenance Cost	September 2012
Trent 772	Rolls - Royce	Rolls-Royce Trent Family Maintenance Cost	September 2012
Trent 877	Rolls - Royce	Rolls-Royce Trent Family Maintenance Cost	September 2012
Trent 892	Rolls - Royce	Rolls-Royce Trent Family Maintenance Cost	September 2012
Trent 895	Rolls - Royce	Rolls-Royce Trent Family Maintenance Cost	September 2012
Trent 970	Rolls - Royce	Rolls-Royce Trent Family Maintenance Cost	September 2012
Trent 977	Rolls - Royce	Rolls-Royce Trent Family Maintenance Cost	September 2012
CF6 - 80E1	General Electric	Big Engine in-service Performance & Maintenance	August 2008
GE 90-90B	General Electric	GE90 Family Maintenance Cost	October 2012
GE 90-90B	General Electric	GE90 Family Maintenance Cost	October 2012
GE 90-94B	General Electric	GE90 Family Maintenance Cost	October 2012
GE 90-110B	General Electric	GE90 Family Maintenance Cost	October 2012
GE 90-115B	General Electric	GE90 Family Maintenance Cost	October 2012
PW 2040 RTC	Pratt & Whitney	PW2000 Maintenance Analysis & Budget	August 2008
PW 4077	Pratt & Whitney	Big Engine in-service Performance & Maintenance	August 2008
PW 4090	Pratt & Whitney	Big Engine in-service Performance & Maintenance	August 2008

Table C-1 Engine Database References

C.2 Producer Price Index and Employment Cost Index

Data extracted on: June 6, 2015 (6:46:48 AM)

Producer Price Index Industry Data

Series Id: PCU336412336412
Industry: Aircraft engine and engine parts mfg
Product: Aircraft engine and engine parts mfg
Base Date: 198512

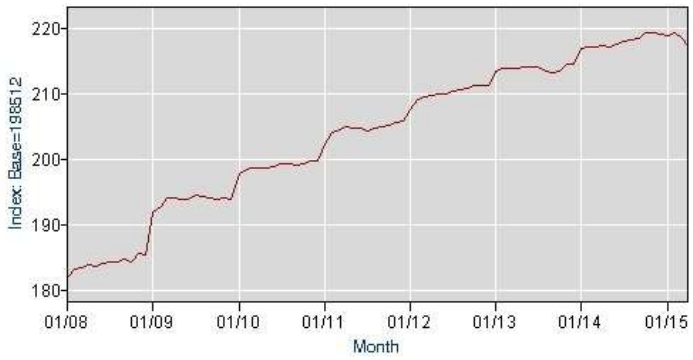

Figure C-1Producer Price Index

Data extracted on: June 6, 2015 (6:54:25 AM)

Employment Cost Index

Series Id: CIU2023211000000I
Not seasonally adjusted
Series Title: Wages and salaries for Private industry workers in Aircraft manufacturing, Index
Ownership: Private industry workers
Component: Wages and salaries
Occupation: All workers
Industry: Aircraft manufacturing
Subcategory: All workers

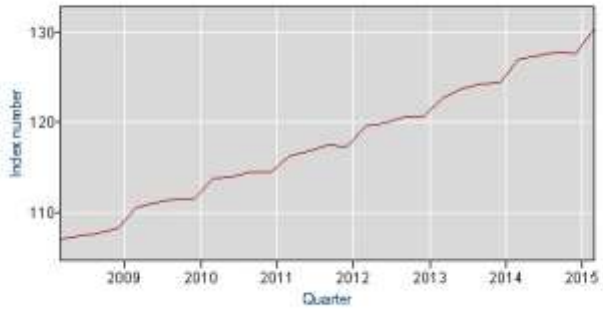

Figure C-2 Employment Cost Index

C.3 Regression Process Results

Non – Mature Removal Interval

Regression Statistics	
Multiple R	0.978544653
R Square	0.957549638
Adjusted R Square	0.934394895
Standard Error	478.8735305
Observations	18

ANOVA

	df	*SS*	*MS*	*F*	*Significance F*
Regression	6	56900259.34	9483376.556	41.35436254	6.43478E-07
Residual	11	2522518.441	229319.8583		
Total	17	59422777.78			

	Coefficients	*Standard Error*	*t Stat*	*P-value*	*Lower 95%*	*Upper 95%*	*Lower 95.0%*	*Upper 95.0%*
Intercept	5901.894092	1814.905341	3.251901881	1%	1907.31437	9896.473814	1907.31437	9896.473814
Thrust	-63.67890851	26.17485351	-2.432827694	3%	-121.2893727	-6.068444374	-121.2893727	-6.068444374
Thrust^2	0.085866494	0.036409473	2.358355823	4%	0.005729783	0.166003204	0.005729783	0.166003204
Weight	5.370140613	1.828361396	2.937133011	1%	1.345944312	9.394336914	1.345944312	9.394336914
Weight^2	-0.000409483	0.000146064	-2.803439263	2%	-0.000730968	-8.79971E-05	-0.000730968	-8.79971E-05
EFH/EFC	475.0094989	177.1226166	2.681811662	2%	85.16524813	864.8537496	85.16524813	864.8537496
ln(EFH/EFC)	-6091.265738	874.3431541	-6.96667631	0%	-8015.682045	-4166.849431	-8015.682045	-4166.849431

Table C-2 NMRI Regression Result

Mature Removal Interval

Regression Statistics	
Multiple R	0.985636652
R Square	0.971479609
Adjusted R Square	0.957219414
Standard Error	339.7499488
Observations	19

ANOVA

	df	SS	MS	F	Significance F
Regression	6	47182208.09	7863701.348	68.12526604	1.43417E-08
Residual	12	1385160.333	115430.0277		
Total	18	48567368.42			

	Coefficients	Standard Error	t Stat	P-value	Lower 95%	Upper 95%	Lower 95.0%	Upper 95.0%
Intercept	79453.11442	26076.25064	3.046953165	1%	22637.84497	136268.3839	22637.84497	136268.3839
Thrust	46.00247056	18.47528576	2.489946362	3%	5.748280919	86.2566602	5.748280919	86.2566602
ln(Thrust)	-17208.79977	6368.43781	-2.702201117	2%	-31084.43377	-3333.16576	-31084.43377	-3333.16576
(EFH/EFC)^2	15.90910013	5.448771635	2.919759021	1%	4.03724659	27.78095368	4.03724659	27.78095368
ln(EFH/EFC)	-4061.641052	360.4800424	-11.26731185	0%	-4847.059593	-3276.222511	-4847.059593	-3276.222511
Weight	4.493623046	1.560095277	2.880351677	1%	1.094467441	7.89277865	1.094467441	7.89277865
Weight^2	-0.000335298	0.000121613	-2.757084136	2%	-0.00060027	-7.03254E-05	-0.00060027	-7.03254E-05

Table C-3 MRI Regression Result

Non – Mature Shop Visit Cost

Regression Statistics	
Multiple R	0.9471124
R Square	0.897021897
Adjusted R Square	0.794043795
Standard Error	31.84695416
Observations	19

ANOVA

	df	SS	MS	F	Significance F
Regression	9	79512.69505	8834.743895	8.710802337	0.001758481
Residual	9	9128.056403	1014.228489		
Total	18	88640.75145			

	Coefficients	Standard Error	t Stat	P-value	Lower 95%	Upper 95%	Lower 95.0%	Upper 95.0%
Intercept	-11191.36854	4668.207112	-2.397359044	0.040071018	-21751.58669	-631.1503838	-21751.58669	-631.1503838
Thrust	-17.46028659	6.113948494	-2.855811854	0.018909095	-31.29099897	-3.629574207	-31.29099897	-3.629574207
Thrust^2	0.04366033	0.016092353	2.713110422	0.023875597	0.007256899	0.080063761	0.007256899	0.080063761
Thrust^3	-3.57521E-05	1.39336E-05	-2.565896112	0.030391722	-6.7272E-05	-4.23217E-06	-6.7272E-05	-4.23217E-06
ln(Weigth)	1862.970807	690.8720022	2.696549868	0.024531922	300.1097581	3425.831855	300.1097581	3425.831855
EFH/EFC	59.50022022	36.62735421	1.624474972	0.138720962	-23.35661146	142.3570519	-23.35661146	142.3570519
1/(EFH/EFC)	-1140.734017	655.3527497	-1.740641232	0.115734523	-2623.244934	341.7768994	-2623.244934	341.7768994
ln(EFH/EFC)	-569.1316476	348.835721	-1.631517684	0.137217281	-1358.252873	219.9895774	-1358.252873	219.9895774
1st EFH	-0.011081221	0.002640645	-4.196407721	0.002318996	-0.017054775	-0.005107668	-0.017054775	-0.005107668
Weight	-0.233515155	0.111917196	-2.086499337	0.066560133	-0.486689441	0.019659131	-0.486689441	0.019659131

Table C-4 NMSV Regression Result

Mature Shop Visit Cost

Regression Statistics	
Multiple R	0.949365979
R Square	0.901295762
Adjusted R Square	0.838483974
Standard Error	34.45014835
Observations	19

ANOVA

	df	SS	MS	F	Significance F
Regression	7	119208.2756	17029.75366	14.34914991	9.97803E-05
Residual	11	13054.93994	1186.812722		
Total	18	132263.2155			

	Coefficients	Standard Error	t Stat	P-value	Lower 95%	Upper 95%	Lower 95.0%	Upper 95.0%
Intercept	11289.90628	5019.791855	2.249078568	5%	241.4188977	22338.39366	241.4188977	22338.39366
Thrust	21.84981902	8.676234612	2.518352718	3%	2.75355539	40.94608264	2.75355539	40.94608264
Thrust^2	-0.012640535	0.00610149	-2.07171291	6%	-0.026069823	0.000788753	-0.026069823	0.000788753
log(Thrust)	-10236.96186	3630.935036	-2.819373455	2%	-18228.59599	-2245.327725	-18228.59599	-2245.327725
Weight^2	-1.51796E-05	6.0677E-06	-2.501711965	3%	-2.85346E-05	-1.82472E-06	-2.85346E-05	-1.82472E-06
log(Weigth)	3443.989583	1122.242053	3.068847379	1%	973.9514786	5914.027687	973.9514786	5914.027687
(EFH/EFC)^2	0.683013913	0.307944864	2.217974687	5%	0.005231837	1.360795989	0.005231837	1.360795989
log(2st EFH)	-822.0388247	142.762887	-5.758070896	0%	-1136.25782	-507.819829	-1136.25782	-507.819829

Table C-5 MSV Regression Result

Life Limited Parts Reserve Cost

Regression Statistics	
Multiple R	0.93610059
R Square	0.876284314
Adjusted R Square	0.814426472
Standard Error	78.3500016
Observations	19

ANOVA

	df	SS	MS	F	Significance F
Regression	6	521770.5188	86961.75314	14.16609882	8.02543E-05
Residual	12	73664.673	6138.72275		
Total	18	595435.1918			

	Coefficients	Standard Error	t Stat	P-value	Lower 95%	Upper 95%	Lower 95.0%	Upper 95.0%
Intercept	27930.77989	7226.156287	3.865233297	0%	12186.33786	43675.22192	12186.33786	43675.22192
Thrust	17.57476292	4.687538288	3.749252131	0%	7.361494353	27.78803148	7.361494353	27.78803148
log(Thrust)	-13238.88944	3726.076552	-3.553037426	0%	-21357.31283	-5120.466043	-21357.31283	-5120.466043
Weight	1.80645404	0.40811289	4.426358699	0%	0.91725244	2.695655641	0.91725244	2.695655641
Weight^2	-0.00014863	3.17717E-05	-4.678062464	0%	-0.000217854	-7.94054E-05	-0.000217854	-7.94054E-05
EFH/EFC	62.42230606	12.67462488	4.924982526	0%	34.80667076	90.03794136	34.80667076	90.03794136
log(1st EFH)	-1324.405661	311.4891168	-4.251852118	0%	-2003.082145	-645.7291771	-2003.082145	-645.7291771

Table C-6 LLPR Regression Result

C.4 T-value and F-value Chart

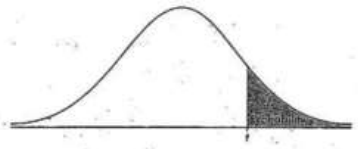

TABLE B: *t*-DISTRIBUTION CRITICAL VALUES

	Tail probability p										
df	.25	.20	.15	.10	.05	.025	.02	.01	.005	.0025	.001	.0005
1	1.000	1.376	1.963	3.078	6.314	12.71	15.89	31.82	63.66	127.3	318.3	636.6
2	.816	1.061	1.386	1.886	2.920	4.303	4.849	6.965	9.925	14.09	22.33	31.60
3	.765	.978	1.250	1.638	2.353	3.182	3.482	4.541	5.841	7.453	10.21	12.92
4	.741	.941	1.190	1.533	2.132	2.776	2.999	3.747	4.604	5.598	7.173	8.610
5	.727	.920	1.156	1.476	2.015	2.571	2.757	3.365	4.032	4.773	5.893	6.869
6	.718	.906	1.134	1.440	1.943	2.447	2.612	3.143	3.707	4.317	5.208	5.959
7	.711	.896	1.119	1.415	1.895	2.365	2.517	2.998	3.499	4.029	4.785	5.408
8	.706	.889	1.108	1.397	1.860	2.306	2.449	2.896	3.355	3.833	4.501	5.041
9	.703	.883	1.100	1.383	1.833	2.262	2.398	2.821	3.250	3.690	4.297	4.781
10	.700	.879	1.093	1.372	1.812	2.228	2.359	2.764	3.169	3.581	4.144	4.587
11	.697	.876	1.088	1.363	1.796	2.201	2.328	2.718	3.106	3.497	4.025	4.437
12	.695	.873	1.083	1.356	1.782	2.179	2.303	2.681	3.055	3.428	3.930	4.318
13	.694	.870	1.079	1.350	1.771	2.160	2.282	2.650	3.012	3.372	3.852	4.221
14	.692	.868	1.076	1.345	1.761	2.145	2.264	2.624	2.977	3.326	3.787	4.140
15	.691	.866	1.074	1.341	1.753	2.131	2.249	2.602	2.947	3.286	3.733	4.073
16	.690	.865	1.071	1.337	1.746	2.120	2.235	2.583	2.921	3.252	3.686	4.015
17	.689	.863	1.069	1.333	1.740	2.110	2.224	2.567	2.898	3.222	3.646	3.965
18	.688	.862	1.067	1.330	1.734	2.101	2.214	2.552	2.878	3.197	3.611	3.922
19	.688	.861	1.066	1.328	1.729	2.093	2.205	2.539	2.861	3.174	3.579	3.883
20	.687	.860	1.064	1.325	1.725	2.086	2.197	2.528	2.845	3.153	3.552	3.850
21	.686	.859	1.063	1.323	1.721	2.080	2.189	2.518	2.831	3.135	3.527	3.819
22	.686	.858	1.061	1.321	1.717	2.074	2.183	2.508	2.819	3.119	3.505	3.792
23	.685	.858	1.060	1.319	1.714	2.069	2.177	2.500	2.807	3.104	3.485	3.768
24	.685	.857	1.059	1.318	1.711	2.064	2.172	2.492	2.797	3.091	3.467	3.745
25	.684	.856	1.058	1.316	1.708	2.060	2.167	2.485	2.787	3.078	3.450	3.725
26	.684	.856	1.058	1.315	1.706	2.056	2.162	2.479	2.779	3.067	3.435	3.707
27	.684	.855	1.057	1.314	1.703	2.052	2.158	2.473	2.771	3.057	3.421	3.690
28	.683	.855	1.056	1.313	1.701	2.048	2.154	2.467	2.763	3.047	3.408	3.674
29	.683	.854	1.055	1.311	1.699	2.045	2.150	2.462	2.756	3.038	3.396	3.659
30	.683	.854	1.055	1.310	1.697	2.042	2.147	2.457	2.750	3.030	3.385	3.646
40	.681	.851	1.050	1.303	1.684	2.021	2.123	2.423	2.704	2.971	3.307	3.551
50	.679	.849	1.047	1.299	1.676	2.009	2.109	2.403	2.678	2.937	3.261	3.496
60	.679	.848	1.045	1.296	1.671	2.000	2.099	2.390	2.660	2.915	3.232	3.460
80	.678	.846	1.043	1.292	1.664	1.990	2.088	2.374	2.639	2.887	3.195	3.416
100	.677	.845	1.042	1.290	1.660	1.984	2.081	2.364	2.626	2.871	3.174	3.390
1000	.675	.842	1.037	1.282	1.646	1.962	2.056	2.330	2.581	2.813	3.098	3.300
∞	.674	.841	1.036	1.282	1.645	1.960	2.054	2.326	2.576	2.807	3.091	3.291
	50%	60%	70%	80%	90%	95%	96%	98%	99%	99.5%	99.8%	99.9%
	Confidence level C											

Table C-7 T-Distribution Chart

F - Distribution ($\alpha = 0.05$ in the Right Tail)

Denominator Degrees of Freedom (df_2) \ Numerator Degrees of Freedom (df_1)	1	2	3	4	5	6	7	8	9
1	161.45	199.50	215.71	224.58	230.16	233.99	236.77	238.88	240.54
2	18.513	19.000	19.164	19.247	19.296	19.330	19.353	19.371	19.385
3	10.128	9.5521	9.2766	9.1172	9.0135	8.9406	8.8867	8.8452	8.8123
4	7.7086	6.9443	6.5914	6.3882	6.2561	6.1631	6.0942	6.0410	5.9988
5	6.6079	5.7861	5.4095	5.1922	5.0503	4.9503	4.8759	4.8183	4.7725
6	5.9874	5.1433	4.7571	4.5337	4.3874	4.2839	4.2067	4.1468	4.0990
7	5.5914	4.7374	4.3468	4.1203	3.9715	3.8660	3.7870	3.7257	3.6767
8	5.3177	4.4590	4.0662	3.8379	3.6875	3.5806	3.5005	3.4381	3.3881
9	5.1174	4.2565	3.8625	3.6331	3.4817	3.3738	3.2927	3.2296	3.1789
10	4.9646	4.1028	3.7083	3.4780	3.3258	3.2172	3.1355	3.0717	3.0204
11	4.8443	3.9823	3.5874	3.3567	3.2039	3.0946	3.0123	2.9480	2.8962
12	4.7472	3.8853	3.4903	3.2592	3.1059	2.9961	2.9134	2.8486	2.7964
13	4.6672	3.8056	3.4105	3.1791	3.0254	2.9153	2.8321	2.7669	2.7144
14	4.6001	3.7389	3.3439	3.1122	2.9582	2.8477	2.7642	2.6987	2.6458
15	4.5431	3.6823	3.2874	3.0556	2.9013	2.7905	2.7066	2.6408	2.5876
16	4.4940	3.6337	3.2389	3.0069	2.8524	2.7413	2.6572	2.5911	2.5377
17	4.4513	3.5915	3.1968	2.9647	2.8100	2.6987	2.6143	2.5480	2.4943
18	4.4139	3.5546	3.1599	2.9277	2.7729	2.6613	2.5767	2.5102	2.4563
19	4.3807	3.5219	3.1274	2.8951	2.7401	2.6283	2.5435	2.4768	2.4227
20	4.3512	3.4928	3.0984	2.8661	2.7109	2.5990	2.5140	2.4471	2.3928
21	4.3248	3.4668	3.0725	2.8401	2.6848	2.5727	2.4876	2.4205	2.3660
22	4.3009	3.4434	3.0491	2.8167	2.6613	2.5491	2.4638	2.3965	2.3419
23	4.2793	3.4221	3.0280	2.7955	2.6400	2.5277	2.4422	2.3748	2.3201
24	4.2597	3.4028	3.0088	2.7763	2.6207	2.5082	2.4226	2.3551	2.3002
25	4.2417	3.3852	2.9912	2.7587	2.6030	2.4904	2.4047	2.3371	2.2821
26	4.2252	3.3690	2.9752	2.7426	2.5868	2.4741	2.3883	2.3205	2.2655
27	4.2100	3.3541	2.9604	2.7278	2.5719	2.4591	2.3732	2.3053	2.2501
28	4.1960	3.3404	2.9467	2.7141	2.5581	2.4453	2.3593	2.2913	2.2360
29	4.1830	3.3277	2.9340	2.7014	2.5454	2.4324	2.3463	2.2783	2.2229
30	4.1709	3.3158	2.9223	2.6896	2.5336	2.4205	2.3343	2.2662	2.2107
40	4.0847	3.2317	2.8387	2.6060	2.4495	2.3359	2.2490	2.1802	2.1240
60	4.0012	3.1504	2.7581	2.5252	2.3683	2.2541	2.1665	2.0970	2.0401
120	3.9201	3.0718	2.6802	2.4472	2.2899	2.1750	2.0868	2.0164	1.9588
∞	3.8415	2.9957	2.6049	2.3719	2.2141	2.0986	2.0096	1.9384	1.8799

Table C-8 F-Distribution Chart